ADVANCED CATHODES FOR NEXT GENERATION ELECTRIC PROPULSION TECHNOLOGY

THESIS

Dustin J. Warner, 2nd Lieutenant, USAF

AFIT/GA/ENY/08-M07

DEPARTMENT OF THE AIR FORCE
AIR UNIVERSITY

AIR FORCE INSTITUTE OF TECHNOLOGY

Wright-Patterson Air Force Base, Ohio

AFIT/GA/ENY/08-M07

ADVANCED CATHODES FOR NEXT GENERATION ELECTRIC PROPULSION TECHNOLOGY

THESIS

Presented to the Faculty

Department of Aeronautics and Astronautics

Graduate School of Engineering and Management

Air Force Institute of Technology

Air University

Air Education and Training Command

In Partial Fulfillment of the Requirements for the

Degree of Master of Science in Astronautical Engineering

Dustin J. Warner, BS

2nd Lieutenant, USAF

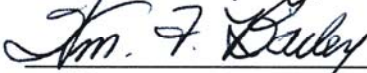March 2008

APPROVED FOR PUBLIC RELEASE; DISTRIBUTION UNLIMITED

AFIT/GAE/ENY/08-M

ADVANCED CATHODES FOR NEXT GENERATION ELECTRIC PROPULSION TECHNOLOGY

Dustin J. Warner, BS

2nd Lieutenant, USAF

Approved:

_____   _____
Richard Branam, Maj, USAF (Chairman)   7 Mar 08
                                                  Date

_____   _____
William F. Bailey (Member)   7 Mar '08
                                                  Date

_____   _____
William Hargus Jr. (Member)   6 Mar 08
                                                  Date

Abstract

The research presented here investigated the feasibility of 6.4 mm Lanthanum Hexaboride (LaB_6) and Cerium Hexaboride (CeB_6) hollow cathodes for low power electric propulsion applications (100-300W). Two orifice geometries, one anode configuration, several anode and keeper currents, and a range of xenon flow rates were tested for the LaB_6 cathode. The CeB_6 cathode underwent the same tests, with the exception of the second orifice geometry due to time constraints.

An oscilloscope measured waveform behavior and a single Langmuir probe for plasma properties. Infrared imaging studied the thermal characteristics of both cathodes and electron microscopy for surface contaminant analysis. High-speed imaging provided visual data for coupling plasma observations.

The CeB_6 cathode operated in spot mode as low as 1.5 A and 1.5 sccm with no heater or keeper power, and as high as 6 A, 1.5 sccm with 1 A keeper current. The CeB_6 cathode was more susceptible to poisoning than the LaB_6 cathode. It also operated at slightly higher temperatures.

The LaB_6 cathode was not affected by poisoning and ran in spot mode as low as 2.5 A, at 1.5 sccm with no heater or keeper power. When the aspect ratio was reduced to 0.25, the cathode operated as low as 1.4 A, with 1.5 sccm. The same spot/plume mode characteristics were observed for LaB_6 as CeB_6. The study of both cathodes is presented here including suggestions for a 3 mm LaB_6 cathode.

Acknowledgments

Table of Contents

List of Figures

Nomenclature

A	Richardson Coefficient
T	Temperature (K)
q	Particle Charge (C)
e	Charge of an Electron (C)
φ	Work Function (electron Volts)
k	Boltzmann's constant
E	Electric Field (V/m)
n	Number Density (cm^{-3})
ε_o	Permittivity of Free Space
ε	Emissivity
λ_D	Debye Length
m_e	Electron Mass (kg)
d	Sheath Thickness (cm)
V	Volts
A_P	Probe Area
I	Current (Amps)

ADVANCED CATHODES FOR NEXT GENERATION ELECTRIC PROPULSION TECHNOLOGY

I. Introduction

Motivation

In 1993, the Air Force Research Laboratory Propulsion Directorate at Edwards Air Force Base formed a committee with the endorsement of leaders from industry and the other branches of the military called Integrated High Payoff Rocket Propulsion Technology (IHPRPT). The aim of this program is to improve and double the performance of United States rocket propulsion by 2010. The goals for these improvements are set out in five-year increments, ending in 2010. In response to this program, entities throughout the United States, including universities and government agencies set out to meet these goals. This program will not only improve high thrust missions, but also low thrust ones suited for electric propulsion.

Electric propulsion exists in many forms, but the technology of interest for this research are ion and Hall thrusters. Both produce low thrust, have high specific impulse, and very high efficiencies when compared to chemical rockets. Satellites requiring precision attitude control and station keeping employ the use of electric propulsion today. The Air Force specifically uses this technology on TacSat - 2, employing a 200 W Busek Hall Thruster identical to the one at AFIT today, the first of its kind used in the US. Ion thrusters however, have been used in US space missions since the early 1970's. Both of these thrusters utilize plasma to produce thrust, which must be ionized by electrons. Hollow cathodes provide the electron source for this technology and are the focus of this research.

Hollow cathodes have been in use for the last several decades. There are various forms of them, but all are used to create electrons. Whether it is a few milliamps or

hundreds of amps, they have proven to be devices of prospect and intense investigation for the electric propulsion field. Hall thrusters, ion thrusters, and plasma contactors all use hollow cathodes in various forms and configurations. Other methods of creating electrons are abundant, but the longevity and peak current capability of hollow cathodes is unrivaled. They have proven their worth in many laboratory investigations, one lasted 28,000 hours.[1] Recently developed hollow cathode technology may alleviate some life-limiting factors that many traditional hollow cathode technologies have.[2] Consequently, long life equipment for spacecraft thruster technology is evolving. The need for low-cost, robust, and efficient hollow cathodes is instrumental in the advancement of the field and fulfillment of the IHPRPT goals.

Problem Statement

The current state-of-the-art hollow cathode for US space propulsion requires nitrogen purging to ensure the impregnated cathode insert is not contaminated by water vapor or oxygen. If this purge system were to fail, the cathode's performance could be adversely affected due to its sensitivity to contaminate species. In addition, high current impregnated hollow cathodes currently used by the US have shorter lifetimes than lower current designs, predominately governed by the evaporation rate of the impregnate. Low current designs however, suffer from several thermal inefficiencies forcing the cathode to consume a large percentage of a sub-300 W thruster's overall power.

Research Objectives

The objectives of this research were to investigate the feasibility of lanthanum hexaboride (LaB$_6$) and cerium hexaboride (CeB$_6$) as low current hollow cathode emitters

(<10A). This research also intended to compare lanthanum hexaboride and cerium hexaboride cathodes' power, flow, and temperature requirements for operation, and determine the benefits of one technology over another.

Research Focus

The work presented here focused on studying the recent developments in emitter technology for hollow cathodes and their feasibility for use in low power applications. LaB_6 and CeB_6 emitters were the two insert materials of choice. The author acquired and evaluated the current state of the art design.[2] While experiments have already studied the use of LaB_6 emitters for hollow cathodes, no work has been published for CeB_6 as a hollow cathode electron emitter. Additionally, all work in the US published on boride hollow cathodes are for high-current applications.[3,4,5,6,7,8,9,10] This study attempted to investigate their prospect for low-current designs, whether it is a hollow cathode configuration or something else.

This research directly compared LaB_6 to CeB_6 for one anode geometry, but for several emission currents, flow rates, and orifice geometries. The primary items of interest were the power and flow requirements of CeB_6 compared to LaB_6, how each emitter material behaved after operation, ways to improve the thermal efficiency of the cathode design, and the operation point at which the plasma transitions from spot to plume mode. A detailed analysis of the plasma behavior of each cathode is included, and compared the cathodes to their impregnated tungsten counterpart.

Investigative Questions

The major question this research attempts to answer is which boride cathode is the best for low current applications? In order to determine this, one needs to know which cathode requires the lowest flow rates and power to maintain spot-mode operation and if this can be improved with orifice geometry. Next, what is the ignition power requirements compared to impregnated cathodes? What is the temperature of each cathode and which is the lower of the two? The lifetime of boride inserts is limited by their evaporation rate, which is a function of temperature. The evaporation rate's temperature dependence emphasizes the importance of measuring the operating temperature of both cathode and comparing them to each other. Temperature data also helps answer the question of how much power the cathode uses and its correlation with temperature. Finally, did any contaminate materials form on the insert surface and affect its performance or lifetime, and what kind of contaminants formed on the surface? After analysis, the best cathode was selected and compared to an impregnated cathode.

II. Literature Review

Hall Thruster Applications

All electric propulsion uses some mechanism to create plasma, which in turn produces the rocket's thrust. Hollow cathodes demonstrate wide use for this technology.[2,3,4,10,11,12,13,14,15,16] The Soviet Union initially flight-tested Hall thrusters in 1972.[14] While invented here, the United States did not actively pursue this technology until 1992.[15] When compared with other electric propulsion devices such as the ion thruster, the Hall thruster demonstrated slightly higher levels of thrust (~up to 5 N) and lower levels of specific impulse (~1000-2000 s). The efficiencies were also lower than

ion thrusters, ~ 50%.[15] Nevertheless, the Hall thruster proved to a very reliable

technology for satellite station-keeping and orbit-raising. The Hall thruster's principle of

operation is illustrated in Figure 1.
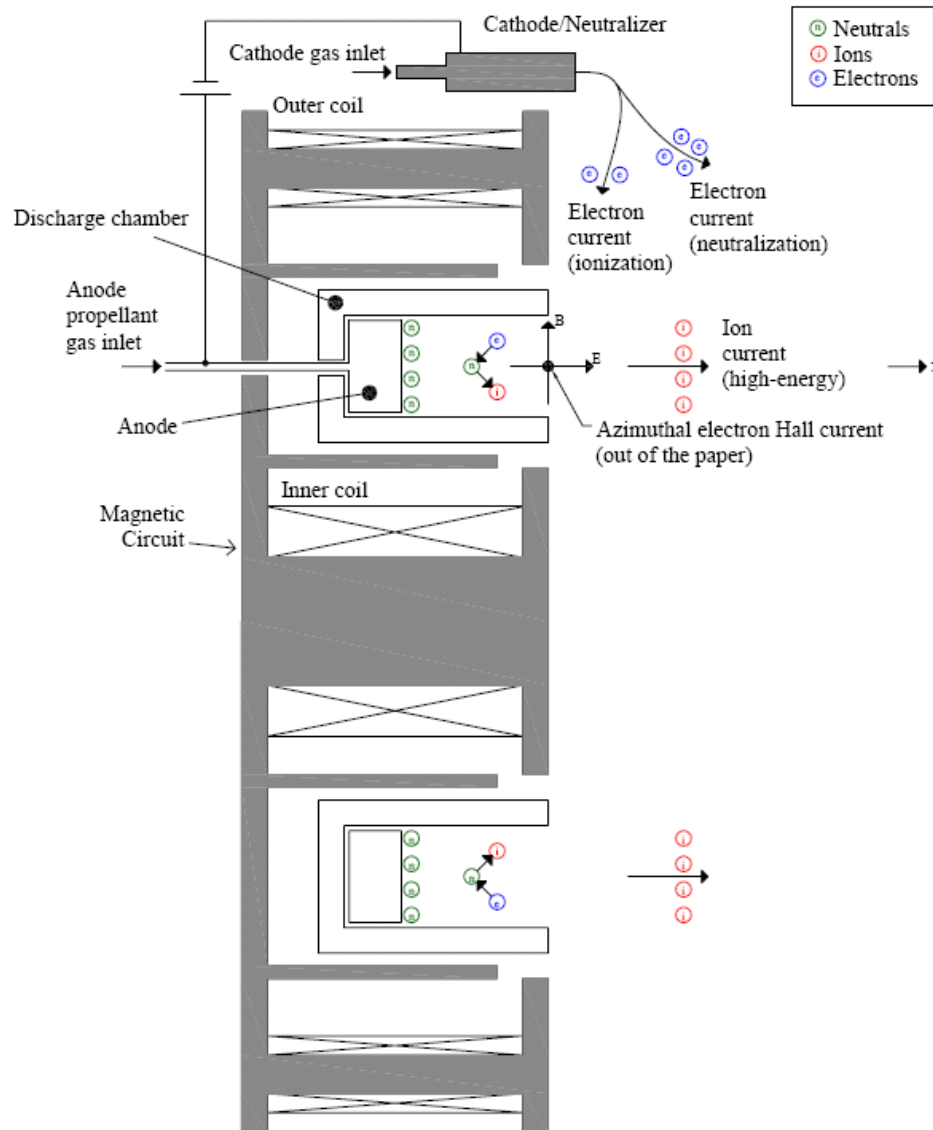
Figure 1. Hall Thruster Schematic[3]

The Hall Thruster's propellant is a neutral gas stored in a pressurized tank (xenon,

argon, or krypton) and a precise mass flow controller system limits the flow to a few

mg/s. This propellant flows into the thruster through a gas diffuser. The diffuser allows

the propellant to spread evenly throughout the thruster. There is an axial electric field

and a radial magnetic field present in a Hall thruster. An anode creates a potential at

approximately 300 V or more, known as the discharge or anode potential.

Electromagnets positioned on the central axis of the thruster create the radially directed

magnetic field. On the outside of the thruster is the hollow cathode (or sometimes a

tungsten wire for terrestrial applications) used to create electrons. Free electrons

generated from the cathode attract to the net positive potential of the anode and flow

toward the thruster itself. The combination of the electric and magnetic field creates the

"Hall" effect and causes the electrons to travel a much longer distance through the

thruster chamber before the anode collects a fraction of them. A stronger magnetic field

increases the ionization efficiency and decreases the frequency of wall-collisions.

Simultaneously, a gyrating region of electrons ionizes the neutral gas as it passes through.

The ions closest to the downstream end of the Hall thruster pass through an acceleration

zone resulting in thrust. The electrons from the hollow cathode continue the ionization or

"discharge" process, but they also act to charge neutralize the plume of the thruster.[15]

For low power applications (100-300 W), the presence of the hollow cathode reduces the

propellant utilization efficiency and power efficiency of the hall thruster, requiring up to

10 percent of the total propellant flow.[17]

Ion Thruster Applications

Like Hall thrusters, ion thrusters also employ hollow cathodes.[15,18,19,20,21] Harold

Kaufman at NASA Glen Research Center (GRC) originally developed an efficient ion

thruster design in the late 1950's. An ion thruster can have total efficiencies as high as

~80% and specific impulses as high as ~8000 s. However, they produce lower thrust

density levels than Hall thrusters. Consequently, ion thrusters prove to be better suited

for deep space missions. See the depiction of the operation of an ion thruster in Figure 2

below.
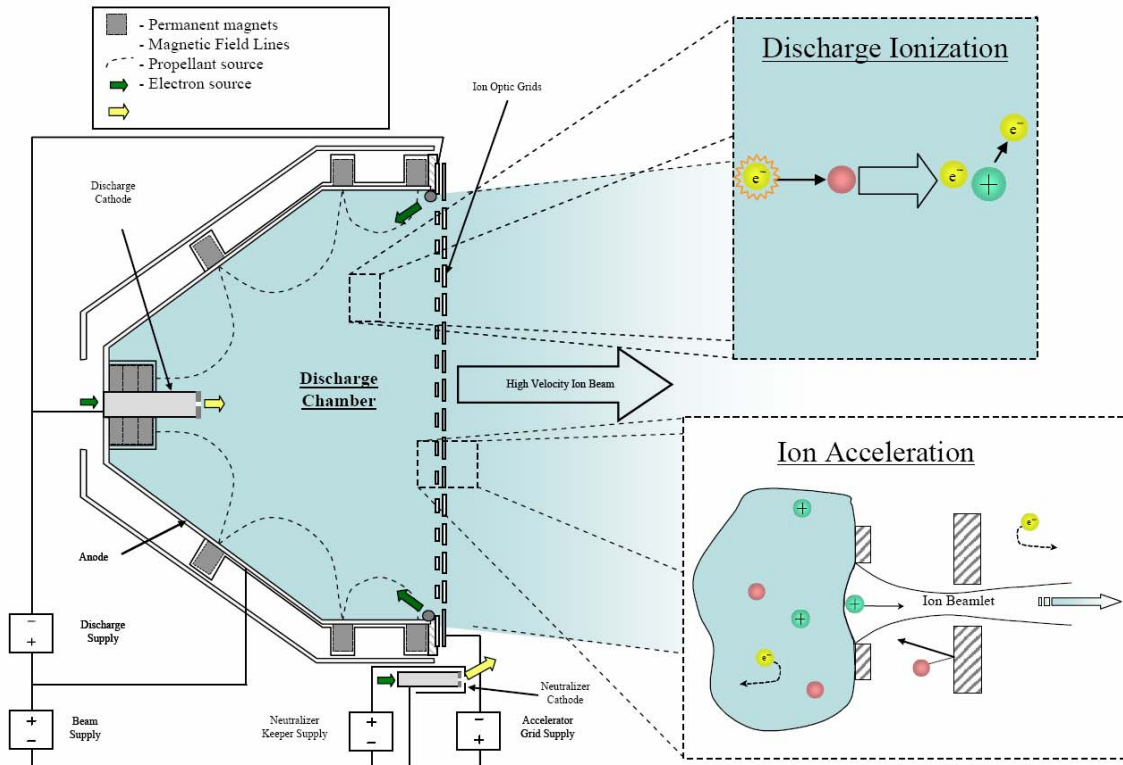
Figure 2. Ion Thruster Schematic[20]

Similar to the Hall thruster, propellant flows through to a diffuser and into the

discharge chamber of the ion thruster. The discharge chamber is at a high positive

potential, 500-1000 V, and the anode is the small plate protruding from it. The anode

potential is typically between 20 and 50 V higher than the discharge chamber. There is a

hollow cathode at the center of the discharge chamber. Electrons leave the cathode and

gyrate along the lines of the magnetic field toward the anode until they are collected. The

magnetic field acts to increase ionization efficiency by increasing the electron mean-free-path and reduce wall-collisions. As the electrons collide with the neutral atoms, plasma is created in the discharge chamber. The end of the thruster usually has two grids, called ion optics (older designs used only one). Without these grids, an ion thruster cannot produce thrust. The first grid is at a slightly lower positive potential than the plasma within the discharge chamber. Closely following the screen grid is the accelerator grid. The accelerator grid is at a large negative potential relative to the screen grid. As the ions migrate towards these grids they pass through a large potential change and are accelerated out the thruster. An additional hollow cathode is outside the grids to charge-neutralize the ion beam.

Plasma Contactor Applications

The third dominant technology utilizing hollow cathodes for space applications is the plasma contactor.[22] Spacecraft can emit electrons from their surface by means of photoemission or obtain large charge buildup due to geomagnetic storms. This creates a net charge relative to the space plasma. The charge presence can damage or perturb instrumentation and sensitive devices on spacecraft by rapid and violent discharging. In order to reduce and sometimes eliminate this phenomenon, a plasma contactor regulates the charge of the spacecraft by emitting or collecting electrons to and from the space plasma. The hollow cathode acts as the electron source for this device. One real world example of a spacecraft using this device is the International Space Station.

Cathode Technology

      Cathodes, the major component of the technologies describe above, have a wide variety of designs. Some cathodes are as simple as a wire passing current through until it glows white hot to emit electrons. Others are more complex, requiring propellant and the presence of other electrodes to create electrons. The first type of cathode is the tungsten filament. Figure 3 shows a tungsten filament used on an ion source.

Figure 3. Ion Source with Tungsten Filament Neutralizer[23]

Tungsten filaments are not used in space applications because of their very short lifetimes and limited performance. High temperatures required to achieve sufficient electron emission, tungsten evaporation, and sputter erosion contribute to the short lifetimes, typically a few hundred hours or less. However, their electron emission behavior is well-described by equation 1, known as the Richardson-Duschman equation. This fundamental behavior is characteristic of most electron emitters.

$$j = A \cdot T^2 \cdot e^{\frac{-q \cdot \phi}{k \cdot T}} \tag{1}$$

The Richardson-Duschman equation describes a relationship between the temperature of the wire and the amount of current it is capable of emitting by thermionic emission. ϕ is

the work function of the material used as the electron emitter. This is a material dependant property, for tungsten, it is 4.5 eV.[19] As one can see, a higher work function requires higher temperature and ultimately more power to achieve the desired electron current density. A is the emission constant, specific to each material as well. One must be cautious when using this equation alone to design an electron emitter. The electron emitter can melt if the temperature is too high. Equation 1 allows the designer to calculate the maximum theoretical emission current assuming the emitter's melting temperature is known. One can also see current density will increase with decreasing work function. Thus, a major pursuit of research is finding robust low work function emitters.

Another consideration for cathode design is the space charge limit. The reason the filament works well as a stand-alone emitter is due to immersion in plasma. Equation 2 shows the "space-charge limit" for an electron emitter immersed in plasma.

$$ j_S = \frac{\kappa}{2} \cdot n_i \cdot e \cdot \sqrt{\frac{k \cdot T_e}{m_e}} \tag{2} $$

For the tungsten filaments used in thrusters, the plasma densities are sufficient to allow the wire to reach the current density required to create a discharge. The dense plasma pulls the electrons away from the filament by the formation of a sheath. As equation 2 shows, this depends on the electron temperature, T_e, and ion density near the filament, n_i. The constant κ is typically 0.5.[19] By knowing or measuring the terms shown in equation 2, one can calculate the maximum emission current the plasma sheath is capable of extracting from the filament. These two equations determine the appropriate emitter and plasma environment to suit a given application.

A second type of cathode is the single crystal emitter. These are widely used in electron microscopes.[24] Due to their low work function (~2.4-2.8 eV), resistance to contamination from trace gases, and their low evaporation rates, the two primary compounds used in these emitters are lanthanum hexaboride and cerium hexaboride.[2,19] Figure 4 depicts a lanthanum hexaboride crystal emitter.
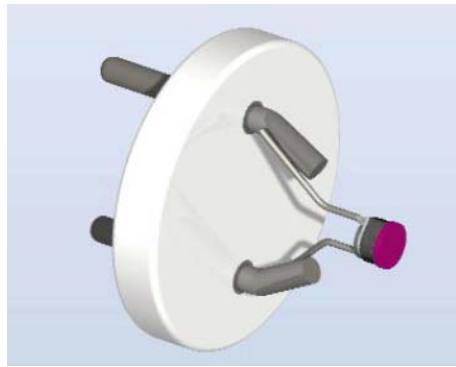
Figure 4. Lanthanum Hexaboride Crystal Emitter[25]

Ohmic heating from electron flow through the mounting posts drives the electron emission from the crystal. Small pyrolytic graphite mounts with high cross-plane resistance reach sufficient temperatures for the crystal to emit electrons. These cathodes require very low levels of power (~10-20 W) to reach useful current levels.[26] Equations 1 and 2 also apply to single crystal emitters. This type of cathode has been proven a viable technology for some electric propulsion applications.[19]

The final cathode technology discussed here is the hollow cathode. There are many different versions of hollow cathodes, but the most common style for space applications is the orificed hollow cathode, shown in Figure 5. The term "orificed" simply means there is a plate present with a small hole in the center at one end of the cathode. Mirtich and Goebel discuss some other designs without orifice plates.[18,15]

26

1. Insert Region
2. Orifice Region
3. Cathode-to-Keeper Region
4. Coupling Region
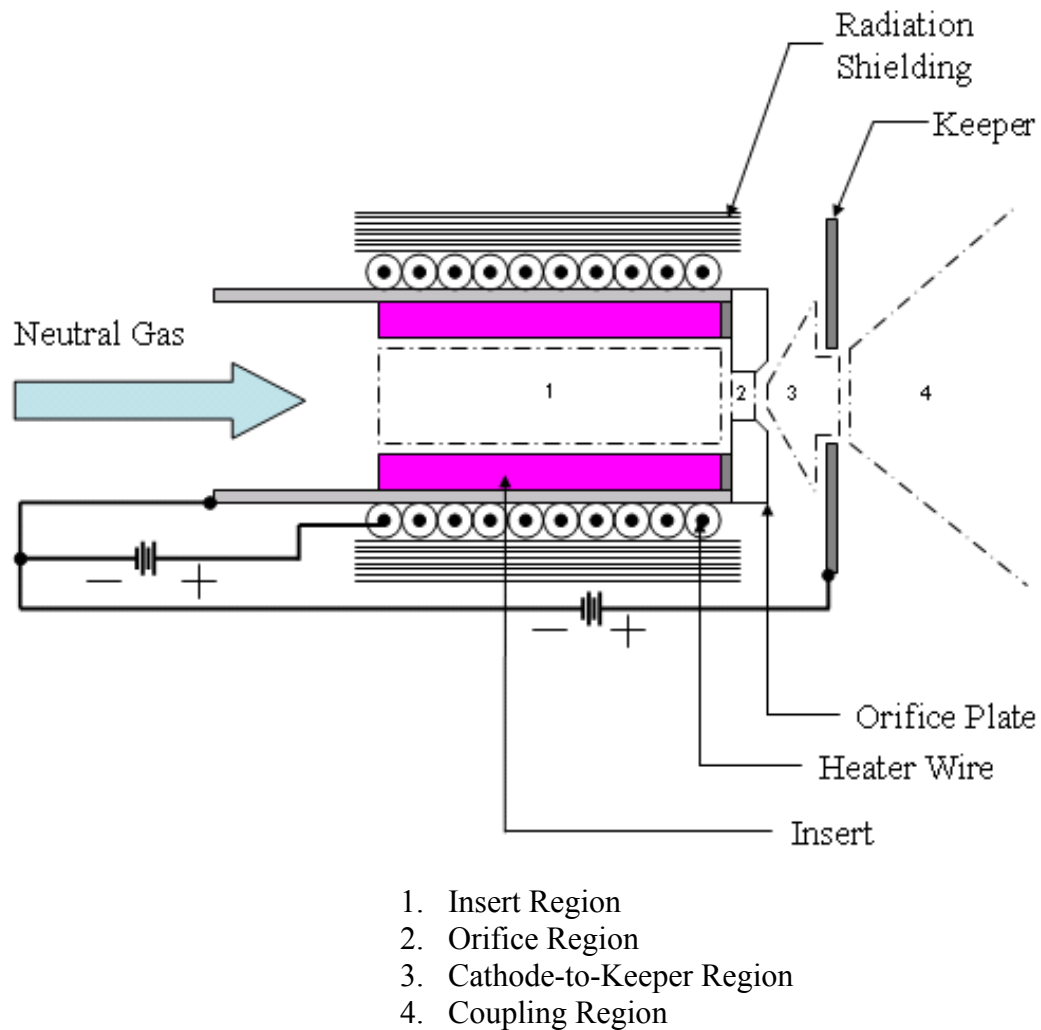
Figure 5. Orificed Hollow Cathode

Instead of using Ohmic heating of a wire or crystal emitter, the hollow cathode

has a tube containing a low work function material called an insert. A heater filament

wrapped around the tube containing the insert heats it to a temperature sufficient for

electron emission. A neutral gas flows into the cathode tube for the creation of plasma in

the insert region. The keeper, a positively biased electrode, extracts electrons from this

plasma through the orifice. The presence of this electric field and the electric field within

the insert region creates a phenomenon known as the Schottky effect. This enhances the

peak current and results in a much lower effective work function, described by equation

3. ε_0 is the permittivity of free space and E is the strength of the electric field.

$$\phi_{eff} = \phi - \sqrt{\frac{q \cdot |E|}{4\pi \cdot \varepsilon_0}}$$

(3)

Hollow Cathode Operation and Physics

Electron Emitter

Field enhanced emission is a major advantage of hollow cathodes over other

cathodes. Utilization of this phenomenon depends heavily on the insert work function

and its dimensions. Some emitters consist of porous tungsten impregnated with barium,

barium oxide, alumina, and calcium oxide mixtures. The impregnate lowers the surface

work function of the insert (~2.0-2.4 eV).[15] As the insert reaches it operating temperature

(~1100°C), the gaseous barium and barium oxide migrates to the surface of the emitter.

This mechanism ultimately lowers the surface work function. These emitters have

demonstrated operation for more than 28,000 hours.[1] However, because impregnated

cathodes rely upon a chemical reaction to maintain the low surface work function they

require very high purity propellant. Consequently, they are very sensitive to oxygen and

water vapor contamination.[2] When the impregnate supply is exhausted, the insert no

longer maintains a low work function. Thus, the lifetime is limited by the evaporation of

the impregnate gases.

Pure tungsten impregnated inserts have been the primary hollow cathode emitter

for a number of years in the United States. However, Polk et al. began investigations into

newer emitter technology involving a range of materials.[27] One material discussed in his

28

paper is a porous tungsten-iridium emitter with the same impregnates as above. The work function for this metal matrix ranges between 4.25 and 4.3 eV. Research suggests this matrix can reduce the loss of barium by a factor of six or more, and may be more resistant to oxygen and water vapor contamination than traditional inserts. In addition, the combination of the matrix and the impregnate produces a work function lower than pure tungsten impregnated emitters.[27] Alternate configurations of the porous tungsten emitter are also investigated. Polk et al. provides a detailed description of that work.[27]

Lanthanum hexaboride (LaB_6) is the next emitter material currently drawing attention in US electric propulsion research.[2,3,4,5,10,19] The potential benefits of LaB_6 emitters over others are their lower evaporation rates and higher resistance to oxygen and water vapor contamination.[2,15,28,29,30,31] LaB_6 is unique because it does not require an impregnate to demonstrate a low work function. Instead, it is either grown in single crystal form or press-sintered into polycrystalline form.

The LaB_6 work function depends on the surface composition of the crystal and its orientation.[15] For stoichiometric (LaB_6) or nearly stoichiometric ($LaB_{6.06}$ or similar) crystals, the work functions have been reported to range as low as 2.67 eV and as high as 2.87 eV resulting in operating temperatures of approximately 1650°C.[2] Studies like the one performed by Storms and Mueller used polycrystalline LaB_6. Polycrystalline emitter work functions are an average of each crystal's work function given its individual composition and orientation.[30] This may present some difficulty in duplicating the work function of polycrystalline inserts from cathode to cathode. Polycrystalline samples have been the primary inserts because single crystals are too difficult to machine into the hollow tube geometry used by most hollow cathodes.[26]

29

The final emitter discussed here is cerium hexaboride (CeB_6). It reportedly has a lower work function (2.5-2.62 eV for single crystal) and evaporation rate than LaB_6.[7,24,28,30,31] It is reported to demonstrate the same resistance to poisoning as the LaB_6 cathodes.[7,24,30] Although there is published data on single crystal CeB_6 emitters, no research has investigated the work function of polycrystalline CeB_6 for hollow cathodes. Its operating temperature is approximately 1500°C.[7,26,30]

Regardless of the emitter material, the plasma physics are largely the same. Figure 6 shows a schematic of the discharge process inside the insert region of an orificed hollow cathode.
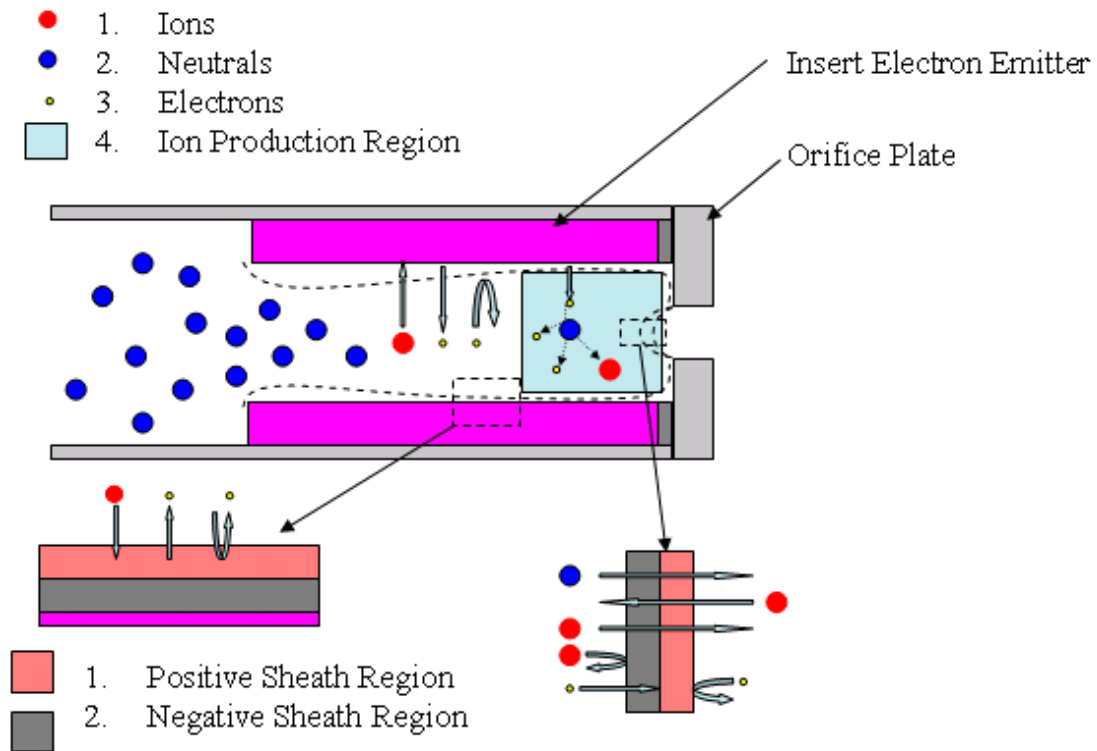
Figure 6. Hollow Cathode Insert Plasma Physics

The cathode insert emits electrons after it has reached a sufficient temperature, usually initiated by an external heater filament. Once this process begins, a negative charge

develops at the insert surface shown by the gray region of the schematic in Figure 6. Due to the high electron densities near the surface, a double sheath develops.[17,38] The electrons predominantly emit in two ways. First, electrons leave the insert as a result of photoelectric emission. Second, electrons accelerate through the developed sheath, known as field enhanced electron emission or the Schottky effect. Equations 1 and 3 describe the Schottky effect. The thickness of the sheath is on the order of a Debye length λ_D.

$$\lambda_D = \sqrt{\frac{\varepsilon_0 \cdot k \cdot T_e}{n_e \cdot q^2}}$$

(4)

The Debye length describes the area of influence each charged species has on another. Equation 4 shows the Debye length in dense plasmas is small. This results in a very strong electric field within the hollow cathode insert.

The insert region has high plasma densities, low electron temperatures, and low plasma potentials. As a result, ion sputter erosion plays a minimal role in the insert's life.[15] In addition, the cathode has effectively no space charge limit due to the high-density levels in the insert plasma. This allows hollow cathodes to produce very high current levels with low voltages and little power compared to the total power of the system. The hollow cathode design also allows it to operate in a self-heating mode. This mode requires no power to the heater and can be divided into three categories.[15] Ohmic heating of the orifice plate drives the first self-heating mode. This mode is characterized by high internal cathode pressures in the insert and orifice. Highly resistive plasma forms within the orifice region. By convection, the orifice plasma transfers heat to the orifice plate then conducts and radiates it to the insert, raising the insert's temperature. Once

31

this process begins, it provides sufficient heat for the cathode to maintain electron emission without operating an external heater. The insert electron temperatures for cathodes using this heating mode are typically higher than the other two and increases with internal pressure.[15] The second self-heating mode results from ions striking the insert surface as they fall through the sheath potential within the insert. The final mode is electron heating that results from Maxwellian electrons having sufficient energy to exceed the sheath potential of the cathode and strike the insert surface.[15] The sheath potential in the insert of all hollow cathodes is relatively low and decreases with internal pressure.

In addition to the cathode's self-heating modes, the insert's length is also an important characteristic. With high current designs, the insert is longer because the plasma attachment point is further upstream.[15] With low current designs, the insert is naturally shorter, which acts to reduce the thermal mass and ultimately power consumption of the cathode.

Orifice Region

The next region, downstream of the insert, is the orifice of the hollow cathode shown in Figure 7. Small orifice diameters with deep lengths (large aspect ratios) similar to the orifice geometry in part A of Figure 7 allow the first self-heating mode to dominate.[15,32] The long narrow channel of the orifice restricts the plasma and increases the cathode internal pressure. The plasma within this region forms an axial electric field and conducts the current from the insert to the coupling plasma. This field penetrates further upstream into the insert with larger orifice diameters and smaller aspect ratios, as depicted in the figure below.
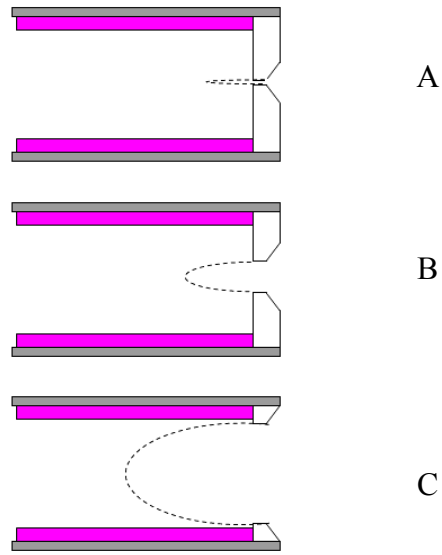
Figure 7. Hollow Cathode Orifice Geometries[15]

A) Large Aspect Ratio B) Medium Aspect Ratio C) Small Aspect Ratio

These parameters also dictate what potential the keeper electrode must start at to initiate the discharge of the cathode. The plasma only penetrates a few millimeters downstream of type A orifice designs. Their long narrow geometries limit the peak current capability of the cathode.[15]

Orifice geometries with medium aspect ratios allow the cathode to run at slightly lower pressures. Cathodes with this intermediate orifice operate by ion heating, electron heating, or a combination of both. The cathode design described in this study falls into this category and is similar to the part B geometry in Figure 7.

As the depth of the orifice increases, more ionization and power consumption occurs. With larger orifice diameters, the peak current capability increases. These require higher flow rates to maintain the spot mode emission described below. Part C of Figure 7, usually called an orifice free cathode, primarily self-heats by ion bombardment.

Cathode-to-Keeper Region

The next section of the hollow cathode plasma is the cathode-to-keeper region. The plasma densities within this region are lower, therefore the Debye lengths of each constituent is larger. In quasi-neutral plasmas, electrons move toward the positively biased electrode, the keeper. This electrode pulls the electrons out of the insert region of the cathode. Once this process begins, the cathode is "lit" and electrons stream out of the cathode. This cathode operates in two plasma region modes, spot and plume. The spot mode is defined by lower discharge voltages (<40 V) and electron temperatures (<4 eV), higher flow rates, and small voltage fluctuations (<1 V). A small luminous spot is present during this mode, expanding monotonically downstream of the cathode. Large, high frequency voltage oscillations (>5 V, >100 kHz), lower flow rates, higher discharge voltages (>40 V) and electron temperatures characterize the other mode of operation, plume mode. Plume mode occurs during higher discharge currents and lower flow rates. During this mode, the spot disappears and a large diffuse plume is present. The plume mode has the potential to accelerate the erosion of the cathode due to the high-energy ion bombardment generated from dense regions of plasma near the hollow cathode.[33,34] The plume mode also acts to increase the impedance of the plasma as observed by Mikellides et. al.[43]

Coupling Plasma Region

Following the cathode-to-keeper plasma region is the coupling plasma-region. The behavior of this plasma region is very dependent on operating conditions and is similar to the cathode to keeper region, exhibiting spot and plume mode as well. Generally, the plasma potential and electron temperature profiles follow a valley shaped

contour without an applied magnetic field and trench-like contours with an applied

magnetic field.[35,36] For some low flow, elevated current conditions, Goebel observed the

formation of a localized plasma density structure he called plasma balls, shown in Figure

8.[15] Martin and Williams also observed the formation of a similar structure they called a

"plasmoid" for similar operating conditions of the coupling region of the hollow cathode.

See Figure 9.
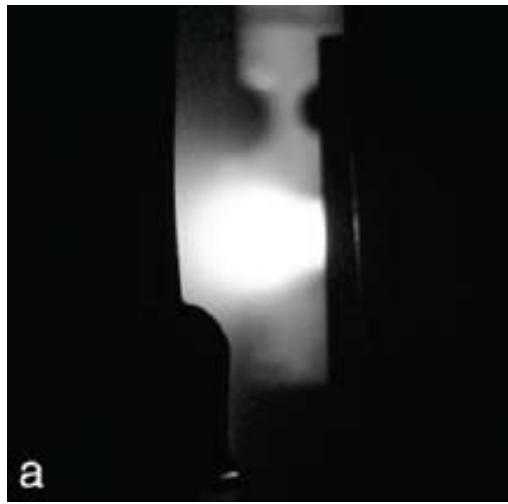
Figure 8. Plasma Ball[15]
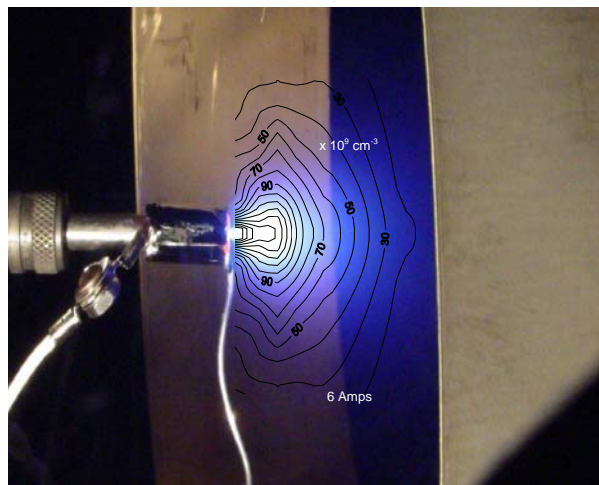
Figure 9. Plasmoid Density Contour[35]

The plasmoid structures produced higher electron temperatures and appeared further away from the cathode under higher flow rates and discharge currents, somewhat indicative of the plume mode. Goebel also observed plasma balls appearing further downstream under higher flow conditions. The plasma was also observed to adjust itself to maintain the current being drawn from it under operation without an applied magnetic field. The behavior of the coupling plasma also differs as the anode geometry changes. Martin and Williams did an extensive study of a variety of anode configurations to show the different characteristics of the cathode plume. The primary concerns with the near keeper regions of the cathode coupling plasma are to determine what causes the erosion of the keeper electrode. The plasma balls and plasmoids may provide regions for high-energy ion creation and accelerate the sputter erosion of the keeper and cathode. This is especially true if the plasmoids form during high amplitude and frequency oscillations. However, these plasma ball and plasmoid structures rarely occur. Most expansions of the cathode coupling region are monotonic.

Boride Cathodes

As discussed above, direct emission cathodes use boride-based materials. The initial use of boride cathodes dates back to the late 1940's.[8] James Lafferty addressed the issue of a need for higher emission current requirements for cathode ray tubes. In his study, he concluded rare-earth borides are better emitters than alkaline earth or thorium borides. He observed LaB_6 was the best emitter of the samples he tested. This emitter technology went largely untouched in the US for electric propulsion applications until the late 1970's. However, it was widely used for electron beam applications in the US and Soviet Union.[2,31] Goebel, et al., first demonstrated use of LaB_6 as an emitter for hollow

36

cathodes in US electric propulsion applications in 1979.[4] Later, Goebel et al.

demonstrated the use of this device for a high current plasma source in 1985.[9] The US

did not seriously consider LaB_6 as an emitter for hollow cathodes used in Hall and ion

thrusters until 2005.[2] The most recent studies revealed the true robust nature of the

emitter and its capability as a high current substitute over other insert materials. Until

now, most LaB_6 crystals were arranged in a manner similar to that shown in Figure 10.
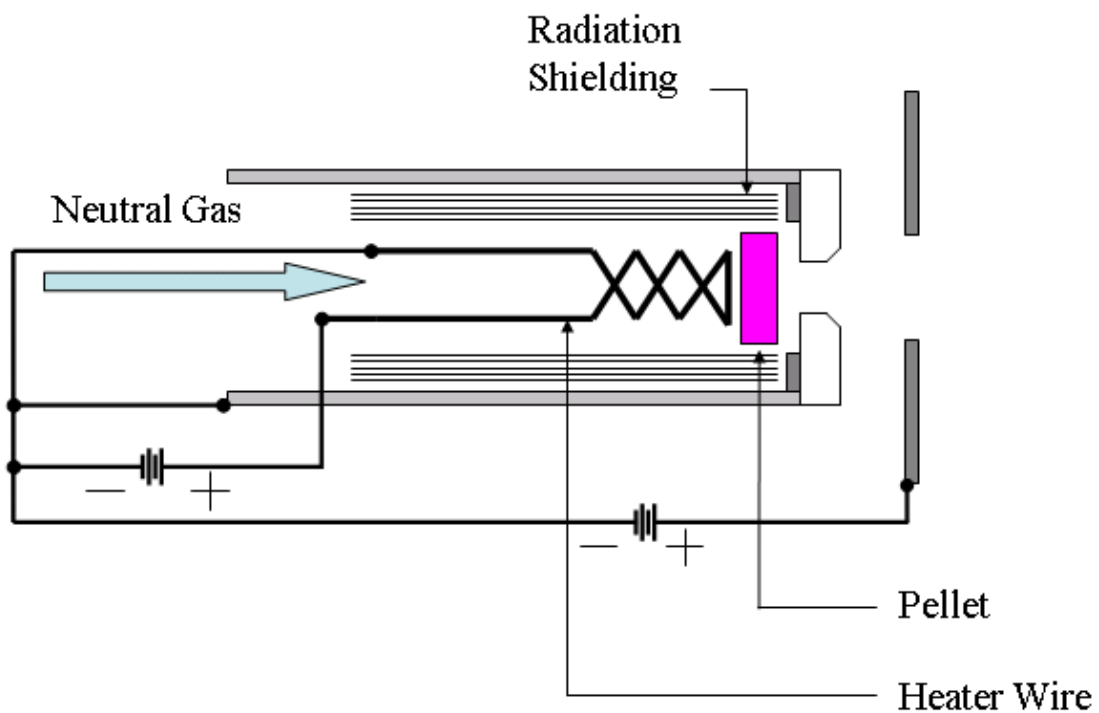
Figure 10. Early Lanthanum Hexaboride Hollow Cathode

As shown in the figure, the emitter is in the form of a solid pellet. Observed in some

research, this cathode design required continuous heater operation to maintain the proper

temperature for the crystal to produce sufficient electrons.[17] Goebel found a hollow tube

insert with an internally mounted heater could self-sustain operation without power to the

heater. However, the cathode required discharge currents above 100 A.[4]

37

The most recent design is similar to conventional hollow cathodes, and is capable of self-sustaining the plasma at currents as low as 10 A.[2] The crystals for all of these studies are polycrystalline, formed by press sintering the compound to approximately 70-90% theoretical density. The work function from polycrystalline samples is an average of each crystal's work function.[2] This may also provide a variation in work function, changing from insert to insert, resulting in a wide range of values as reported in the literature.[2] However, a more likely candidate is the variation in density between inserts. An alternative to LaB_6, reducing the power requirements for cathodes, would be beneficial for low power applications (100-300 W). One possible candidate for this is cerium hexaboride (CeB_6).

No work has been published investigating the use of CeB_6 as a hollow cathode electron emitter. However, Wirz completed the first study to use this crystal as an emitter in a direct emission configuration for miniature ion thrusters.[19] CeB_6 has been used in electron beam applications just as LaB_6, primarily because the work functions and evaporation rates are lower than LaB_6.[7,8,28,31] Work functions for CeB_6 range from 2.3-2.5 eV.[37] Like LaB_6, they also depend on the chemical composition of the surface of the crystal. Nevertheless, CeB_6 has demonstrated superior emission current densities at lower temperatures than LaB_6.[7]

All of the former studies for CeB_6 used single crystal borides. No press-sintered studies were presented for CeB_6 because the single crystal form is known to have a consistent and repeatable work function. It not only depends on the composition of the material, but the crystal plane orientation as well. Some planes have lower work functions than others do. The difficulty arises when tube geometries used in hollow

cathodes are required. The single crystal emitter cannot be machined into a hallow tube because of its brittle nature, a problem common to CeB_6 and LaB_6. As a result, easier to machine polycrystalline inserts for LaB_6 have been used for hollow cathodes in the past. As a result, this experiment used polycrystalline material for the CeB_6 insert as well.

Experimental Considerations

Important parameters to understand the performance of hollow cathodes include propellant flow rates, insert and heater operating temperature, insert material evaporation rates, and poisoning effects. The voltages, currents, and waveforms of each cathode component are also important. The electron temperature, plasma potential, and plasma densities are three other parameters studied as well.

The first experimental consideration is propellant flow rates. Most research has employed precision mass flow controllers from various vendors, able to control the flow over a wide range. Xenon has been the primary propellant researched.

To determine the desired operating temperature, some studies have simply spot welded thermocouples to the desired locations of the hollow cathode.[17,27] Type K thermocouples have been used as well as type R and C. The assumption was the orifice plate temperature was approximately equal to the insert temperature. This was possible because the orifice plate was electron beam welded to the cathode tube and it directly interfaced with the insert. Floating thermocouple readouts to prevent the thermocouples from acting as a short to ground is also common practice. Others used thermocouples as a calibration point but then used an optical pyrometer to measure the insert operating temperature.[27,38] An additional method employed by Domonkos was the use of an infrared camera, calibrated by spot-welded type R thermocouples. The advantage of

39

using this camera over other methods was the ability to see the temperature distribution along the length of the cathode tube. This allowed one to quantify the amount of heat conducted to the base of the cathode. Another reason for measuring the temperature is to ensure the insert operates at the ideal temperature to prevent contamination, reduce evaporation, and maximize insert life.

To determine the evaporation rate of a LaB_6 insert, Lafferty used a configuration allowing him to heat the material to its operating temperature under vacuum and open a shutter for the material to pass through to a sheet of cooled tungsten. A molybdenum anode masked the cold tungsten sheet used for LaB_6 condensation. Knowing his exposure area, temperature, duration, amount of material, and distance to the collector, he calculated the evaporation rate of the material.[8] Another study simply measured the diameter of the material in combination with some other calculations after operation to determine the amount of material lost due to evaporation and subsequent sputtering.[24]

In addition to evaporation, another life limiter for hollow cathodes is contamination. To determine how much of a contaminant is present, auger electron spectroscopy or energy dispersive x-ray analysis is often employed.[19] This method detects the constituents of the surface of a material, a reliable procedure for determining if a cathode insert has been contaminated.

The next experimental consideration is the potential and current of the keeper, anode, and heater. Previous studies employed the use of an oscilloscope to monitor the waveform behavior of the anode and keeper voltages and multi-meters for the raw anode, keeper, and heater voltage and current.[17,35] Spot or plume mode operation can be determined from the oscilloscope. Another method used Langmuir probe data to

40

determine the transition from spot to plume mode.[32, 34,35,39] When the cathode operates in plume mode, there is a significant increase in electron temperature. A Langmuir probe is well suited to measure this increase and may be a more sensitive method than the waveform monitoring.

The Langmuir probe also measures plasma potential, electron temperature, and plasma densities. Plasma potential allows one to calculate the energy of the ions hitting the cathode and deduce erosion rates for a given operating point. Electron temperature indicates whether the cathode is in spot or plume mode operation. Plasma densities give information regarding mechanisms for wear of the cathode. Regions of high-density ions are more likely to accelerate wear of the cathode during plume mode operation.

III. Methodology

Vacuum Facility

Cryo-Pumps

Helium Refrigerators
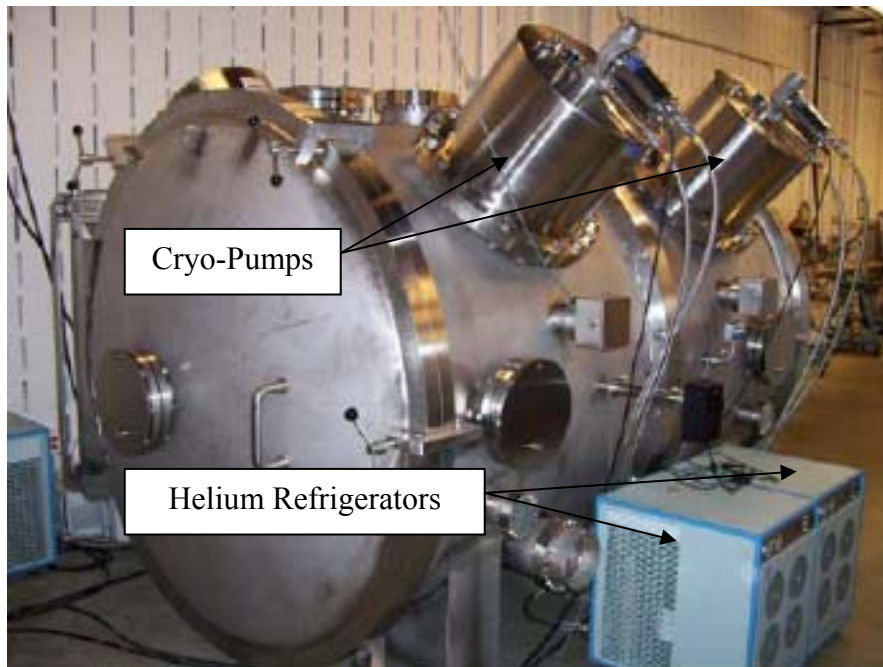
Figure 11. SPASS Facility

All testing was performed in the AFIT Space Propulsion Analysis and Simulation System (SPASS) vacuum chamber, Figure 11. In September of 2006, the author assisted Maj. Richard Branam in the procurement of this facility. Due to the nature of the experiments, every effort was made to ensure the facility met the thruster pumping requirements for testing and stayed within the budget, however one major constraint made this a challenge.

There are several pumps used in vacuum chambers, one of which is a cryogenic pump. Others include turbo molecular pumps, ion pumps, and mechanical roughing pumps. Most vacuum chambers use a mechanical roughing pump to draw the pressure of the chamber down to around 100 mTorr. This is standard practice and implemented for the SPASS facility using a Leybold Trivac D65B rotary vane mechanical pump. Then there is a secondary pump used to bring the chamber down to even lower pressures. Turbo pumps use turbine blades to trap the gas molecules and a roughing pump draws them from the turbo pump. Turbo pumps are only capable of one or two thousand liters per second of nitrogen and do not have the pumping speed required for many electric thrusters. The ideal pump used by most space propulsion facilities is the cryogenic pump. This pump acts as a cold trap for the gases as they condense on the surface of the cooled pump, lowering the pressure.

Many facilities achieve these low temperatures by using liquid nitrogen for the first stage of the two stage cryogenic pumps. Some pumps are capable of speeds of up to 40,000 l/s on xenon gas. The building did not have a supply of liquid nitrogen; therefore, the chamber was constrained to using an alternative refrigerant. The challenge came in finding a chamber that could maintain a high pumping speed and not require liquid

nitrogen. The solution was from another cooling method employed by cryogenic pumps, helium refrigeration. The blue boxes in Figure 11 are of the helium compressors used in the SPASS chamber. These allowed the cryo-pump to drop to temperatures as low as 15-20 K. However, as the pumps grow in diameter, the helium refrigerators reach a limit. After some investigation, the largest helium refrigerated pumps available were from CVI Torrmaster at 0.5 m diameter. One of these pumps is capable of 4,000 l/s for xenon gas. Four of these provided sufficient pumping and allowed experiments to run at flow rates as high as 10 sccm and maintained pressures around $3*10^{-5}$ Torr. After posting these specifications, the chamber was built and delivered by PHPK Technologies in June of 2007.

Hollow Cathode Assembly

Two hollow cathodes based on the design from Goebel were fabricated.[2] The author completed all assembly and testing described herein. One was for testing LaB_6 and the other for CeB_6 inserts. With the exception of the insert material, both cathodes were identical. Figure 12 shows an engineering drawing of the hollow cathode design.
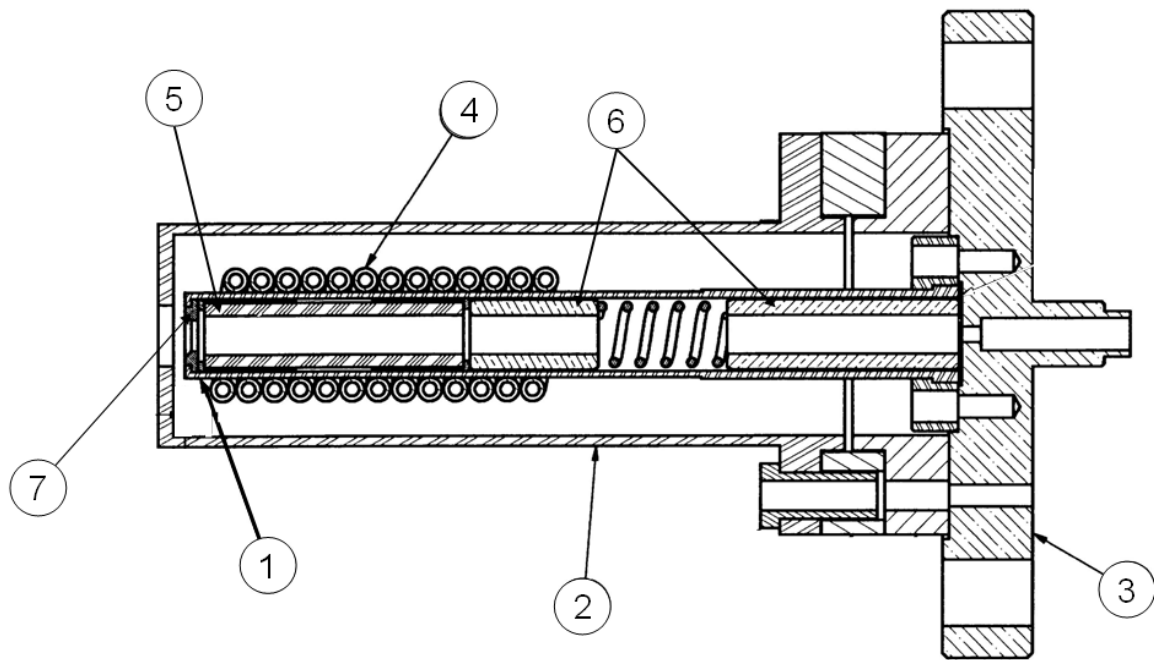
1. Hollow Cathode
2. Enclosed Keeper
3. Mounting Flange
4. Heater Filament
5. Insert
6. Graphite Support Tubes
7. Orifice Plate

Figure 12. Hollow Cathode Assembly

Every part of a hollow cathode is designed around the electron emitter. The first

consideration for many designs is how to contain the emitter. Simply due to the nature of

the insert's geometry, a hollow tube is fitting. The diameter of the tube is obviously a

function of the diameter of the insert. The insert's diameter must be greater than that of

the mean free path of an electron.[38] Otherwise, the electrons would collide with the walls

of the insert and plasma would be difficult to generate. The peak current capability is

also a function of the insert's diameter. Larger inserts have more surface area, making

more current available when needed. The length of the insert is a function of the plasma

attachment length and the peak current requirement. Longer inserts increase the surface

44

area and total current capability of the cathode. If the insert is too short, then there is little current drawn from it and the plasma will not be able to attach where needed. A picture of the CeB_6 and LaB_6 inserts are shown in Figure 13 and Figure 14 respectively. Each is 6.4 mm outside diameter, 3.8 mm inside diameter, and 25.4 mm long. The theoretical density of the CeB_6 insert was approximately 70% and the LaB_6 80-90%.

Figure 13. Cerium Hexaboride Insert

Figure 14. Lanthanum Hexaboride Insert

Typical materials used for hollow cathode tubes include molybdenum-rhenium alloys due to their resistance to oxygen adsorption, tantalum, titanium, molybdenum, and sometimes graphite. For this particular design, the hollow cathode was constructed out of molybdenum, shown in Figure 15.

Figure 15. Molybdenum Hollow Cathode Tube

However, the reader must be aware that molybdenum is not as resistant to oxygen

adsorption like a molybdenum rhenium alloy. This is an important consideration for

impregnated cathodes, but is not an issue with the boride based ones. For the case of

boride cathodes, one has to be careful when selecting materials. Most refractory metals

including molybdenum allow the boron to diffuse into its lattice and starve the emitter of

its required chemistry for electron emission.[8] To reduce this effect, graphite (99.5%pure)

is commonly used when interfacing with boride emitters. However, a previous version of

this design had arcing problems between the keeper electrode and the orifice. In this

case, the orifice was graphite, which has a low sustaining current and was damaged by

the arcing. Originally, a thoriated tungsten orifice plate with a 3mm orifice was included.

This orifice plate optimized for high current designs was not suited for the low current

work presented here. As a result, the author had tantalum orifice plates cut by electron

discharge machining from a 0.25 mm sheet, shown in Figure 16. Multiple orifice plates

allowed the depth of the orifice to vary by stacking the plates on top of each other. The

orifice diameter for these plates is 1 mm. This investigation examined two aspect ratios (L/D) for each cathode, 0.5 and 0.25.

Figure 16. Tantalum Orifice Plates

Figure 17. Graphite Protection Sleeves

Figure 17 displays the graphite sleeves used to protect the emitter from the molybdenum tube. Figure 18 shows these tubes when slipped over the insert.

Figure 18. Graphite Protection Sleeves with Insert

Other materials such as tantalum carbide and rhenium also resist boron diffusion.

Another consideration for the material used in the cathode tube is its thermal

conductivity. For high power applications, thermally insulating the insert is not of great

concern because the power used by the cathode is a small percent of the total power of

the thruster. However, for low power applications, improving the thermal efficiency of

the design can provide advantages. The heat loss rate along the length of the cathode

tube is higher when using materials with higher thermal conductivities. Since this design

was intended for medium power applications, the thermal efficiency was not a big

concern and is not optimal for low power applications. However, it provides a proof of

concept platform. In response to this, improved design suggestions presented later in this

paper take advantage of the findings of Domonkos for low power applications.[17]
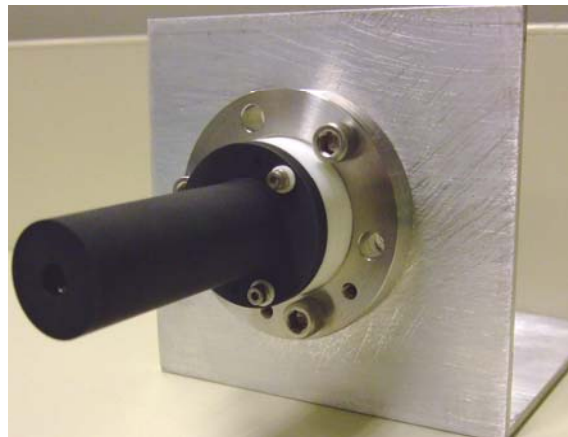
Figure 19. Cathode with Graphite Keeper

The keeper electrode was fabricated out of a single piece of Poco graphite, grade

AXF-5Q, see Figure 19. This grade has a similar coefficient of thermal expansion to that

of LaB_6.[2] It also has a higher purity than most other graphite available. While the

coefficient of thermal expansion is not important for the keeper electrode, other parts

such as the support tubes and sleeves require it. Graphite also has a lower sputter yield

than most materials, thus it provides a robust keeper capable of lifetimes greater than

other cathode keeper designs. In addition to heat shielding, the enclosed keeper electrode

also helped to reduce radiation losses. The keeper orifice was 6 mm and spaced 1 mm

from the cathode orifice. While the large orifice was optimized for higher current

applications, it may have provided some advantage. Goebel observed larger keeper

orifice diameters like the one used here reduced the plume mode transition point for

certain operating conditions.[2]

The only electrical current conducted to the keeper electrode was that emitted

from the orifice of the cathode. Ceramic insulators placed between the keeper electrode

and mounting plate ensured this. Small shoulder insulators between mounting screws

and the electrode provided additional isolation from cathode potential surfaces such as

the mounting plate. In addition to Figure 19, Figure 20 and Figure 21 show these

insulators as well.

Figure 20. Ceramic Insulators between Keeper and Cathode Base

Figure 21. Shoulder Insulators between Mounting Screws and Keeper Electrode

49

Figure 22. Tantalum Sheathed Heater Wire

The heater filament was a tantalum sheathed alumina insulated wire, Figure 22. According to vendor data, these filaments operate as high as 1800°C.[2] This provided a higher operating temperature than the typical magnesium oxide insulated wires. Wrapping the filament around the cathode tube 12 times ensured uniform heat distribution along the length of the insert. Placed upstream from the orifice, this filament position reduced the heat conduction to and from the heater and the orifice plate. Wrapping 0.127 mm thick Tantalum foil around the heater 12 times provided the required shielding for self-heating operation. The author loosely wrapped the shield around the heater filament to increase the conduction length and contact resistance. Allowing the foil to relax after mounting created a small gap between each layer. Other than loosely wrapping and relaxing the foil after mounting, the author did not take any other measures to improve the heat shield. An additional 0.254 mm thick piece of tantalum foil secured the thinner shielding and kept it from un-winding. Figure 23 shows the cathode with the keeper electrode removed and heat shield present.

Figure 23. Cathode with Keeper Removed

Test Assembly

The hollow cathode previously described was mounted to the flange shown in Figure 24. An aluminum plate secured to the desired test platform acted as the mounting surface for the flange. A compression fitting threaded into the rear of the mounting flange provided the propellant line connection. For these experiments, the author aligned the keeper exit plane with the anode entrance plane. The 304L stainless steel anode had a 5 cm diameter and was 13 cm long. Figure 24 shows the cathode assembly in its entirety, just before testing.
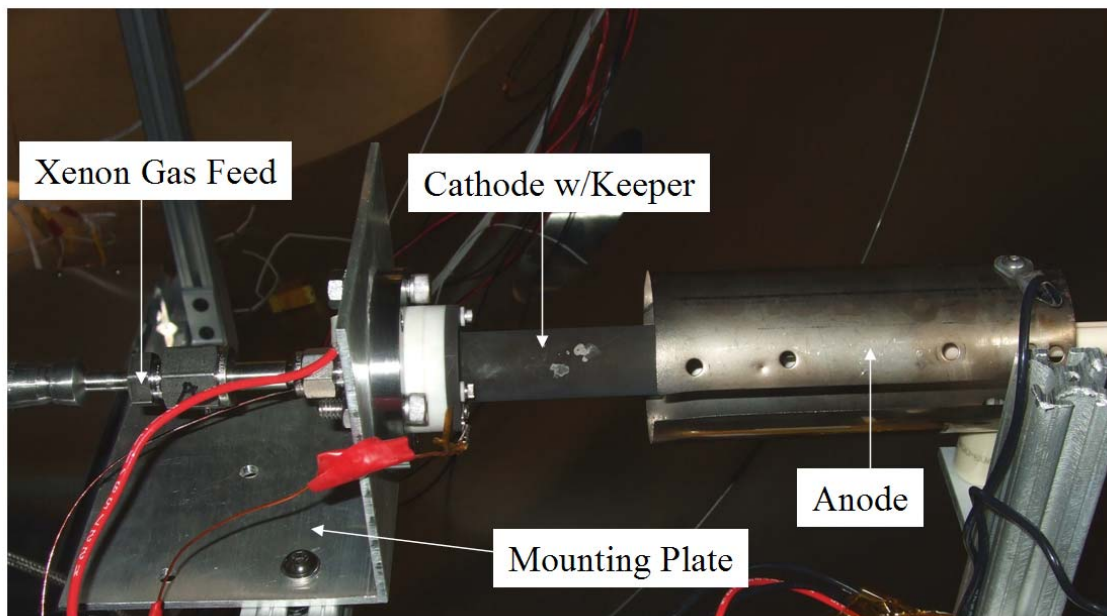
Figure 24. Hollow Cathode Base Test Assembly

All wiring used for the cathode assembly was low out gassing vacuum compatible materials including Kapton® and Teflon® insulated wires and nickel-plated high-temperature electrical connections.

Figure 25 is the electrical schematic for the assembly displayed in Figure 24. This experiment emulated the basic electrical configuration of Hall and ion thrusters. However, there is no magnetic field present and the geometry of the anode is different from ion and Hall thruster anodes. However, it still provides basic electron transport properties of the plasma critical to cathode evaluation and thruster design.
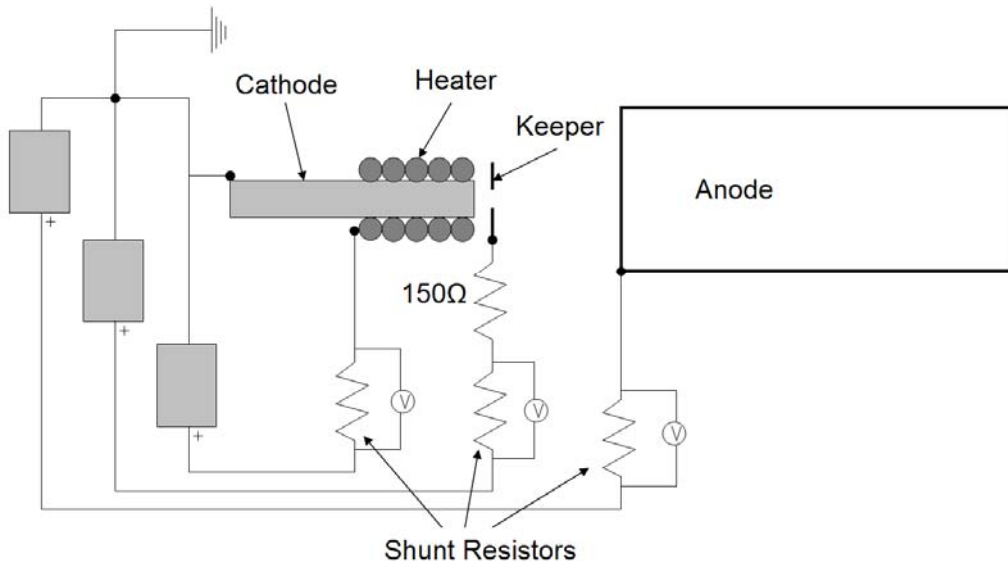
Figure 25. Cathode Assembly Electrical Schematic

A Hewlett-Packard 6038A DC power supply controlled the anode. It was capable of 0-60 V and 0-10 A output. The maximum power level of this supply was 250 W, well suited for the low power range investigated here. The Hewlett-Packard 6033A heater power supply was also a 250 W DC power supply, but its output ranges were 0-20 V and 0-30 A. Finally, the keeper power supply was a Matsusada REk650-2.5 DC power supply. Capable of 650 V and 2.5 A with 1625 W of total output power. All negative leads of the power supplies were grounded. A low-pass filter not included in the schematic attenuated voltage oscillation frequencies above 10MHz.

The next portion of the base test assembly is the propellant feed system. The

propellant used here was 99.9995% pure xenon, also called "grade 5". The flow

requirements of hollow cathodes are very low when compared to other rocket

technologies, about one mg/s or less. A precision MKS mass flow controller calibrated

for 0-10 sccm of xenon controlled the cathode flow. Figure 26 is the schematic for this

propellant feed and control system.
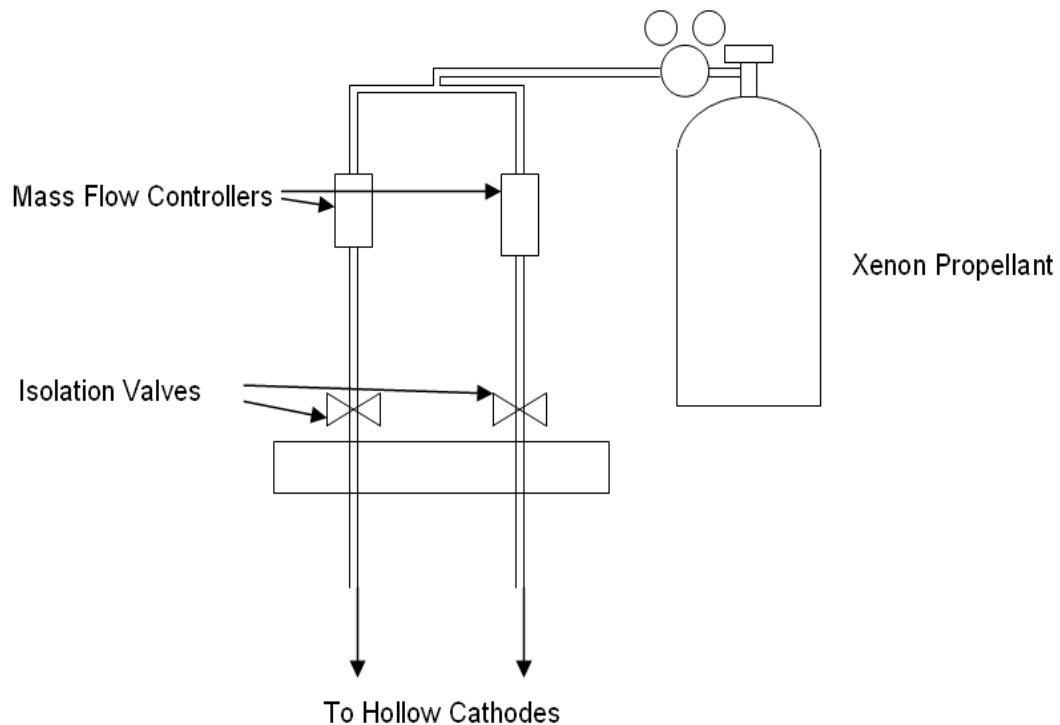
Figure 26. Xenon Propellant Feed Schematic

Data Acquisition and Measurement Equipment

Several measurable parameters during cathode operation provided information

about its stand-alone and integrated thruster performance. The first two fundamental

quantities measured here were current and voltage. Connected in series with the anode,

heater, and keeper, calibrated shunt resistors provided an accurate way to measure the current in a circuit. A National Instruments® SCXI- 1321 4-channel readout measured and logged the voltage across each resistor and a LabVIEW® program used Ohm's Law to calculate the current through each one. Figure 25 shows the resistors and their locations within the overall circuit. A Tektronix® 420 A, 200 MHz digitizing oscilloscope monitored the anode voltage and keeper waveforms during cathode operation. The voltages reported were slightly higher than the actual component voltage. There was a potential drop across the eight feet of wires to the oscilloscope. This difference was only one or two volts.

The National Instruments readout had 8-bit resolution and a sampling rate of 50 kHz. With this low sampling rate, any oscillations above 25 kHz were aliased or attenuated. As a result, the readout could not collect reliable data about plume mode oscillations. Rather, the readouts provided average currents and qualitative information about the behavior of the cathode and stability information. The author neglected the voltage drop across the wires from the shunt resistors to the readout because signal current was low and the length was negligible.

The oscilloscope had a 400 mV resolution and a sampling rate of 200 MHz. The oscilloscope records 500 data points for each sample time. Signal resolution drops with larger sample times and may cause small jumps in voltage. However, this will not introduce any considerable error because the difference between spot and plume mode voltage behavior is significant. Additionally, plume mode voltage oscillations are much higher than 400 mV, typically at 5 volts or more.

Langmuir Probe

In addition to voltage and current, the cathode plasma properties provide information on how it affects the life and efficiency of the cathode and ultimately its respective space application. Many measurement instruments are available for collecting plasma data, one of which is a single Langmuir probe. Other types of probes include a Faraday probe, double Langmuir probe, emissive probe, ExB probe, and retarding potential analyzer. Hutchinson provides a comprehensive text for most of these devices.[40] The single Langmuir probe was used in this research due to availability. The probe was built by Scientific Systems and contains all the control and acquisition electronics in one package. The data analysis component was included in the supplied Smartsoft® software. Figure 27 is an image of the Langmuir probe during hollow cathode operation.
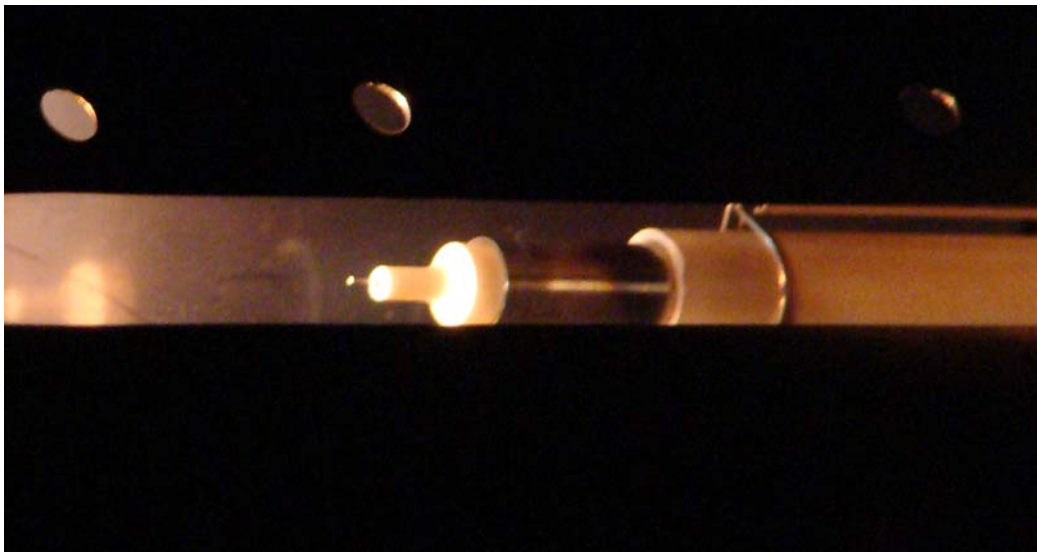
Figure 27. Langmuir probe

The concept behind the operation of this measurement device is relatively simple. In this case, the probe was a small tungsten wire, 0.19 mm outside diameter with

2.41 mm exposed length. The whole coupling plasma is not isotropic but the small

region exposed to the probe's tip is assumed to be. There are some density gradients over

the length of the probe. The isotropic approximation will introduce some uncertainty not

quantified in the data presented here. A Macor® ceramic insulator contained the probe

tip and a shielded co-axial cable carried the signal to the computer. All single Langmuir

Probes collect current by applying a voltage to the probe wire. This voltage typically

starts at a negative value (~-10 V) and linearly increases to a positive value (~40 V). The

plasma response to this voltage sweep develops the distinct curve in Figure 28.
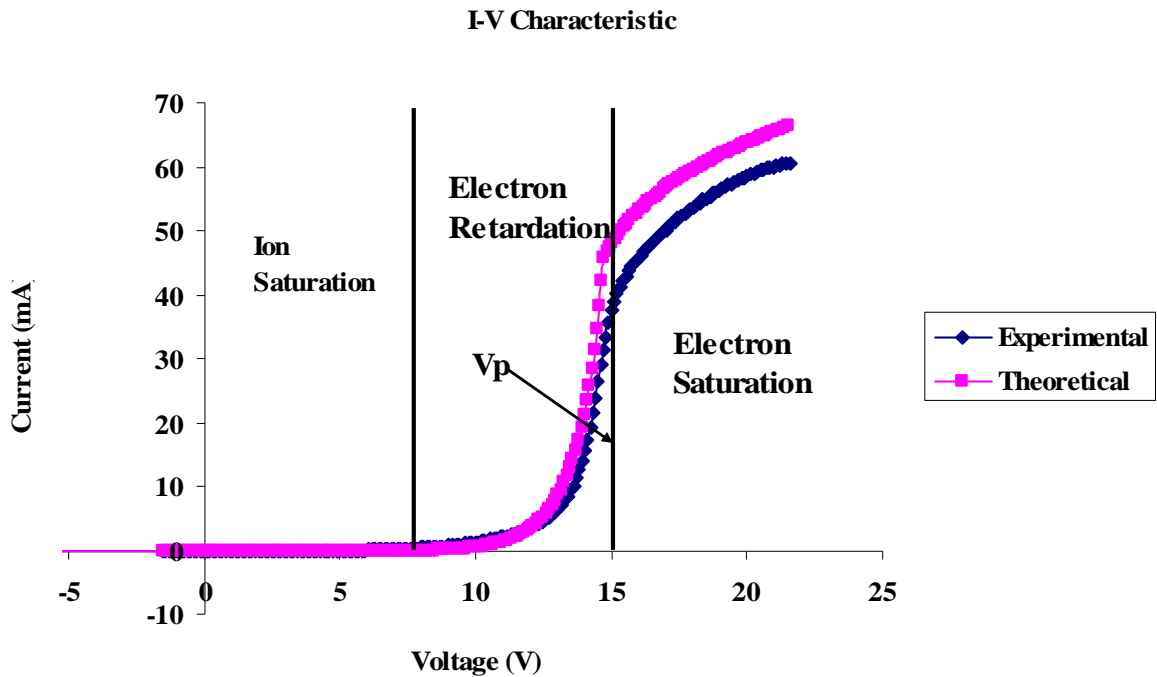
Figure 28. I-V Curve for 10 A Anode Current and 8 sccm Xenon

The region of the curve called the ion saturation region is when the probe is at a

large negative potential relative to the voltage of the plasma. Here the probe is at a

sufficient negative voltage to repel all of the electrons in the plasma and saturates itself

with ion current. This region of the curve allows the calculation of ion current, number density, and flux. Additionally, the plasma floating potential is calculated near the end of this region when the ion and electron flux is equal. Smartsoft® software employs the theory developed by Laframboise to calculate ion number density.[41] This theory accounts for the sheath that develops around the probe, described by equation 5.

$$d_s \cong \lambda_d \sqrt{\left| \frac{V - V_P}{kT_e} \right|} \qquad (5)$$

V is the applied potential to the probe, d_s is the sheath width, and λ_D is the Debye length. Laframboise developed a family of curves, showing the relationship between ion current, a range of Debye lengths, and probe radii.[41] Smartsoft® uses an algorithm that condenses this family of curves into a series of equations to calculate ion current, and ion number density. The sheath thickness expands with probe potential and lower plasma density effectively increasing the collection "area". Without considering the sheath expansion, the current collected would be different than the true current. For this research, the Langmuir probe diameter was much larger than the Debye length of the plasma, resulting in a smaller sheath. With sufficiently large probe diameter, the sheath around the probe is thin and the ion current saturates well.[42] More information on this specific algorithm is included in the SmartProbe® user manual.

The next portion of the I-V curve called the electron retardation region is when the electrons with enough energy to overcome the potential barrier of the probe are collected. Assuming thermal equilibrium for the electron distribution, the electron current grows exponentially relative to the probe potential. Smartsoft® uses this portion of the curve to calculate the electron temperature. See equation 6.

$$\frac{I(V_p)}{\int_{V_f}^{V_p} I(V)dv} = \frac{1}{kT_e} \qquad (6)$$

The final section of the curve is the electron saturation region. This region is just after the "knee" in Figure 28. Here the probe is at a higher potential than the plasma and becomes saturated with electrons. Plasma potential is calculated from the slope of this region and the electron retardation region. Here Smartsoft® employs the method of intersecting slopes. A line is drawn along the slope of the 2nd and 3rd regions of the curve and the point of intersection is the plasma potential. At the knee of the curve, the probe potential equals the plasma potential. Any current draw in this region results from slow thermal electrons and ions. With the plasma potential determined, SmartSoft® uses equation 7 to calculate the electron number density.

$$n_e = \frac{I(V_p)}{A_p} \left(\frac{2\pi m_e}{e^2 kT_e} \right)^{1/2} \qquad (7)$$

The I-V curve described above is for one voltage sweep. Typically, spatial measurements and averaged stationary measurements are desirable. The control electronics applied a saw-tooth voltage waveform to the probe and collected multiple I-V curves. The probe generated 200 data points for each curve. For each data point, five samples were taken and averaged before making up the respective I-V curve, like that in Figure 28. Then the two curves recorded and averaged resulted in one final I-V curve for one location in the coupling plasma region. The sampling rate of the probe was 200 kHz. This equated to a collection time per data point of 0.025 ms. The entire curve was collected in 5 ms. The details described above allowed electron temperature, plasma potential, floating potential, and number densities to be calculated. As previously

58

mentioned, these help describe the nature of the coupling plasma and its relation to life, performance, and efficiencies with the cathode integrated into a thruster.

For spatial Langmuir probe data, an Aerotech® x-y translation stage positioned the cathode relative to the probe. Figure 29 shows the locations of these data points along the centerline of the cathode. This stage used encoders to measure position and regulated the stage velocities to 1 mm/s. Closed-loop feedback integrated with Aerotech® software provided positional data.
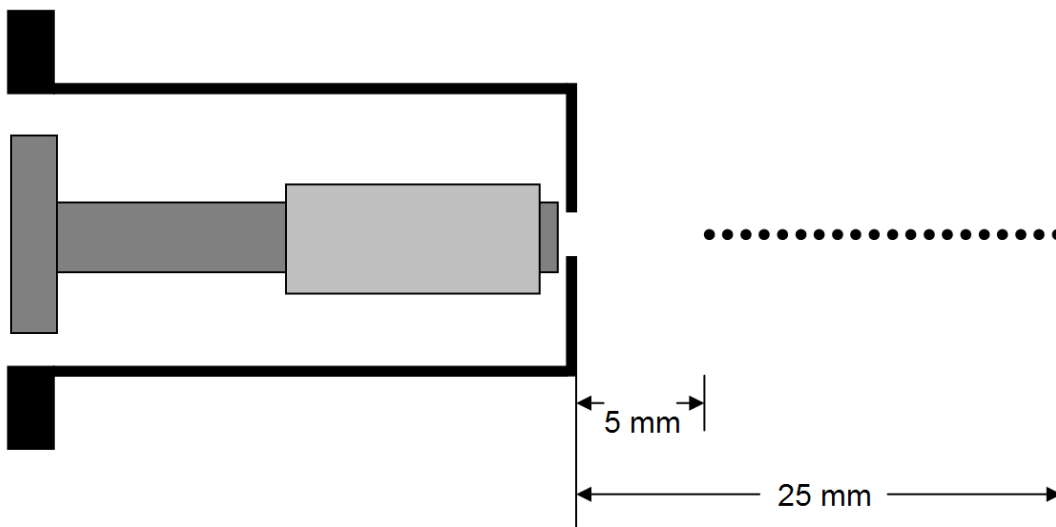
Figure 29. Data Collection Locations

When the probe is close to the orifice of the keeper, the current draw becomes much higher and has the potential to melt the probe tip or cause it to emit electrons. Three precautions mitigated this. First, compressed air blew through the ceramic shaft to cool the probe. Second, ranges set for the translation stage limited how close the probe could get to the keeper orifice. For most of these measurements, the probe was at least 5 mm from the keeper orifice exit plane and no further than 25 mm at 1 mm increments.

3 mm was the closest any trace came to the keeper orifice. The final precaution was the collection routine designed by Scientific Systems. The probe control electronics limited the maximum voltage when the probe exceeded plasma potential.

Infrared Imaging

To study the temperature behavior of the cathode, the author used a forward-looking infrared (FLIR®) imaging camera. Accurate temperature measurements gave insight into which cathode operated at a higher temperature. Using this information, the author made definitive observations and conclusions about each cathode's relative work function. If the CeB_6 work function was indeed lower, it should operate at slightly lower temperatures for equal electron emission as LaB_6. The temperature data also determined if the cathodes were operating at levels that make them susceptible to poisoning. The FLIR® camera was capable of detecting infrared wavelengths from 7.5 to 13 μm, and provided a non-intrusive method for measuring cathode temperature. This temperature collection method was advantageous over thermocouples because did not affect the discharge process or act as a heat sink for the cathode. A Zinc Selenide (ZnSe) window mounted to the vacuum chamber allowed transmission of the IR waves. Figure 30 is a picture of the camera as it looked through the ZnSe window during cathode operation.
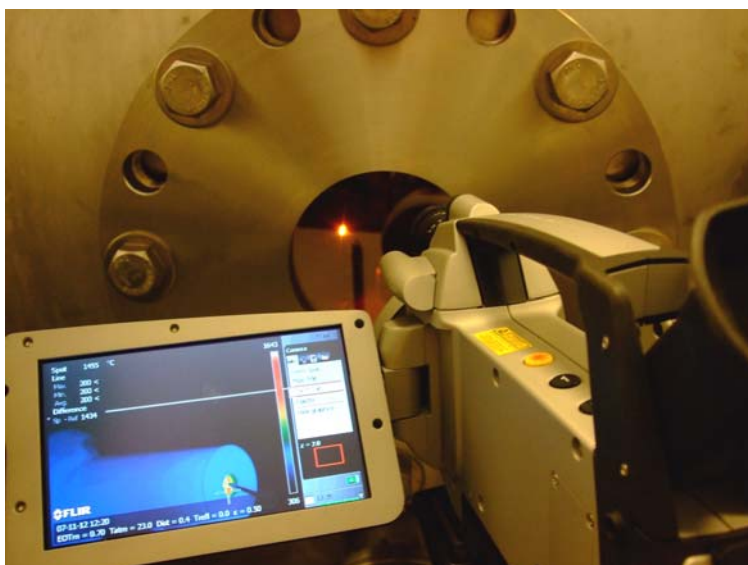
Figure 30. FLIR® Camera Looking Through ZnSe Window

For simplicity, the only region of the hollow cathode quantitatively studied and corrected for emissivity was the tantalum orifice plate. A tantalum sheathed, insulated type C thermocouple pressed against the orifice plate provided the reference temperature necessary to obtain emissivity values for the orifice. Then the camera was calibrated with these emissivity values for the remainder of testing when the thermocouple was removed. The insulated tantalum sheath electrically isolated the thermocouple from surfaces at cathode potential. There was no plasma discharge during the calibration of the camera for these tests. By setting the heater filament current to a range of values, the cathode temperature was varied as desired. The cathode was positioned 13 cm from the ZnSe window. The temperature range tested was 300-700°C. Basic radiation heat transfer methods were implemented to calculate the emissivity using four data points from the both the thermocouple and the camera for each temperature.

After calibration, side-by-side and positioned in the center of the chamber, the cathodes faced the ZnSe window at a distance of 3 m. Each cathode operated

independently from the other to prevent any unintentional coupling between them. Each test point ran for 15 minutes, then two images were taken with the camera. Because the cathode required more time to reach stable operation when changing the propellant flow, the anode current was varied first. When the desired range of current levels was tested, starting from lowest to highest, the flow was decreased and the procedure repeated.

After collecting the IR images, the emissivity corrections obtained were applied to each image using the software provided by FLIR®. The orifice plate was 10 pixels across and the temperature reported included the maximum and minimum.

The camera automatically corrected for the transmission of the window from a user-defined value. The ZnSe window had a transmissivity of 0.68, which was determined in the lab. The FLIR® camera also corrected for atmospheric transmission between the camera lens and the window. The user only had to specify the distance between the two for this correction to be included. For this experiment, the camera lens was 10 cm from the ZnSe window. Each temperature recorded by the camera was accurate to within +/- 2% over a range of 300-2100°C.

Microscope Imaging

Microscopes documented the state of the hollow cathode inserts before and after testing. A light microscope capable of 10-x magnification captured real color images of the inserts before and after the experiment. These images revealed any signs of damage, dimensional changes, and contamination. They also provided a visual reference to the location in which spectral analysis was completed. The microscope described here is in Figure 31.

Figure 31. 10x Microscope

An Edax electron microscope provided more information for understanding the effects of poisoning on the cathode insert, shown in the figure below. This device measured concentrations of the elements that formed on the cathode insert surfaces. The microscope can detect materials with activation energies up to 15 keV. This machine cannot detect elements such as molybdenum, because the applied electric field in the electron microscope cannot exceed 30 kV due to hardware limitations. Specified by the vendor, any elements with activation energies more than half the maximum applied potential are undetectable or the machine cannot provide accurate data for those elements.

Figure 32. Edax Electron Microscope

High-Speed Imaging

The final device used to collect data for this experiment was an X-Treme XS-4 high-speed imaging camera. This camera is capable of frame rates as high as 100 kHz. However, at higher frame rates, the resolution is lower and the amount of light collected is much smaller. This requires larger apertures or lower frame rates to collect sufficient light to distinguish an image. This camera provided the time dependant behavior of the plasma and the data necessary for additional insight into spot and plume mode behavior.

Cathode Operation Test Points

All of the aforementioned equipment collected information about the cathode during and after it ran with several xenon flow rates, anode currents, keeper currents, and orifice geometries. The test points included 2 A, 4 A, and 6 A of anode current with 4.5,

3, and 1.5 sccm of xenon, maintaining constant vacuum pressure by bleeding in background xenon. The keeper was turned on and off for each of these test points, totaling 18 test points per cathode. When the keeper was off, it electrically floated relative to ground. Some cathodes with higher work functions like the ones used here require the keeper to operate while others do not. This variation determined if either cathode is capable of operating without the help of a keeper. However, when operating in space, it is required the cathode keeper be kept on to ensure the main thruster discharge can be quickly re-started if needed.

Both cathodes operate at the 18 test points previously described. The CeB_6 cathode was tested at these operating points for one orifice geometry (aspect ratio of 0.5), while the LaB_6 was tested for two orifice geometries (0.5 and 0.25). The author originally intended for both cathodes to be tested with two orifice configurations, but time only permitted this for the LaB_6 cathode.

IV. Analysis and Results

Cathode Ignition

The LaB_6 cathode was the first cathode tested. The term "ignition" or "breakdown" describes the beginning of the cathode discharge. As previously discussed in the background section, the keeper begins the extraction of electrons from the cathode orifice. During ignition, the keeper is set to a constant voltage, which stays constant until the potential barrier of the insert plasma sheath is broken and electrons begin to flow. After breakdown, the keeper voltage drops and the power supply maintains a constant current. For ignition to occur, impregnated cathodes require conditioning procedures similar to the following description:

1. Pump propellant lines out to the bottle valve.

2. Purge the propellant lines with 5-10 sccm of propellant for 1-2 hours.

3. Set heater current to 2-3 A for 1 hour.

4. Increase heater current to 3-5 A for an hour.

5. Increase heater current to 6-8 A for 30 minutes.

6. Start flow, turn on keeper electrode

The cathode lights once this procedure is completed. The propellant flow can be turned off after the purge and turned back on when ready to light. The above conditioning sequence is only required after the cathode has been open to atmosphere. Once the conditioning is complete and the cathode is under vacuum, the ignition procedure is as follows:

1. Pump propellant lines out to bottle valve.

2. Set heater current to 6-8 A for 10-15 minutes

3. Start flow and turn on keeper.

The voltages required to light impregnated cathodes are typically much lower than LaB_6 cathodes due to their lower work function. In addition, after the keeper starts, the heater is typically turned off. When the insert is poisoned or the work function begins to rise over time and the cathode performance degrades, higher flow rates and more heater power are required to re-light the cathode.

Due to the higher work function of LaB_6, the initial ignition procedure began with slightly higher flow rates than impregnated cathodes needed. The same heater power and

keeper power were used throughout all ignition tests. For both the 0.5 and 0.25 aspect ratio cathodes, the ignition procedure was as follows:

1. Pumps propellant lines out to the bottle valve.

2. Set heater to 11.25 A until its voltage reaches 11 V (10 minutes)

3. Set flow to 4.5 sccm and run for 2 minutes

4. Set keeper to 650 V, 1 A and turn on.

The LaB_6 cathode was able to start at these conditions consistently with no measurable degradation in performance. With the deeper orifice, the heater filament needed 30-40 W for the cathode to maintain discharge at low anode currents (<2.5 A) and flow (<2 sccm) with the keeper electrode off. However, the shallower orifice operated smoothly with no heater power at low anode currents (~1.5 A) and flow (~1.5 sccm). The shallower orifice also allowed the LaB_6 cathode to run with no heater or anode power. Only the keeper was on during this condition. Below is an image of the LaB_6 cathode at the moment of ignition, captured with a high-speed camera.
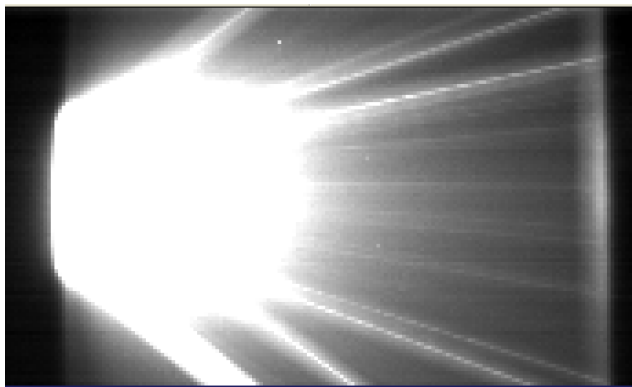
Figure 33. LaB_6 Cathode Ignition

Both cathodes underwent the same ignition process. During initial tests, the CeB_6 cathode started at the same conditions as the LaB_6 cathode, noting that only the deeper

orifice geometry was tested. The author changed the limits of ignition for the CeB_6 cathode to investigate the validity of the reported lower work function. The lowest voltage required to start the CeB_6 cathode was 500 V at 1 A of keeper current, maintaining heater power and flow at a constant level. After ignition, no heater power was required to maintain keeper only operation. After further investigation, the heater filament of the CeB_6 cathode was superior to the LaB_6 cathode, and the actual power delivered during ignition was 9 Watts more than the LaB_6 cathode received. This may explain the lower keeper power levels, and requires temperature data to clarify.

Spot and Plume Mode Characterization

Because the anode and orifice configuration is different for many experiments, it is difficult to make direct comparisons to other impregnated cathodes. However, the data collection techniques are similar to other studies and provide the same insights into the plasma behavior. This first section discusses the results obtained for both the LaB_6 and CeB_6 cathodes by analysis of the anode and keeper voltage waveform, as well as Langmuir probe I-V curves. The error include in these plots is the statistical variance between the 10 samples collected per data point and location.

LaB_6 Cathode

The tests begin with the highest anode current and flow rates. This reduced run time because it took longer for the propellant system to stabilize while increasing the flow rates rather than decreasing them. The error included for all the Langmuir probe data is the statistical variance between samples. The variance is usually so small the error bars cannot be seen in most the graphs. The possible perturbations from the probe were not quantified in the sake of time and were not included in the error. The vacuum

chamber maintained a pressure of $6.5*10^{-6}$ Torr +/-5% during all testing by bleeding additional background xenon gas when the cathode flow rate decreased. Positioning the inlet far from the pressure gauge and anode prevented inadvertent discharge or false readings. The first data presented are from a Langmuir probe centerline scan for the LaB_6 cathode having an aspect ratio of 0.5 (AR.5). When the keeper electrode was off it was left floating relative to ground potential.
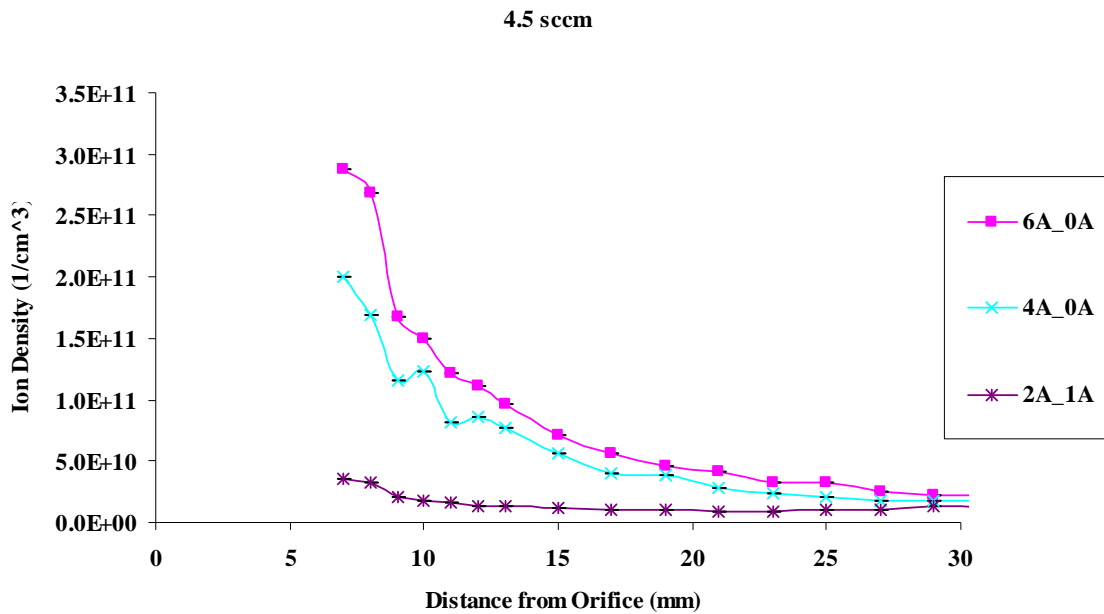
4.5 sccm

Figure 34. Ion Density for AR.5 at 4.5 sccm

Figure 34 displays the ion number density for three anode currents. The second number after the underscore denotes the keeper current. The AR.5 LaB_6 cathode could not maintain a stable discharge for this flow at 2 A anode current without the operation of the keeper. This additional current draw allowed the insert temperature to be high enough to maintain sufficient electron emission for discharge. Due to the restrictive nature of the orifice, the peak emission occurred close to the exit plane of the keeper,

quickly dropping off with increasing axial distance. In addition, lower anode currents clearly show lower ion densities, as expected. This is simply because less plasma is required from the cathode to conduct lower current. The next figure is a comparison between two operating conditions, one with the keeper on and one with it off for one flow condition.
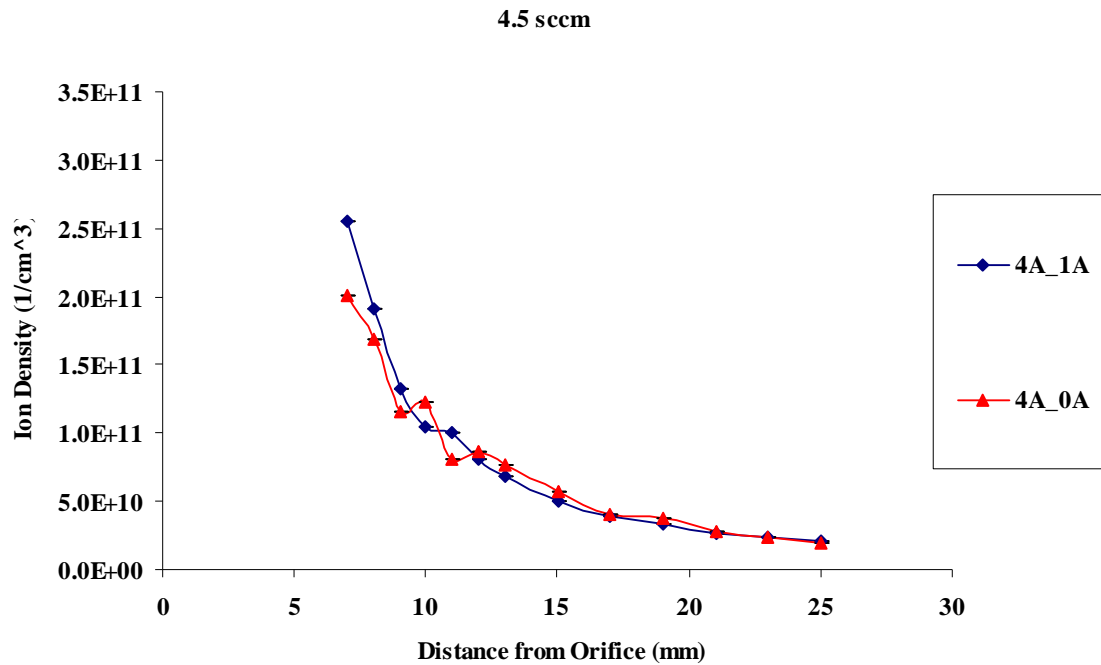
4.5 sccm

Figure 35. Ion Density with Keeper on and off for AR.5 at 4.5 sccm

For the case displayed in the above plot, the ion density appears to increase with increasing keeper current. However, it did not appear to have any considerable affect on how far the peak ion density extended from the keeper orifice.

Electron density exhibited a similar behavior as ion density, decreasing with decreasing anode current and peak densities occurring near the orifice, Figure 36 and Figure 37. The number densities were not indicative of the plasmoids or plasma ball

structures characteristic to plume mode behavior. The keeper also did not appear to have a significant effect on the penetration of the electrons downstream of the keeper. Plasma potential and electron temperature provided more information on the mode the LaB$_6$ cathode was running at for the 4.5 sccm cases presented.
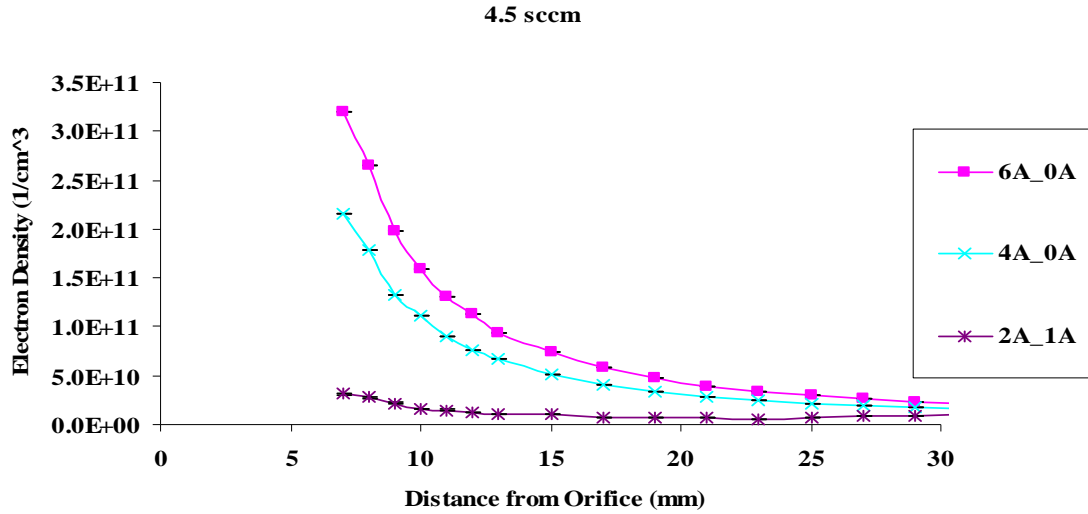
4.5 sccm

Figure 36. Electron Density for AR.5 at 4.5 sccm
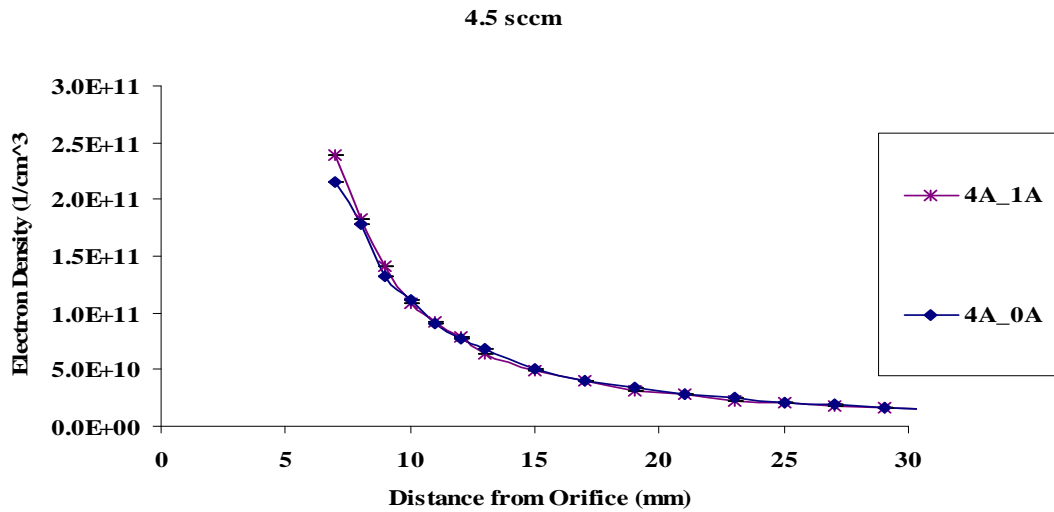
4.5 sccm

Figure 37. Electron Density with Keeper on and off for AR.5 at 4.5 sccm

71

Confirmed by other literature, higher anode currents and lower flow rates induced higher electron temperatures within the plasma.[15,35,36] All of the electron temperature data collected followed this trend and the AR.25 LaB_6 had the clearest depiction of this behavior. The plots in the section discussing the AR.25 LaB_6 cathode definitively show the correlation between electron temperature, anode current, and flow rate discussed above.

Plasma potential negatively correlated with anode current and flow rate for these test conditions. Figure 38 depicts the relationship between plasma potential and anode current. Ion energy cost increases with higher plasma potentials, lowering the efficiency of the thruster. Ideally, a cathode would require very low flow rates and maintain low plasma potentials, reducing the ion energy cost and maximizing the propellant utilization efficiency of the thruster. Running the keeper lowered the plasma potential by a very small amount, but showed the negative correlation between plasma potential and anode current. However, keeper operation does not provide any efficiency advantage because its power input is a loss for a thruster. So leaving it is more for ensuring the discharge is maintained and is not used to improve cathode plume performance. There were oscillations in plasma potential from 7-11 mm, possibly induced by the Langmuir probe. Scientific Systems did not design the probe for low plasma perturbation. Other studies have taken several measures to limit the effects of the probe on the plasma.[15,35,36] It is difficult to predict how and to what degree the probe will affect the coupling plasma, but not difficult to measure it. A later section quantifies and discusses the probe effects.
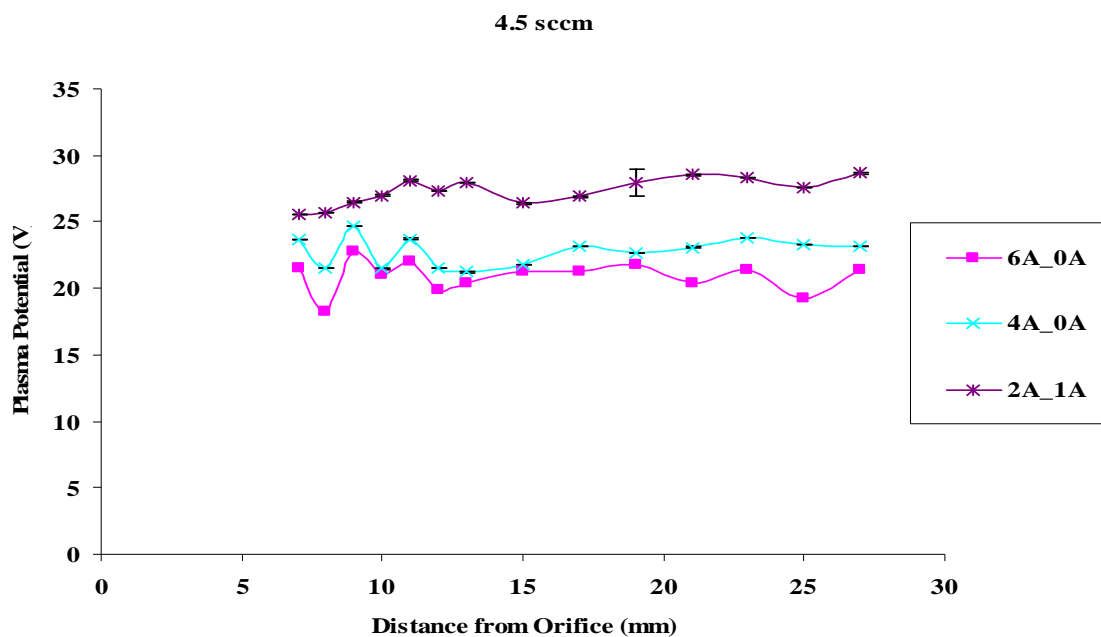
4.5 sccm

Figure 38. Plasma Potential for AR.5 at 4.5 sccm

The voltage waveforms presented below give further insight into the behavior of the cathode during these 4.5 sccm operating conditions.
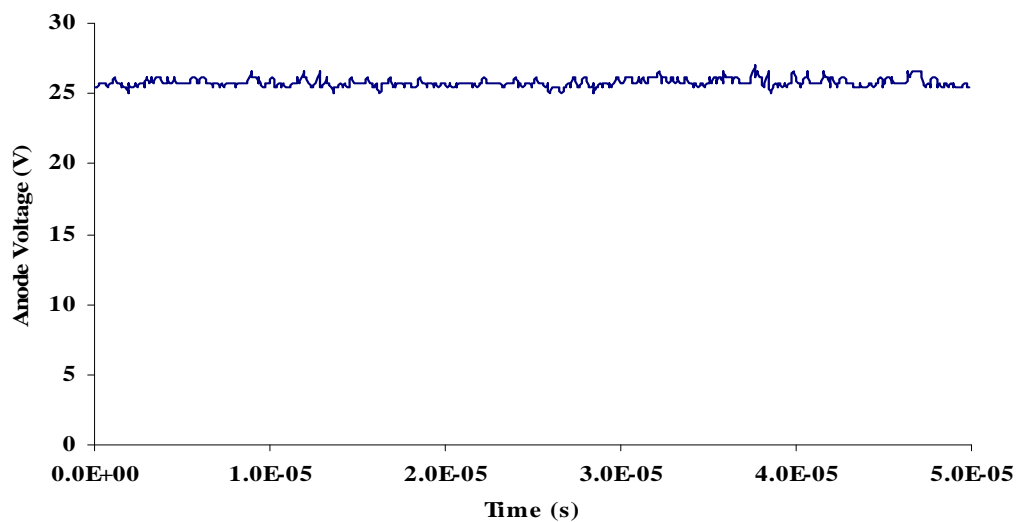
Figure 39. Anode Waveform for 4A Anode, 1A Keeper, 4.5 sccm

All operating points for 4.5 sccm displayed very similar waveform behavior as Figure 39, having virtually no AC component in the discharge, characteristic of spot mode operation. The keeper voltage also displayed such behavior, depicted in Figure 40.
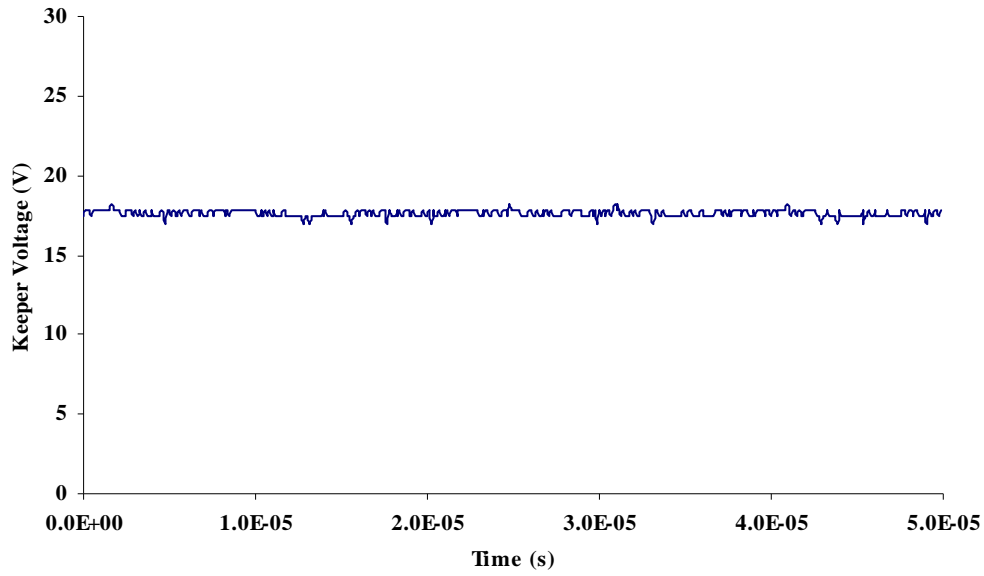
Figure 40. Keeper Waveform for 4 A Anode, 1 A Keeper and, 4.5 sccm

The keeper maintained a relatively low potential, despite the cathode having a higher insert work function than an impregnated cathode. This shows the significant impact of field enhanced emission caused by the plasma and is one of the primary advantages of hollow cathodes over direct emission cathodes.

Overall, the LaB$_6$ cathode operated in spot mode for all the anode and keeper current ranges tested at 4.5 sccm. The expansions were monotonic and the ion densities were similar to the electron densities. The anode voltage levels did not exceed 40 V or exhibit any large AC voltage oscillations. The electron temperatures were also below 4 eV and no plasma balls or plasmoids were observed. Surprisingly, the LaB$_6$ cathode was able to operate at all the 4.5 sccm test conditions without any heater power. For this

74

flow condition, it also demonstrated the ability to run at low anode currents (3 A) without any power to the keeper electrode.

After decreasing the flow to 3 sccm, the same data were collected. The graphs include each plasma parameter at different anode and keeper currents. Figure 41. shows a similar trend as that observed for the 4.5 sccm case, with the exception of 6 A anode current with 1 A keeper current. It appears there was a localized region of dense plasma forming at the exit of the cathode. As stated by both Martin and Goebel, these regions occur further downstream of the cathode under higher flow conditions.[35,15] This may explain why the localized region was several millimeters from the orifice. Interestingly enough, the localized dense region only occurred with the keeper on for this case.
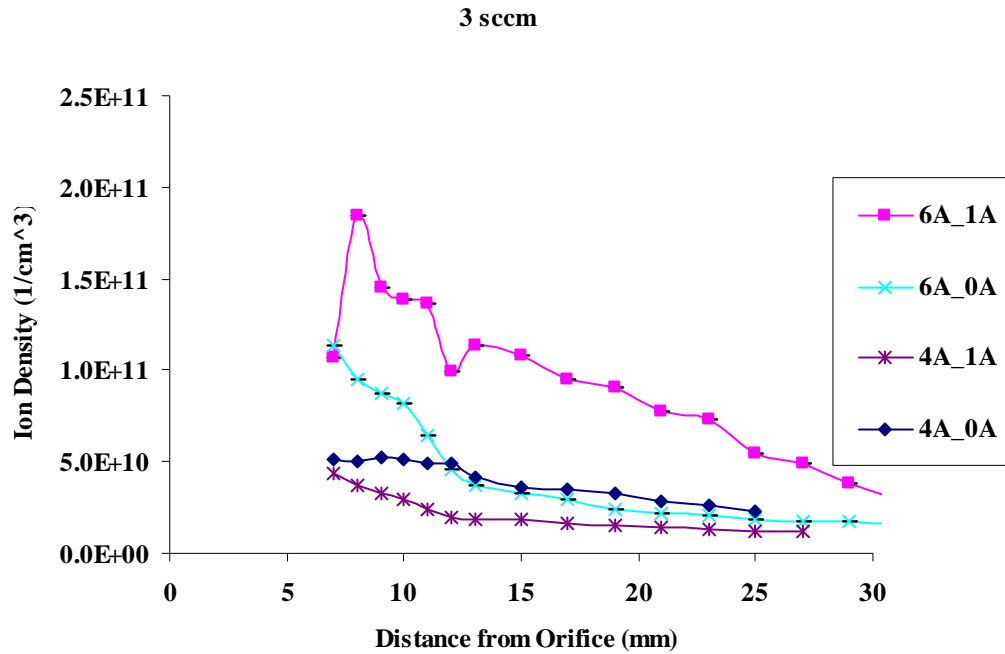
3 sccm

Figure 41. Ion Density for AR.5 at 3 sccm

For every case but the 6 A anode current with 1 A keeper current, the electron density was higher than the ion density and both curves had the same general shape. See Figure 42. As for the exception, its electron density is much lower than the ion and followed a trend similar to the ion density curve, but with less prominence. In the event of large AC voltage oscillations, this region of dense plasma may provide the ingredients necessary to create high-energy ions that accelerate the wear of the keeper and ultimately the cathode. However, it may not be a significant threat because it is so far away from the cathode, the voltage at this operating condition was below 40V, and there were no significant oscillations.
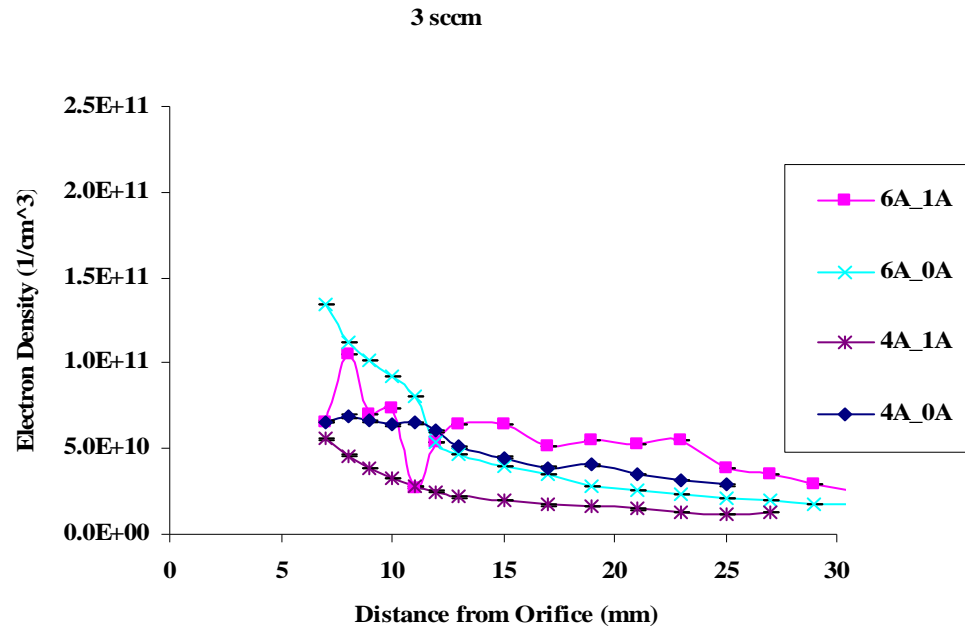
Figure 42. Electron Density for AR.5 at 3sccm

The electron temperature for 3 sccm followed a similar trend as that of the 4.5 sccm test point. The exception was again the 6 A anode current, 1 A keeper current

76

case. The temperatures for that operating condition were much lower than the rest. This

was not indicative of plume mode at all, since higher electron temperatures are

characteristic of this mode. However, because the densities were much higher, the

electron temperatures were lower, which is an expected phenomena.

The plasma potential curves in Figure 43 are similar to that of Figure 38. This

figure shows how plasma potential increased with lower anode currents and decreased

with higher ones, the same relationship seen during the 4.5 sccm test point. As the figure

shows, the plasma potential stayed relatively constant along the axis of the cathode.

However, the overall plasma potential at 3 sccm was only slightly lower than the

4.5 sccm case. See Figure 44.
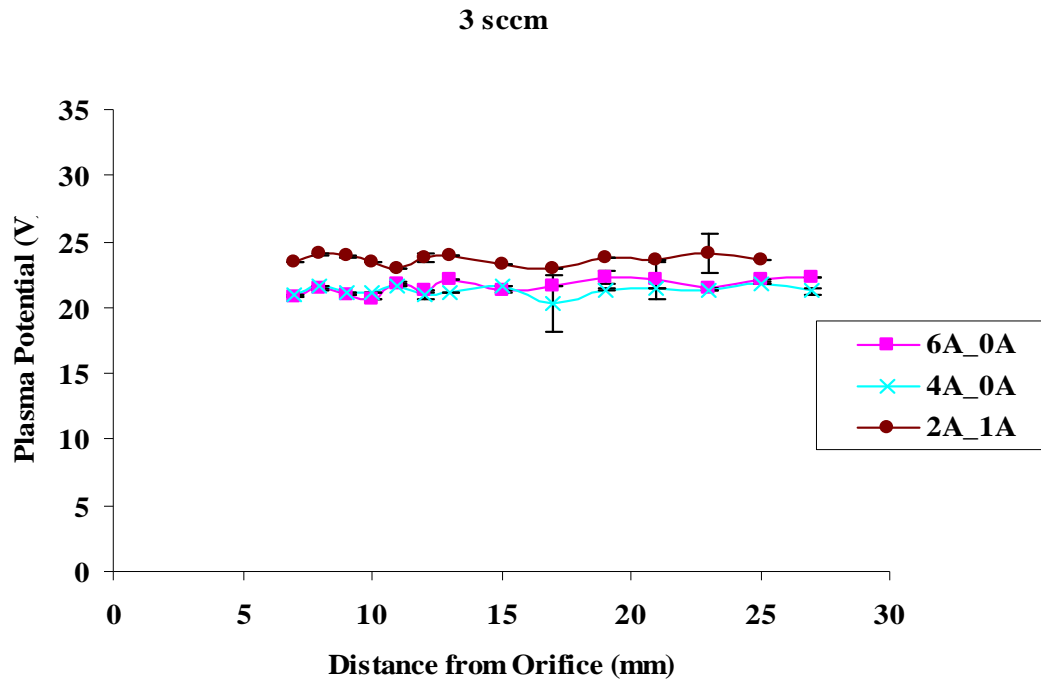
3 sccm

Figure 43. Plasma Potential for AR.5 with Keeper on and off at 3 sccm
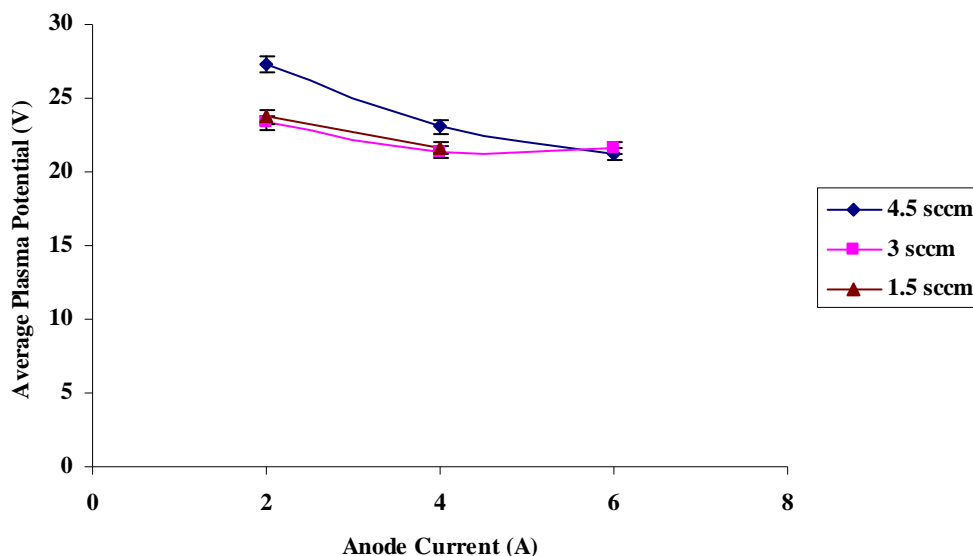
Figure 44. Average AR.5 LaB$_6$ Cathode Plasma Potential with Keeper Off

It also appears the plasma potential experienced the greatest change with flow at low anode currents. As the anode current approaches 6A, the flow had little effect on the plasma potential for the conditions examined here. The keeper also had a small effect on plasma potential. These data are higher than plasma potential values reported for impregnated cathodes.[35]

The waveform data collected for the operating points at 3 sccm had no AC voltage oscillations, increased anode, or keeper voltages. As for the 6 A anode and 1 A keeper current case, its anode and keeper voltage waveform are displayed in Figure 45, and Figure 46, respectively. A purely DC waveform was not observed here, atypical of the other current levels, possibly indicating an intermediate mode. There were some small voltages fluctuations, but they were only a volt or two and did not occur very frequently, confirmed by Fourier analysis.
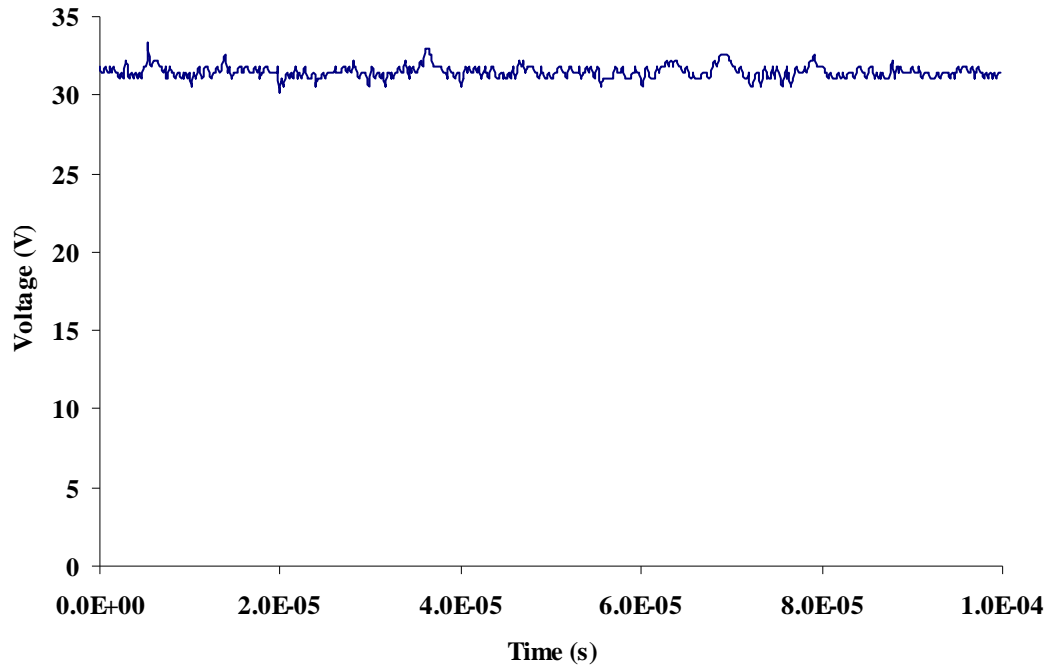
Figure 45. Anode Voltage for 6 A Anode Current and 1 A Keeper Current
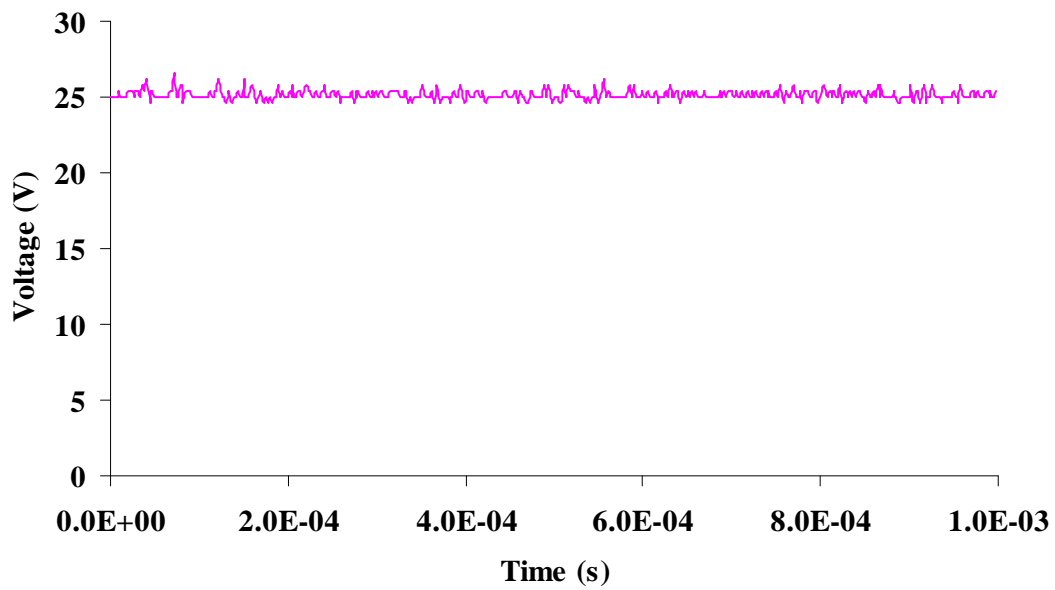
Figure 46. Keeper Voltage for 6 A Anode Current and 1 A Keeper Current

The final flow condition was 1.5 sccm for this orifice geometry. The ion densities in Figure 47 were lower than the previous flow conditions. 30-40 W of heater power were required to run the cathode at currents below 3 A, therefore no Langmuir probe traces were taken for these operating conditions. In some instances, anode currents above 5 A at 1.5 sccm exceeded the maximum 250 W output of the power supply. The cases presented here were of the times this did not occur.

There were localized regions of plasma here as well, the following plots are only for those instances. The peak density for 4 A anode current here was much higher than the 3 sccm case, but the average density was less than twice the average ion density at 1.5 sccm.
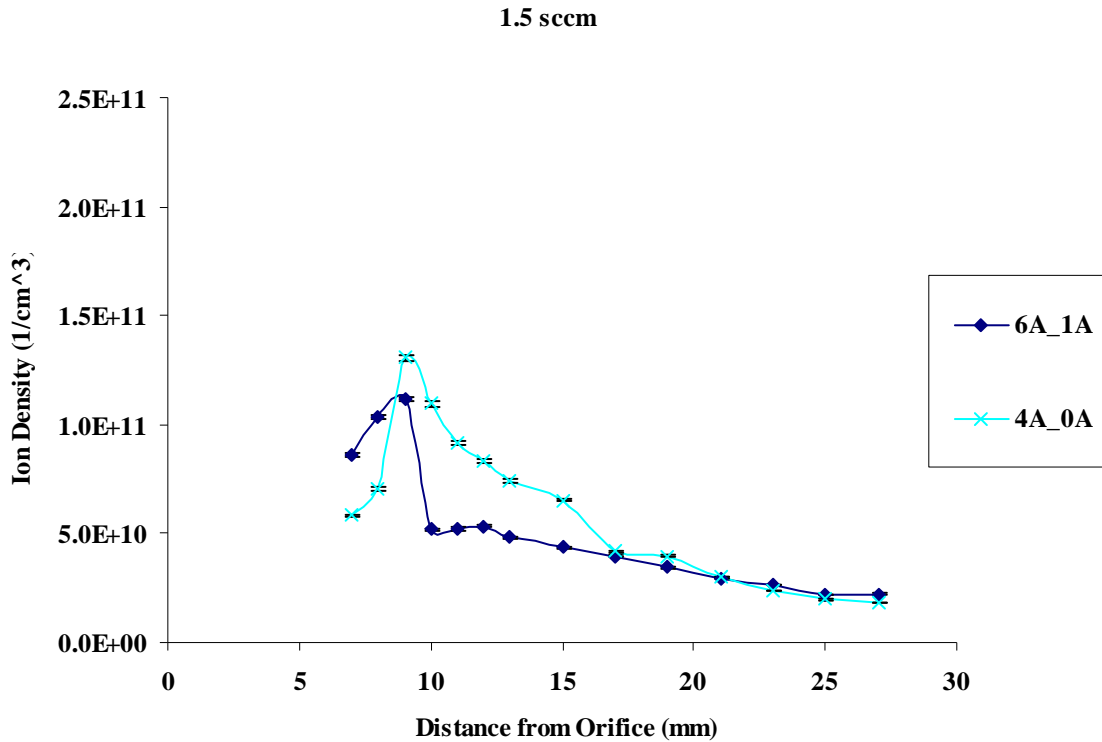
Figure 47. Ion Density for AR.5 at 1.5 sccm
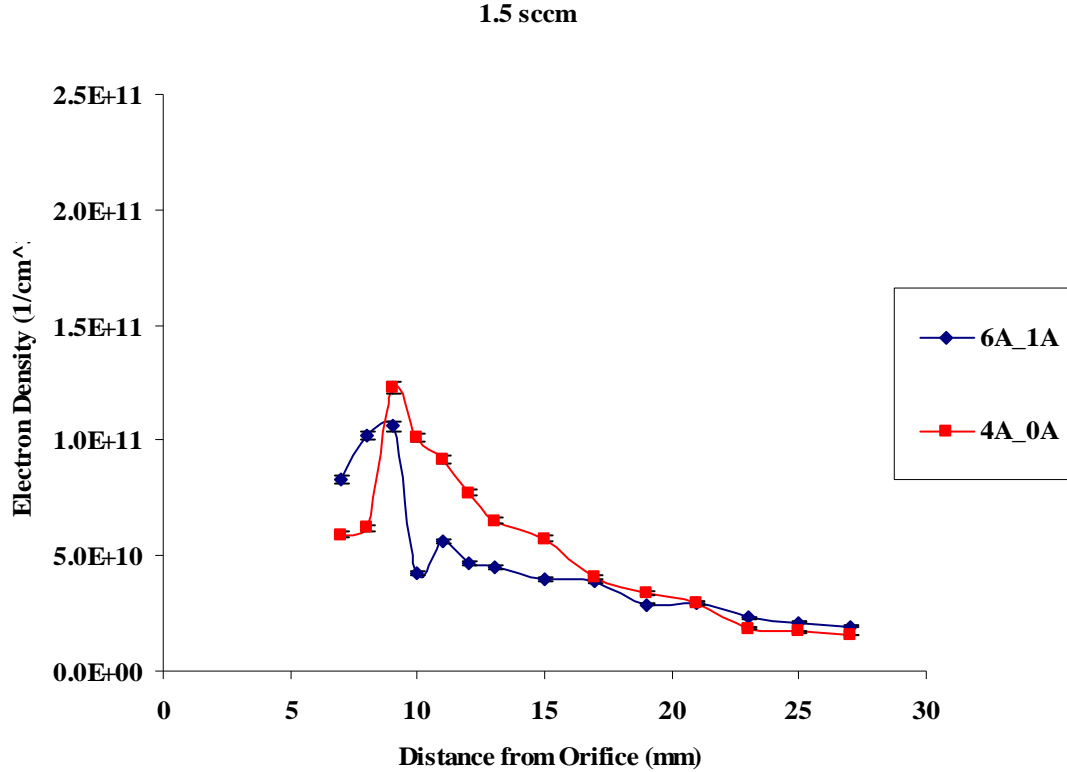
Figure 48. Electron Density for AR.5 at 1.5 sccm

The electron densities in Figure 48 are lower than the 4.5 sccm flow condition, also an expected trend. They were about equal to the ion density however, slightly different from previously observed. The peak densities also occurred closer to the keeper orifice than observed by others for lower flow conditions.[15,35] As previously mentioned, keeper operation takes the cathode out of plume mode, but the graphs presented above show plasmoid structures for cases with the keeper on and off. The plasmoids can still form while the cathode is not in full plume mode, they key was measuring how close they are to the keeper. With the keeper off, as in the 4A case above, the highest plasma densities were further from the cathode. The plasma pulled in and concentrated over a smaller distance when the keeper was on, as in the 6A case. The probe did not measure

localized plasma with the keeper off at 6A anode current, perhaps because it was within

the first 5 or 6 mm of the keeper orifice.

The electron temperature did not show much change between either flow

conditions. The average electron temperatures of each current setting varied less than

0.2 eV and were all below 3 eV. The temperatures were not indicative of a full plume

mode. With the localized regions of plasma, these conditions may also be an

intermediate mode. Additional data from waveform monitoring helped to define this

mode of operation, discussed below.

Again, it was unclear from the probe traces taken for the 1.5 sccm condition

whether the cathode was in plume mode or some kind of intermediate. Martin and

Williams also found it difficult to determine the mode of operation from Langmuir probe

data alone.[35,36] The voltage waveform for most of the 1.5 sccm tests showed very small

AC oscillations. However, some oscillations were present for the anode and keeper at

6 A anode current and 1 A keeper current, Figure 49 and Figure 50 respectively.
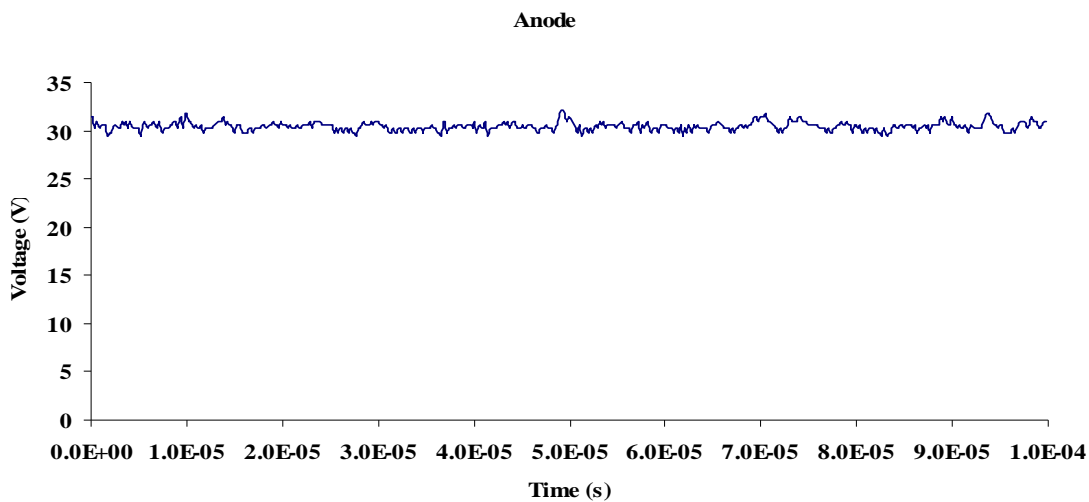
Anode

Figure 49. Anode Voltage Waveform for AR.5 6 A Anode and 1 A Keeper at 1.5 sccm
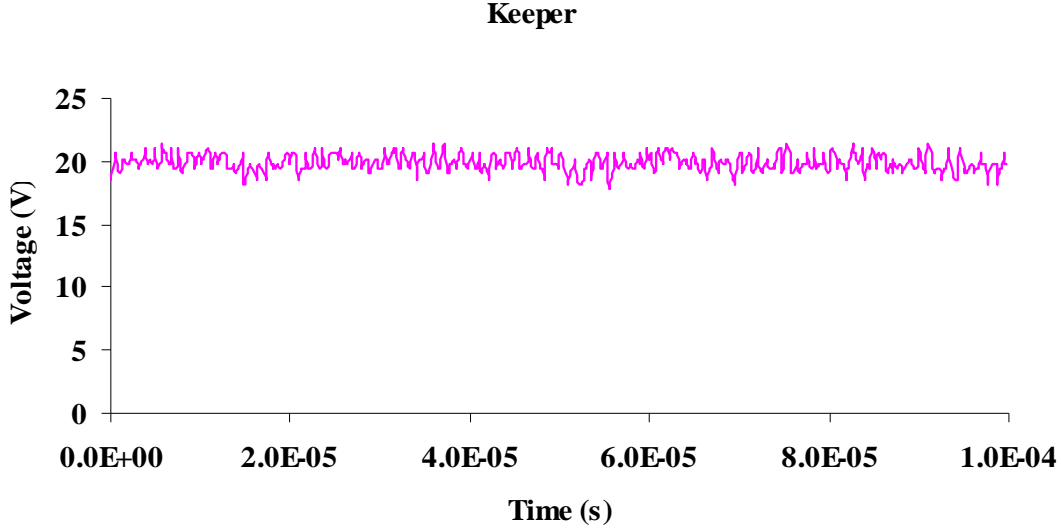
Keeper

Figure 50. Keeper Voltage Waveform for AR.5 6 A Anode and 1 A Keeper at 1.5 sccm

Fourier analysis revealed a primary frequency of 195 kHz for the anode voltage signal. The keeper voltage oscillated at 937 kHz, much higher than the anode oscillations. The keeper may experience plume mode before it propagates through the entire coupling plasma while operating between spot and plume mode. Large AC fluctuations and higher anode voltages would have answered the question about what mode the cathode was in at this test point. However, since the waveforms showed some oscillations that are not similar to others at the same flow condition, and there were localized plasma regions, the cathode was determined to be in an intermediate mode again. However, after running it a little longer, the cathode displayed some interesting behavior when the keeper was off.

Almost immediately after turning the keeper off and after the Langmuir probe collected data, the discharge voltage suddenly began to oscillate. Not only were there some oscillations in the voltage but in the current as well, see Figure 51. Here one can

83

see the change in the anode current as soon as the keeper current is zero. While the oscillations in anode current seemed small in amplitude, the voltage told a different story.
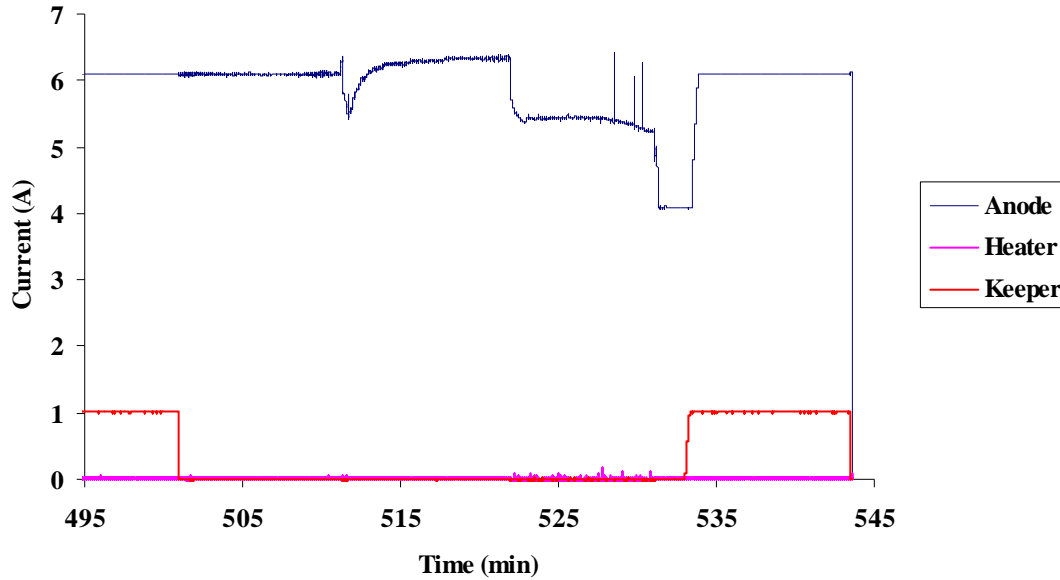
Figure 51. LaB$_6$ Current Waveform during possible Plume Mode Operation

The voltage waveform was not captured during the event, but with the keeper turned off at 6 A anode current and 1.5 sccm, the discharge became unstable. The anode voltage drastically increased, exceeding the limit of the power supply. This explains why the anode current dropped several times in the above figure. This mode was determined to be plume mode due to the higher discharge voltage (>50 V) and higher frequency oscillations. On the other hand, when the keeper was on, the discharge was relatively smooth and the voltage oscillations small. A phenomena cited by Kamhawi, stating more keeper current helps to inhibit plume mode.[13] No Langmuir probe data is available for this event, making it unclear whether there was localized plasma or not.

One property that may help explain why the localized plasmas form is the plasma floating potential. Upon comparison of Figure 47 and Figure 52, the plasma densities drop when the floating potential rises sharply, and the plasma density sharply rises when there is a sudden decrease in floating potential. This phenomenon occurred every time a plasmoid formed. Which property is the dependant variable is unclear.
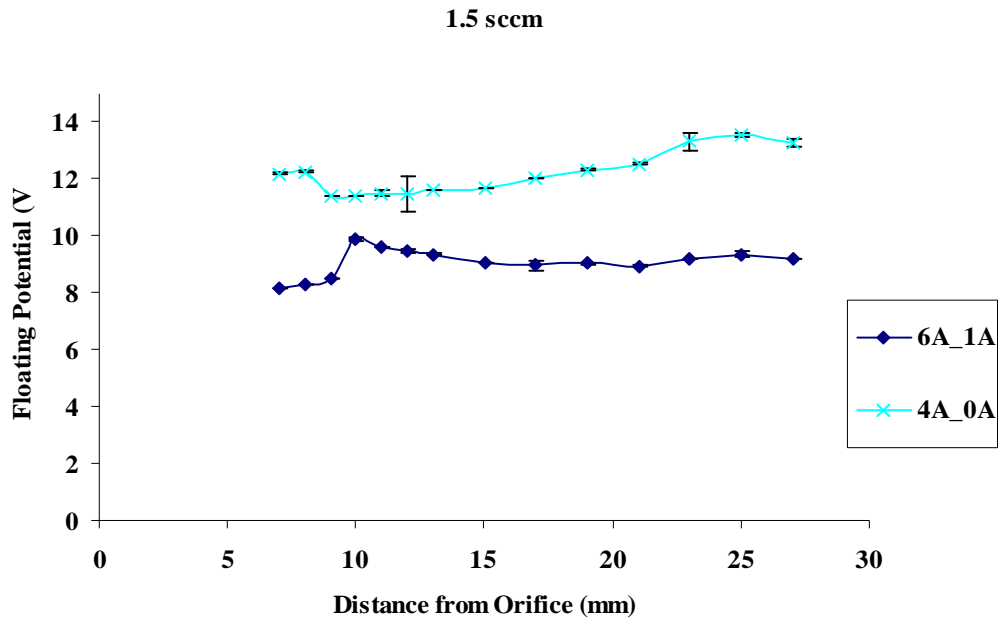
1.5 sccm

Figure 52. Floating Potential for AR.5 at 1.5 sccm

After the LaB_6 cathode performed successfully with an aspect ratio of 0.5, the aspect ratio was decreased to 0.25 (AR.25). The data presented in the next section is for this orifice geometry under the same anode current and flow conditions as the others. However, for the smaller aspect ratio, the keeper was turned off after the cathode coupled with the anode because keeper effects were already observed during the initial LaB_6 and CeB_6 tests. Only a few select cases have the keeper turned on and set to the standard 1 A.
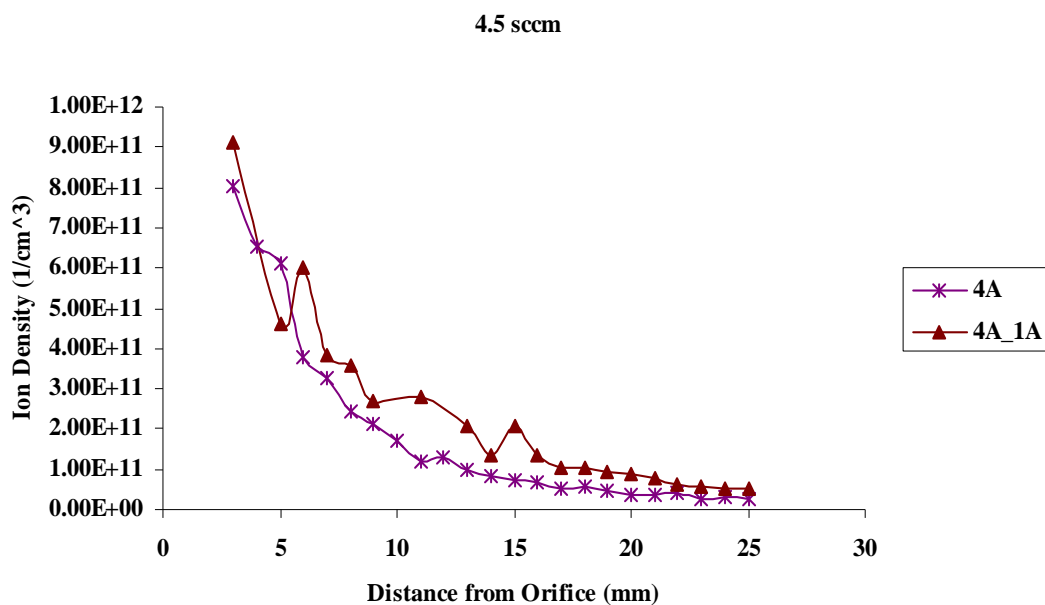
4.5 sccm

Figure 53. Ion Density for AR.25 at 4.5 sccm
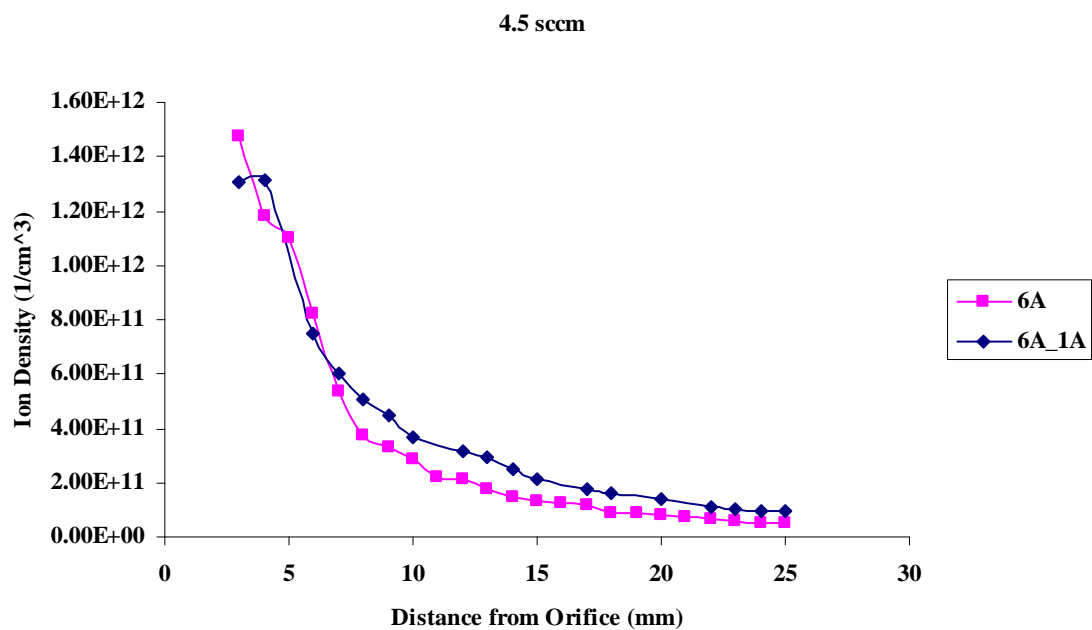
4.5 sccm

Figure 54. Ion Density for AR.25 at 4.5 sccm (2)

The keeper slightly increased the ion density close to the cathode as well as further downstream, Figure 53 and Figure 54. The AR.5 LaB$_6$ cathode exhibited the same behavior for the same flow condition. The keeper had little effect on the electron density, also observed with the AR.5 cathode. Ion density was slightly higher than electron density in most cases. The density curves along the centerline of the AR.25 geometry in Figure 53-56 show the expected increase with higher currents. Even after reducing the aspect ratio, the penetration of the peak ion density still occurred close to the cathode. Nevertheless, the average ion density was higher for the AR.25 cathode than the deeper AR.5 one.

Figure 55 is a clear comparison of ion density between the two orifice geometries, AR.25 having higher levels as one would expect with a smaller aspect ratio. This was because the smaller aspect ratio allowed the electric field to penetrate further upstream into the insert and extract more plasma.[15] This behavior was less apparent with electron density, Figure 56. For this property, the orifice had little effect on the electron density. It is actually lower at some locations for the smaller aspect ratio with 6 A to the anode. The keeper also did not affect the electron density by any significant amount. As for the mode of operation at 4.5 sccm, all of the anode current levels tested were very stable and exhibited no plume mode characteristics. The oscillations were less than one volt and all of the anode voltages were below 40 V. As the density curves will soon prove, all expansions were monotonic, and all other plasma properties exhibited no signs of plume mode.
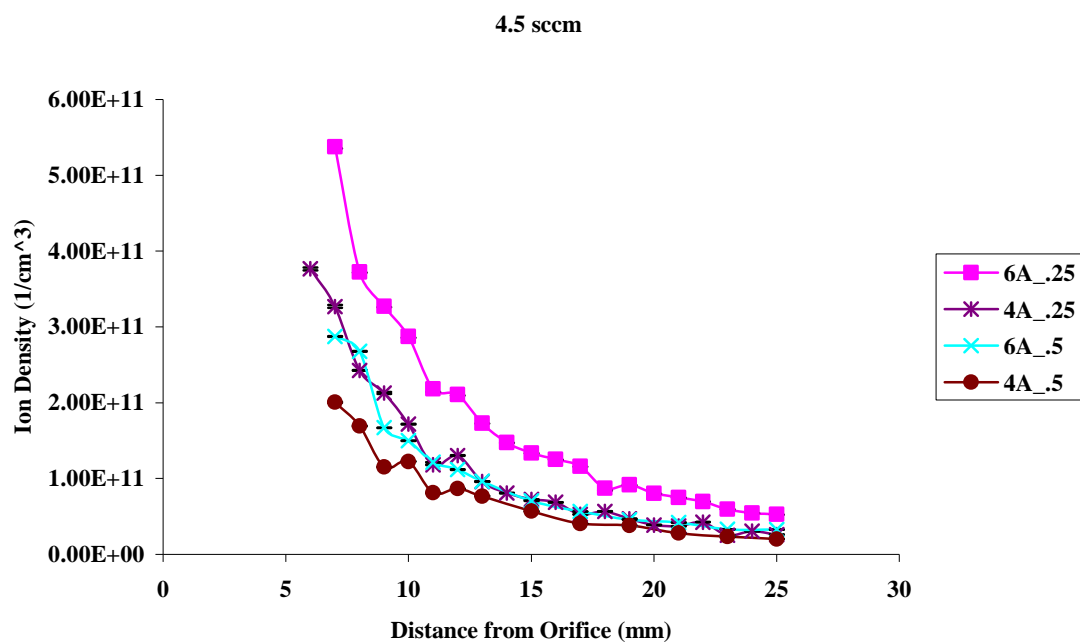
4.5 sccm

Figure 55. Comparison between AR.5 and AR.25 Ion Density at 4.5 sccm
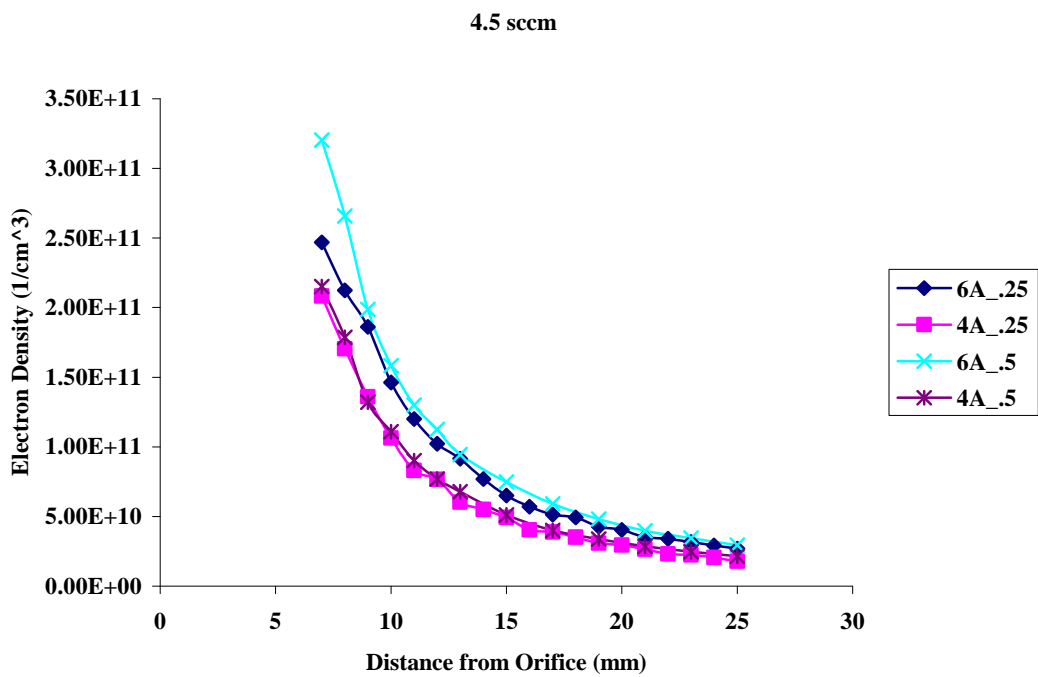
4.5 sccm

Figure 56. Comparison between AR.5 and AR.25 Electron Density at 4.5 sccm
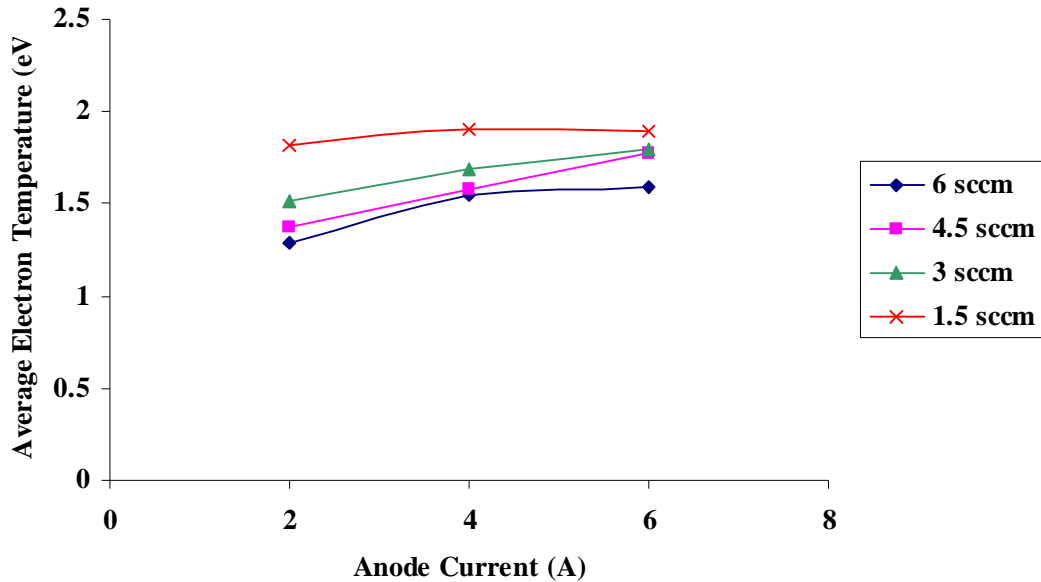
Figure 57. Electron Temperatures for AR.25 with Keeper Off

Figure 57 shows a clear relationship between anode current, flow rate, and electron temperature. As expected, the temperatures were the highest for the 6 A case, decreasing with anode current for a given flow rate. At 4.5 sccm of xenon, the average electron temperatures were much higher for AR.5 than AR.25, Figure 58.

The plasma potential for both aspect ratios and all flow rates are included in Figure 59 and Figure 60. For one aspect ratio, the plasma potential was unaffected by changing flow rate for anode currents above 4 A. Once the current dropped below 4 A, the curves begin to separate. As plasma potential increased with decreasing anode current, the highest plasma potential occurred at 2 A anode current and 4.5 sccm, also observed with the AR.5 cathode. The lowest plasma potential occurred at 2 A for the 3 sccm flow condition, also observed for the AR.5 cathode. Interestingly, the plasma potential was higher with the smaller aspect ratio, Figure 60.
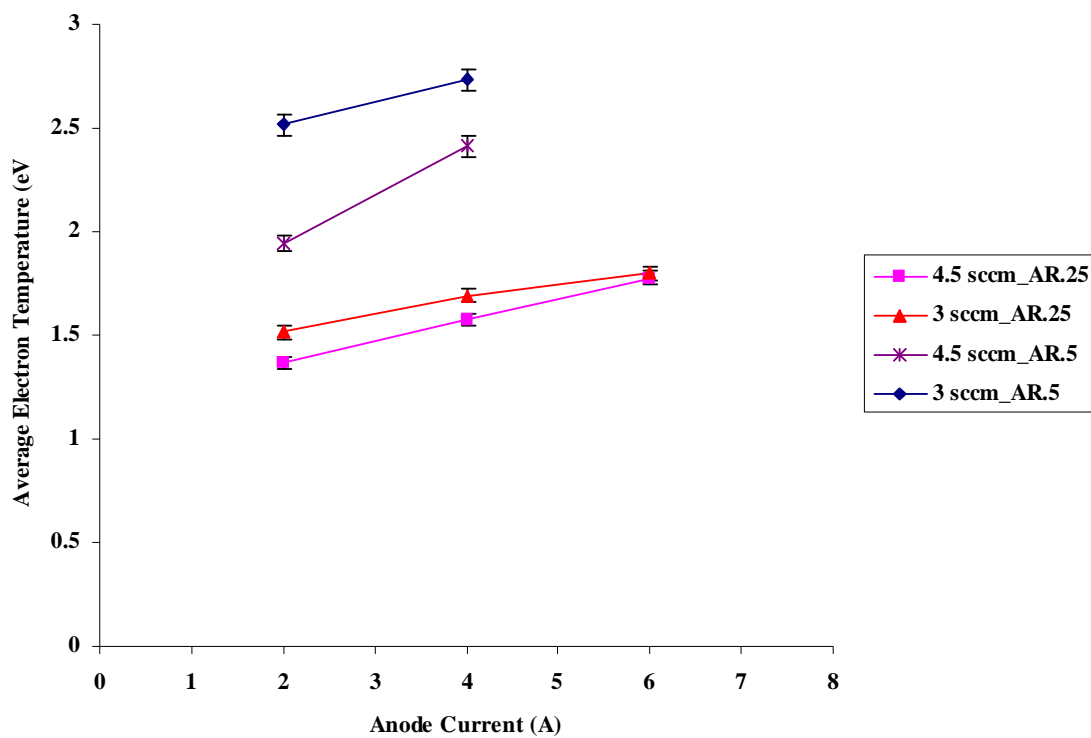
Figure 58. Comparison between AR.5 and AR.25 Average Electron Temperatures
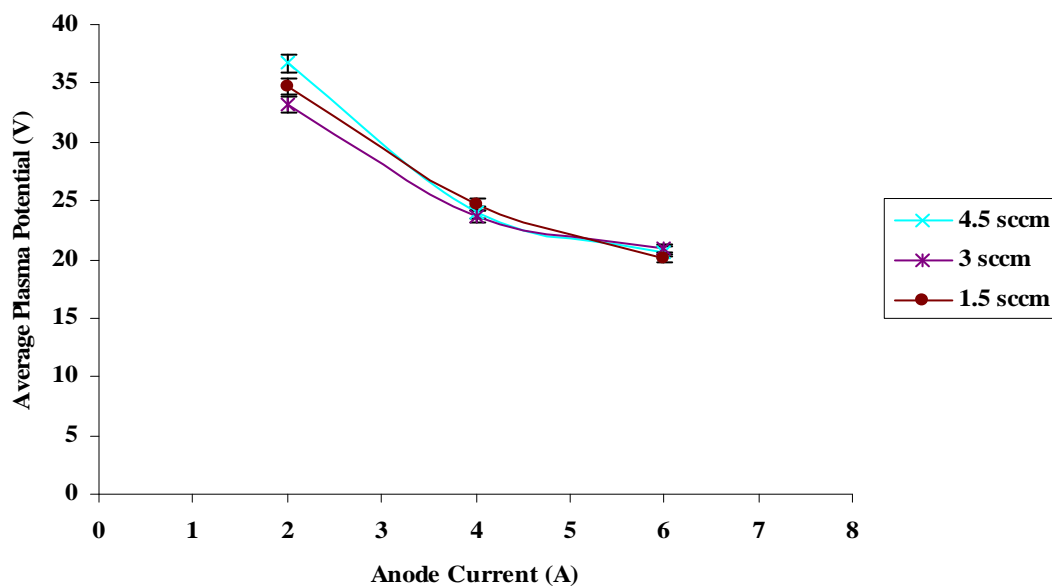
Figure 59. AR.25 Average Plasma Potential
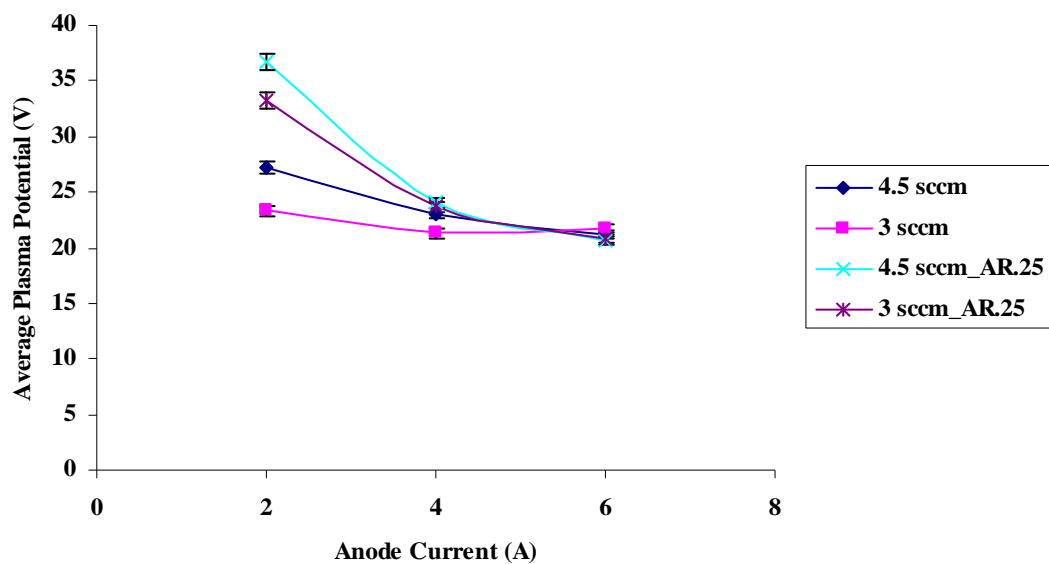
Figure 60. Comparison between AR.5 and AR.25 Average Plasma Potential

The change in plasma densities was more noticeable with different aspect ratios at 3 sccm. Figure 61 shows just how significant this influence was.
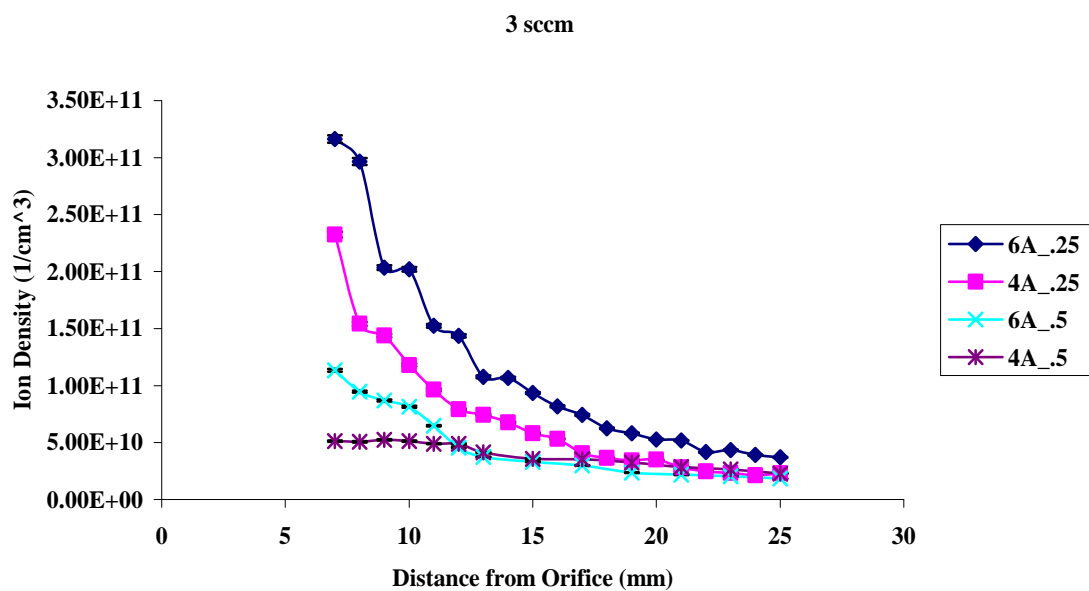
Figure 61. Comparison between AR.5 and AR.25 Ion Density at 3 sccm
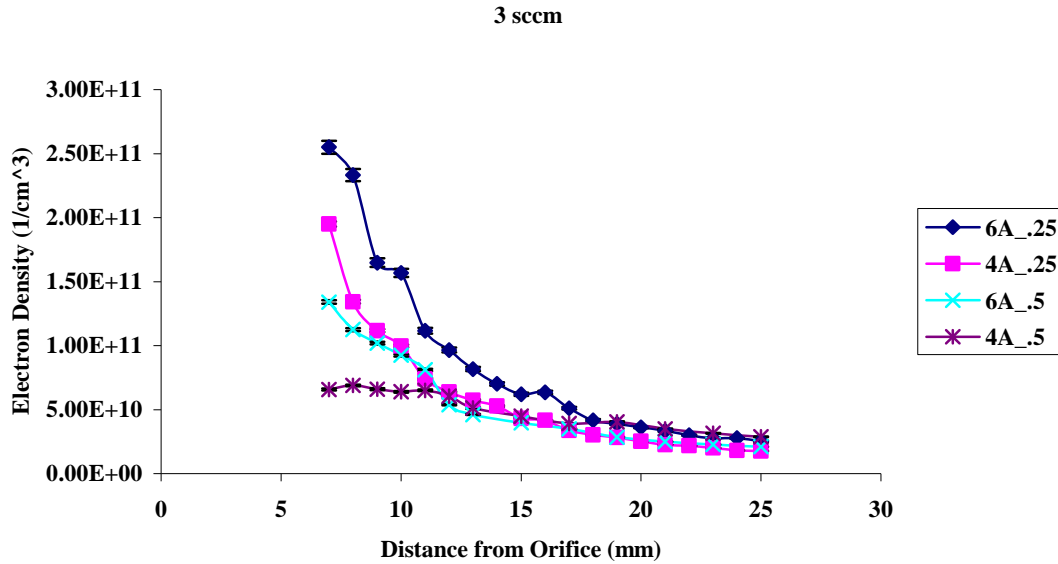
3 sccm

Figure 62. Comparison between AR.5 and AR.25 Electron Density at 3 sccm

Not quite as apparent in Figure 62, the aspect ratio's impact on electron density was slightly less than seen with ion density. As previously discussed, a smaller aspect ratio allowed deeper electric field penetration into the insert and enhanced the performance of the cathode by consuming less power.

With the flow reduced to 1.5 sccm, ion and electron densities for both aspect ratios were lower than the other flow conditions. Yet between them, AR.25 had higher densities. A localized region of plasma formed with 6 A to the anode for both aspect ratios, portrayed in Figure 63 and Figure 64. Note however, the keeper was on for AR.5, which lowered the anode voltage and mitigated the plume mode transition based upon the observations of this research. Despite having a localized region of dense plasma, the anode and keeper voltages had a small AC component as previously discussed, with one exception. One operating condition transitioned to plume mode after the probe entered the near keeper region, discussed here shortly.
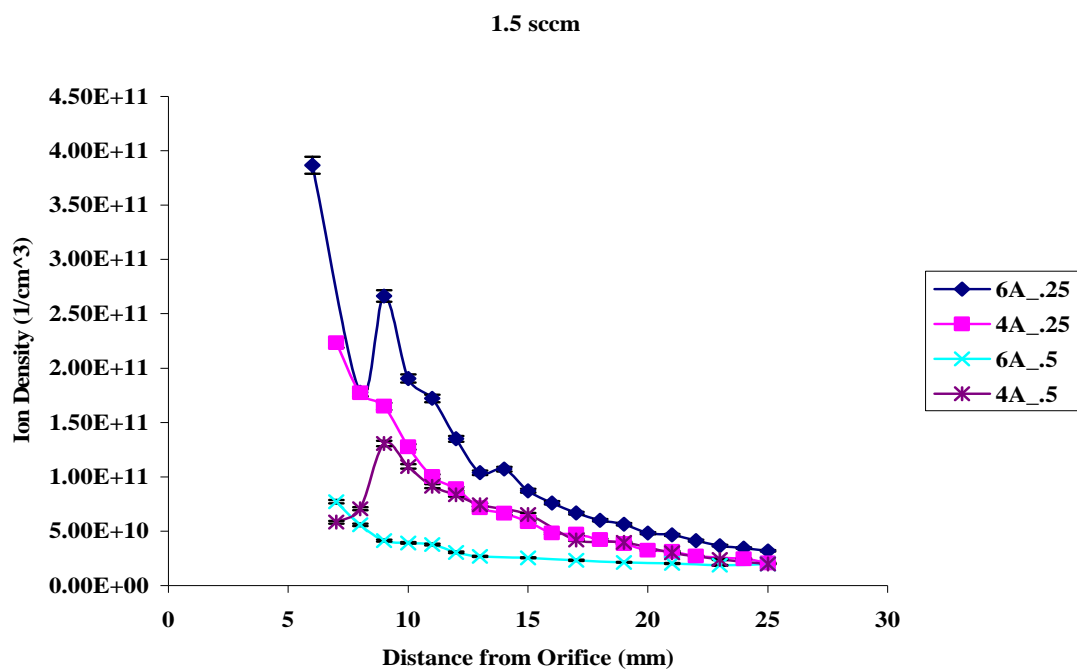
Figure 63. Comparison between AR.5 and AR.25 Ion Density at 1.5 sccm
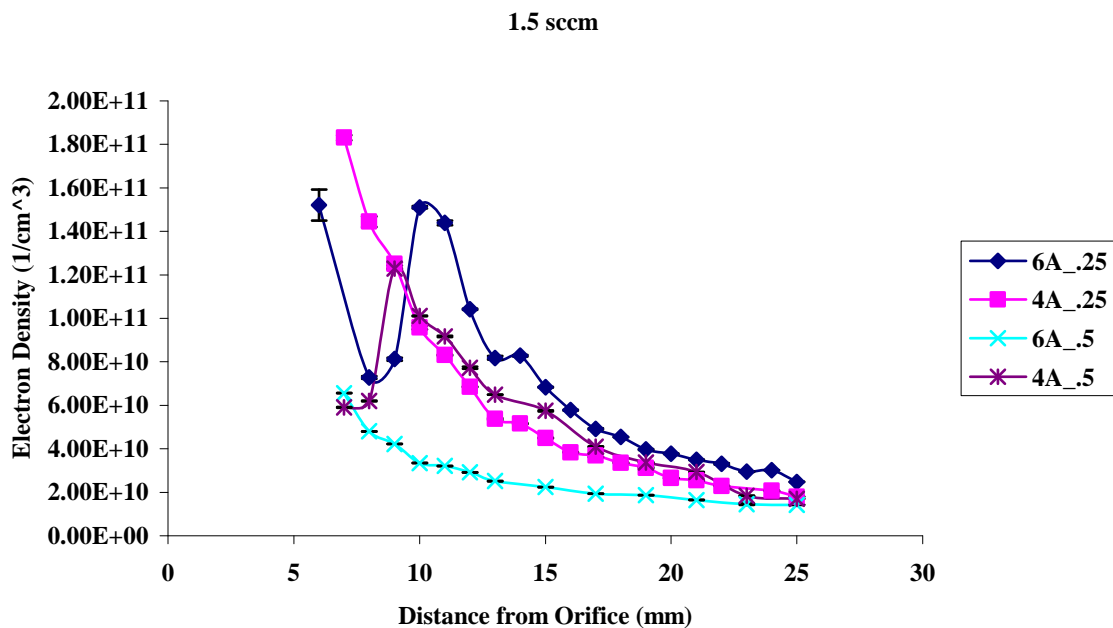
Figure 64. Comparison between AR.5 and AR.25 Electron Density at 1.5 sccm

The plasma potential for the AR.25 cathode was higher than the AR.5 cathode for low flow rates and anode currents. At 1.5 sccm, the electron temperatures were lower with the AR.25 cathode than the AR.5 one. After reviewing the floating potential curves, they were lower by 2-3 volts in the regions of higher plasma density; otherwise, the floating potential was nearly constant along the axis of the cathode with no jumps.

With the anode current set to 6 A at 1.5 sccm with the keeper off, it was the only condition evident of any plume mode-like behavior for all the AR.25 test points. Initially the voltage showed no signs of any large oscillations, then once the probe got close to the cathode orifice, it suddenly induced plume mode, Figure 65. The highest amplitude oscillation here was from the power supply trying to regulate the anode voltage as the impedance of the plasma increased.
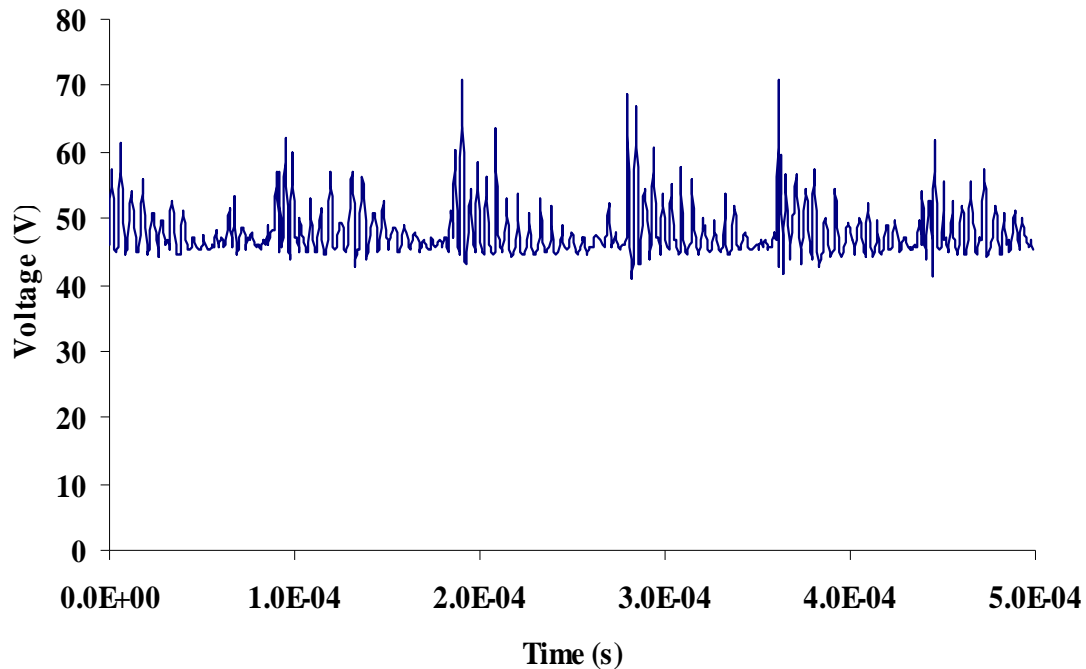
Figure 65. Plume-Mode for AR.25 with 6A Anode Current at 1.5 sccm
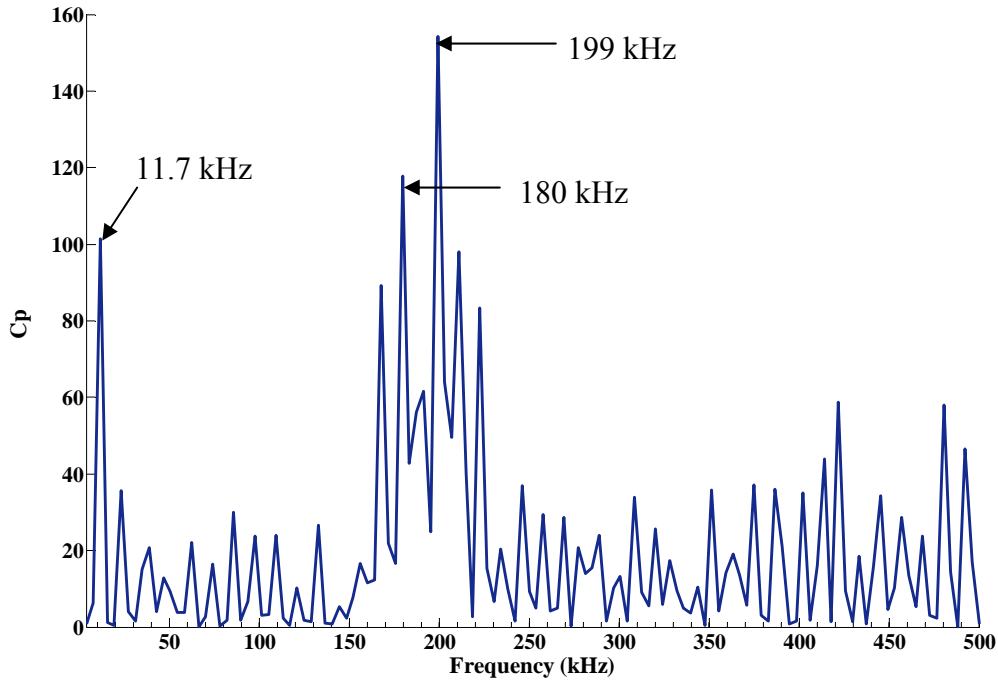
Figure 66. FFT Analysis of Anode Voltage for 6A anode current at 1.5 sccm for AR.25

Cathode

Figure 66 is the Fourier analysis power spectrum of the anode voltage waveform in Figure 65. The three dominant frequencies observed are 11.7, 180, and 199 kHz. The lowest harmonic could be from power supply regulation. The latter two frequencies are within the same range observed by Goebel et al for energetic ion production within and at the edge of plasmoids.[34] The waveforms above do not indicate a location of the oscillations within the plasma. Instead they indicate the presence of oscillations throughout the coupling plasma and its effects on the anode and keeper voltage.

As the anode voltage drastically increases, the ionization percentage in the plume becomes significant and can lead to ionization instabilities.[15] The plasma uses up a large portion of the neutral gas and the discharge collapses within the time it takes neutral flow

to replenish the starved region.[15] During the significant ionization event, high energy

ions may be created from localized plasma regions and accelerate cathode erosion.

The plume mode oscillations in the above figure were apparent in the I-V curve as

well. A phenomenon also observed by Martin and Williams.[35] After pulling the probe

away from the cathode, it stayed in plume mode until turning the keeper back on.

Additionally, after turning the keeper off, the cathode did not return to plume mode until

the probe re-entered the plasma near the orifice. The probe induced plume mode after

repeated attempts to measure close to the keeper orifice. However, the density curves

presented in Figure 63 and Figure 64 were collected before the cathode made the

transition. This shows the state of the coupling plasma before the onset of plume mode.

As observed in other cases, when a localized region of plasma forms with no AC

oscillations or elevated anode voltages, I concluded the cathode was at an intermediate

between spot and plume mode.

This phenomenon showed how much this Langmuir probe affected the plasma

and ultimately the data collected. The Langmuir probe's presence increased the anode

voltage the closer it was to the cathode because it introduced additional impedance

between the cathode and anode and geometrically interfering with the plasma discharge.

For 2 A anode current at 1.5 sccm, the anode voltage increased by 1.5 volts when the

Langmuir Probe was within 10 mm of the keeper orifice. See Figure 67.

Anode
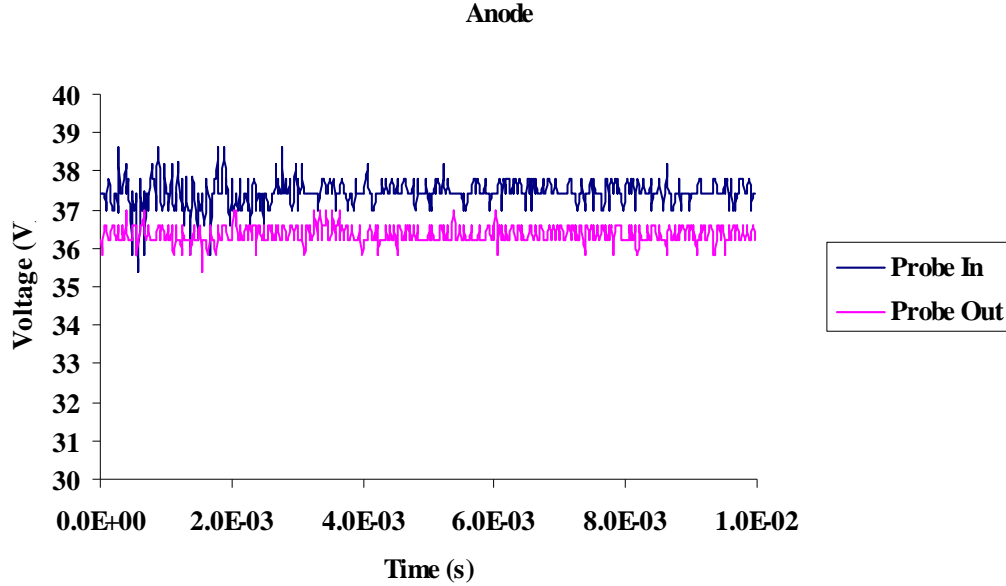
Figure 67. Langmuir Probe Perturbation

The impedance of the plasma increases during plume mode.[33,43] For the 6 A low flow condition, the cathode could be at a transition point, only needing a small perturbation to affect its impedance, and ultimately tip it into plume mode operation. However, despite the measured electron temperatures being slightly higher in this case, they were not indicative of "full plume mode" characteristic of average electron temperatures as high as 8 eV.[35,36] Martin and Williams also observed some measurable perturbation using high-speed probes, designed to minimize perturbations to the plasma. With their research, the probe had a larger effect on the coupling plasma at lower flow rates, also observed here.

In summary, the LaB_6 cathode showed better performance with a smaller aspect ratio. The electron temperatures were lower, the ion and electron densities were higher, but the plasma potential was higher for some conditions. The key observation about the

97

smaller aspect ratio, was it allowed the cathode to run as low as 1.4 A with the heater and

keeper turned off at 1.5 sccm of xenon flow. The only reason the cathode did not operate

any lower was because the anode voltage exceeded the voltage limit of the power supply.

The smaller aspect ratio also allowed the cathode to run in a stable intermediate similar to

spot mode as high as 6 A at 1.5 sccm with the keeper on and heater off. Tables 1 and 2

are the complete sets of test conditions for the LaB_6 cathode and its mode of operation for

each aspect ratio. Anode and keeper voltages, currents, and flow rates are included.

Mass Flow (sccm)	J_a (A)	J_k (A)	V_a (V)	V_k (V)	Mode
6	6	1	26.26	15.89	Spot
		0	25.57	N/A	Spot
	4	1	27.91	18.22	Spot
		0	27.72	N/A	Spot
	2	1	30.44	20.34	Spot
		0	31.18	N/A	Spot
4.5	6	1	26	16.22	Spot
		0	26.72	N/A	Spot
	4	1	27.43	17.83	Spot
		0	27.84	N/A	Spot
	2	1	30.23	20.63	Spot
		0	30.95	N/A	Spot
3	6	1	28.46	17.06	Spot
		0	29.36	N/A	Spot
	4	1	30.16	19.24	Spot
		0	30.89	N/A	Spot
	2	1	37.51	25.51	Spot
		0	39.18	N/A	Spot
1.5	6	1	32.17	19.48	Intermediate
		0	48.17	N/A	Plume w/probe
	4	1	31.62	21.31	Spot
		0	34.36	N/A	Spot
	2	1	38.89	25.46	Spot
		0	42.34	N/A	Spot

Table 1. AR.25 LaB_6 Performance Summary

Mass Flow (sccm)	J_a (A)	J_k (A)	V_a (V)	V_k (V)	Mode
4.5	4	1	26.1	17.6	Spot
	2	1	32.4	23.6	Spot
3	6	1	27.78	25.15	Spot
		0	31.45	N/A	Spot
	4	1	28	18.4	Spot
	2	1	33.3	23.75	Spot
1.5	6	1	30.43	19.88	Intermediate
		0	34	N/A	Intermediate
	4	1	31.9	24.05	Spot
		0	35.24	N/A	Intermediate

Table 2. AR.5 LaB$_6$ Performance Summary

Only some data is available for the AR.5 geometry. The cathode did not

transition into plume mode at 6 A anode current at 1.5 sccm. However, it seemed as if it

were at an intermediate operating condition. Much higher electron temperatures were

expected for plume mode than observed. Consequently, I chose to rely more heavily

upon waveform monitoring and density curves when distinguishing between modes. A

combination of the localized plasmas, high anode voltages, and high frequency

oscillations may allow for the creation of high-energy ions that limit cathode life, and is

more indicative of plume mode rather than localized plasma alone. The only operating

condition indicative of plume mode is 6 A anode current at 1.5 sccm with the keeper

turned off for the AR.25 cathode.

Direct conclusions about the performance of this cathode in an ion or hall thruster

require some additional work (i.e. including a magnetic field for ion thruster

applications). Without a magnetic field, the ionization efficiency is poor, shown by the

purple plasma in Figure 87, indicative of high neutral densities rather than ions. These

data can be used to better understand cathode phenomena as a whole, in addition to how the boride cathodes behave as a part of this family and that they demonstrate the ability to operate over the same current and flow ranges as other hollow cathodes.

CeB_6 Cathode

The CeB_6 cathode underwent tests for one aspect ratio of 0.5. The plots included in this section have a comparison to the LaB_6 cathode with the same aspect ratio. The ion densities from the CeB_6 cathode were higher than the LaB_6 cathode, Figure 68 and Figure 69. The exception was for the highest anode current, where the density dropped off after 13 mm from the CeB_6 cathode. The same trend was apparent in Figure 70 and Figure 71 for electron density.
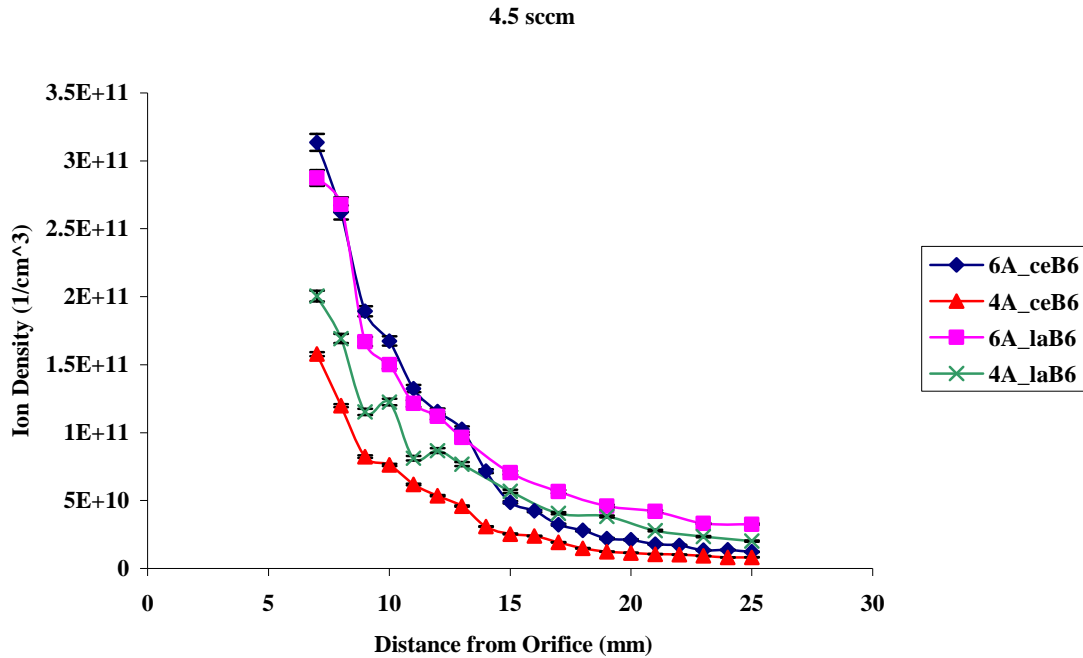
4.5 sccm

Figure 68. CeB_6 & LaB_6 Ion Density Comparison at 4.5 sccm
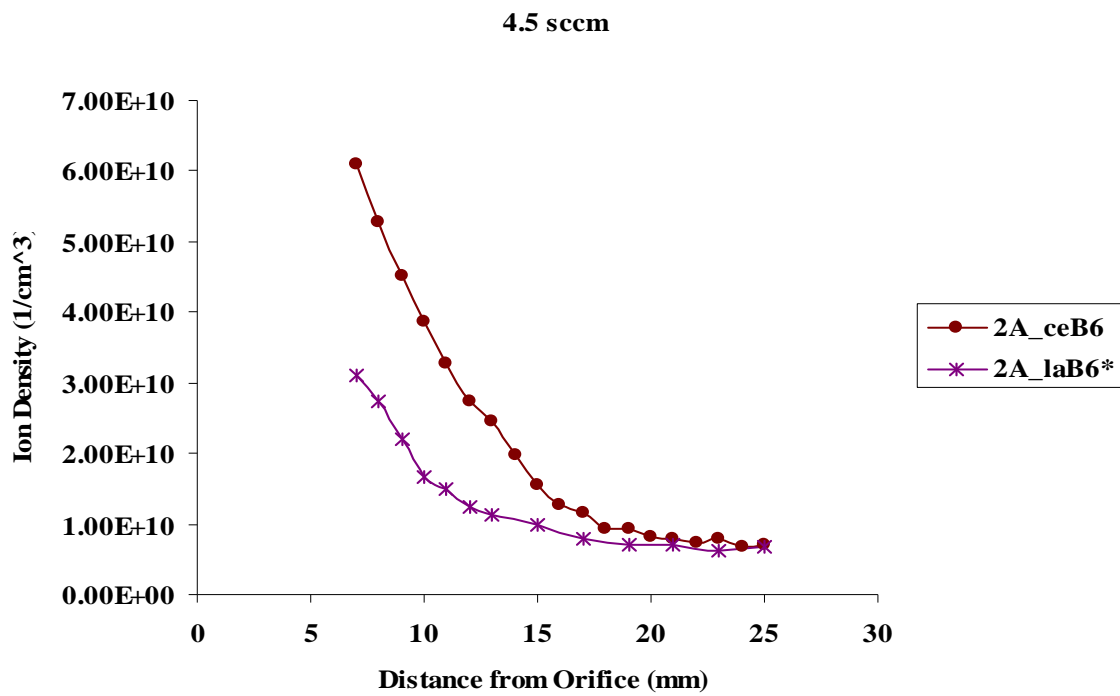
4.5 sccm

Figure 69. CeB$_6$ & LaB$_6$ Ion Density Comparison at 4.5 sccm (2) *Keeper On
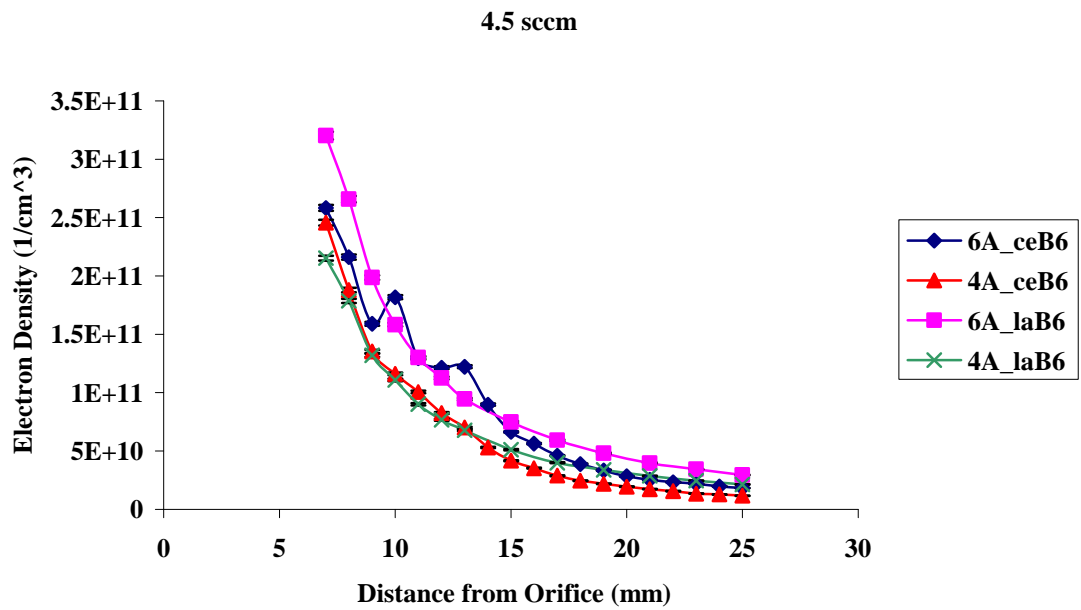
4.5 sccm

Figure 70. CeB$_6$ & LaB$_6$ Electron Density Comparison at 4.5 sccm

101
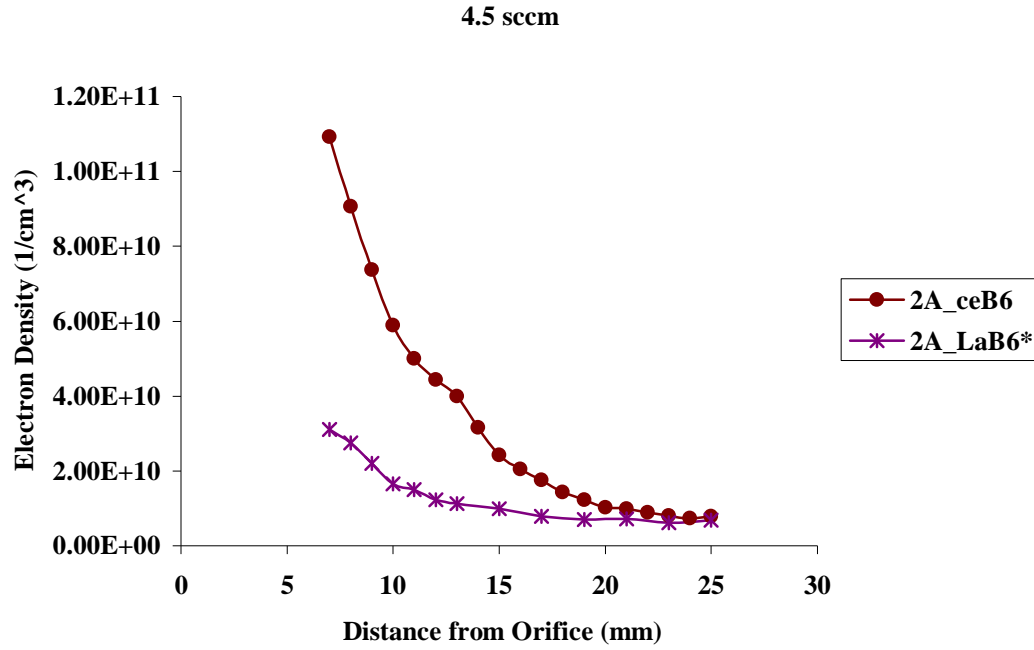
4.5 sccm

Figure 71. CeB$_6$ & LaB$_6$ Electron Density Comparison at 4.5 sccm (2)

As a whole, the LaB$_6$ cathode had the highest electron temperature and the CeB$_6$ the lowest, in Figure 72, which only shows the case for 4.5 sccm. For plasma potential however, the LaB$_6$ cathode had the highest potentials at 4.5 sccm. At 3 sccm, the plasma potential was slightly higher from the LaB$_6$ cathode for two of the three anode current settings. Plasma potential did not change considerably between flow rates; the most significant factor was the anode current. Figure 73 is a plot of the average plasma potential as a function of flow rate and anode current. Neither cathode had a significant advantage over the other. This demonstrated the similarities CeB$_6$ and LaB$_6$ have rather than the differences. Up to this point, CeB$_6$ produced slightly higher densities but with similar electron temperatures and plasma potentials as LaB$_6$.
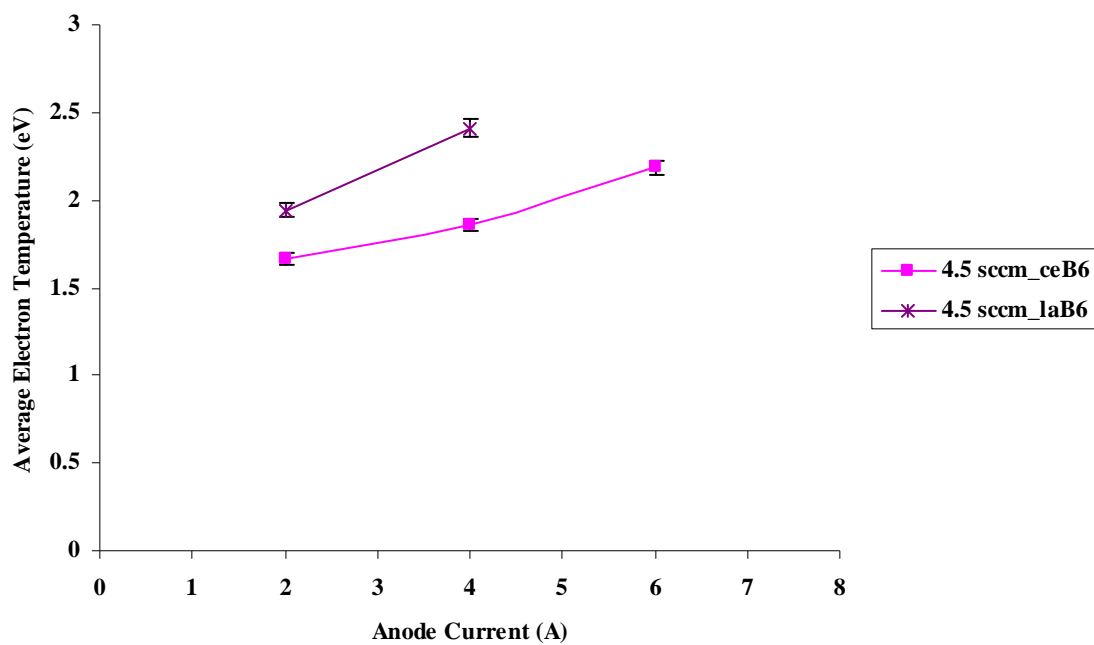
Figure 72. CeB$_6$ & LaB$_6$ Average Electron Temperature Comparison

Figure 73. CeB$_6$ & LaB$_6$ Average Plasma Potential Comparison

At 3 sccm no localized regions of plasma appeared within the plume of the CeB_6 cathode in either Figure 74 or Figure 75. The CeB_6 cathode had slightly higher ion and electron densities at 3 sccm than the LaB_6 cathode. This difference was more apparent between the cathodes at lower flow rates. None of the above conditions was indicative of plume mode behavior at all after reviewing their anode and keeper voltage waveforms.
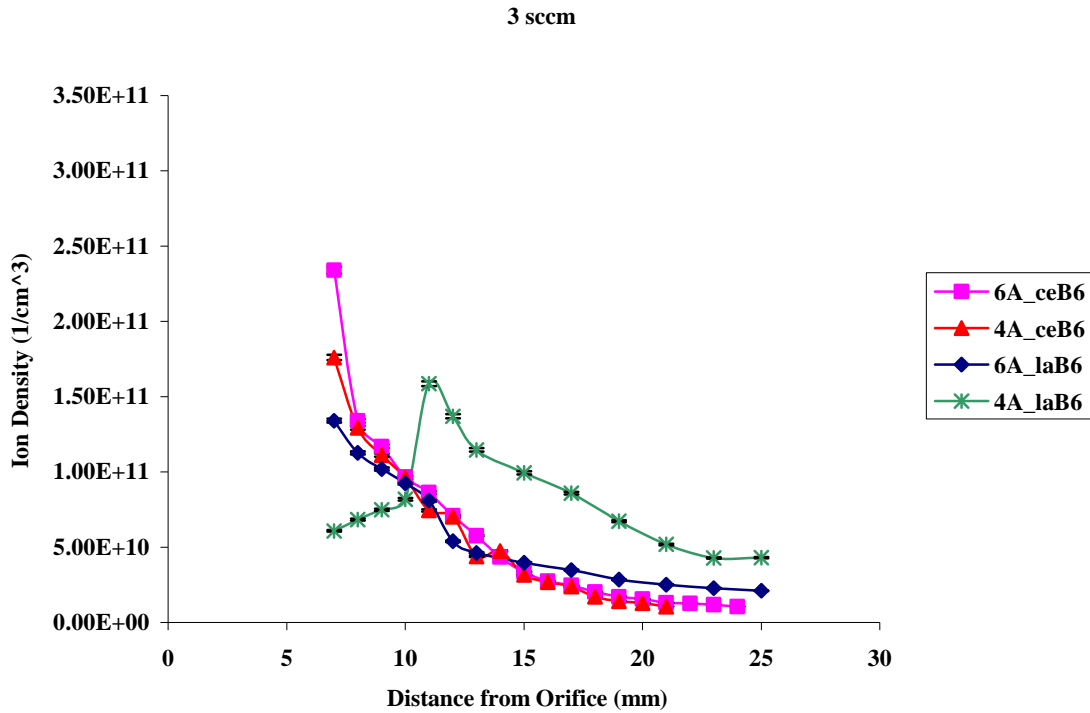
3 sccm

Figure 74. CeB_6 & LaB_6 Ion Density Comparison at 3 sccm
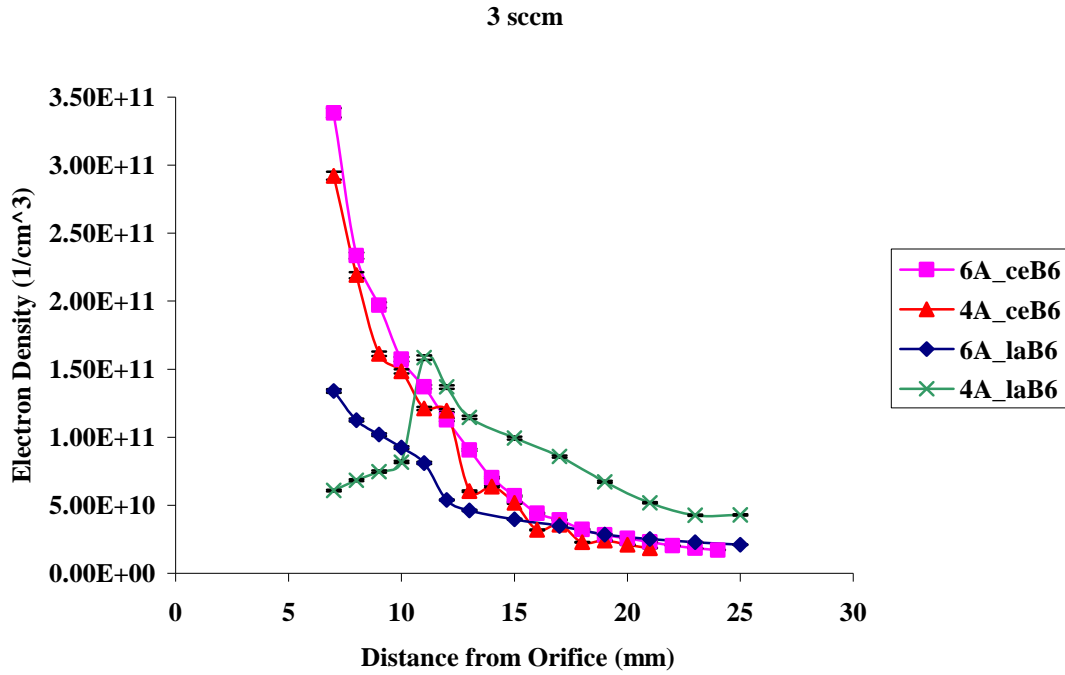
3 sccm

Figure 75. CeB$_6$ & LaB$_6$ Electron Density Comparison at 3 sccm

Localized regions of plasma appeared for both cathodes at 1.5 sccm in Figure 76 through Figure 79. As described by Goebel and Martin, the plasma balls/plasmoids form closer to the cathode at lower flow. For instance, the LaB$_6$ cathode peak density occurred at 9 mm at 1.5 sccm and 11 mm at 3 sccm. While plasma balls were not present in Figure 75 for most conditions, there are some jumps in density observed for 4 A anode current from the LaB$_6$ cathode. It is not clear why there was such a significant jump in electron density for the CeB$_6$ cathode at 4 A anode current. However, the ion densities agreed well between cathodes.
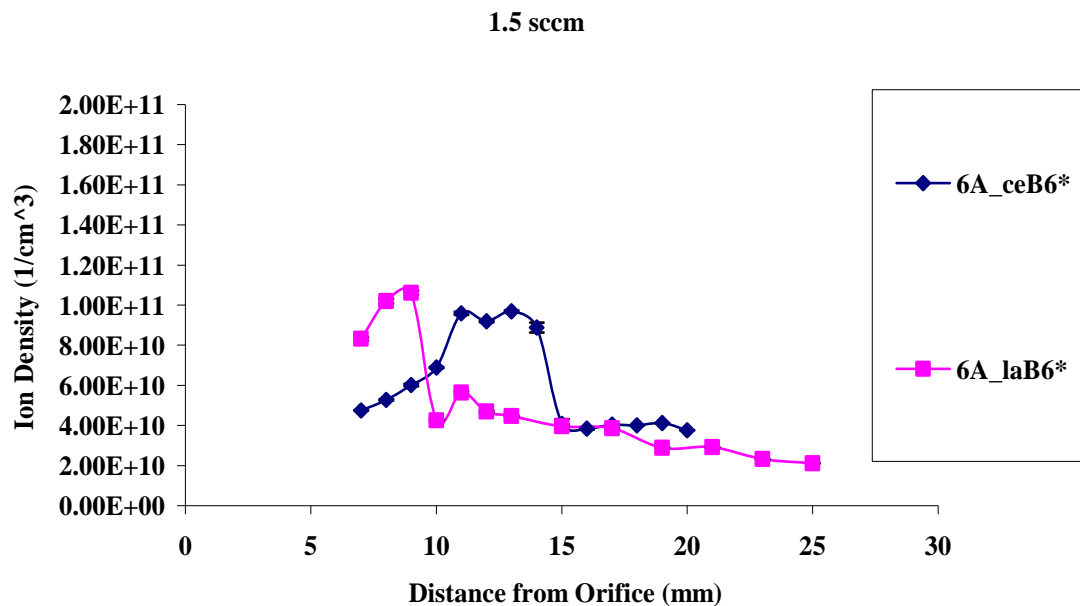
Figure 76. CeB$_6$ & LaB$_6$ Ion Density Comparison at 1.5 sccm

*Keeper on
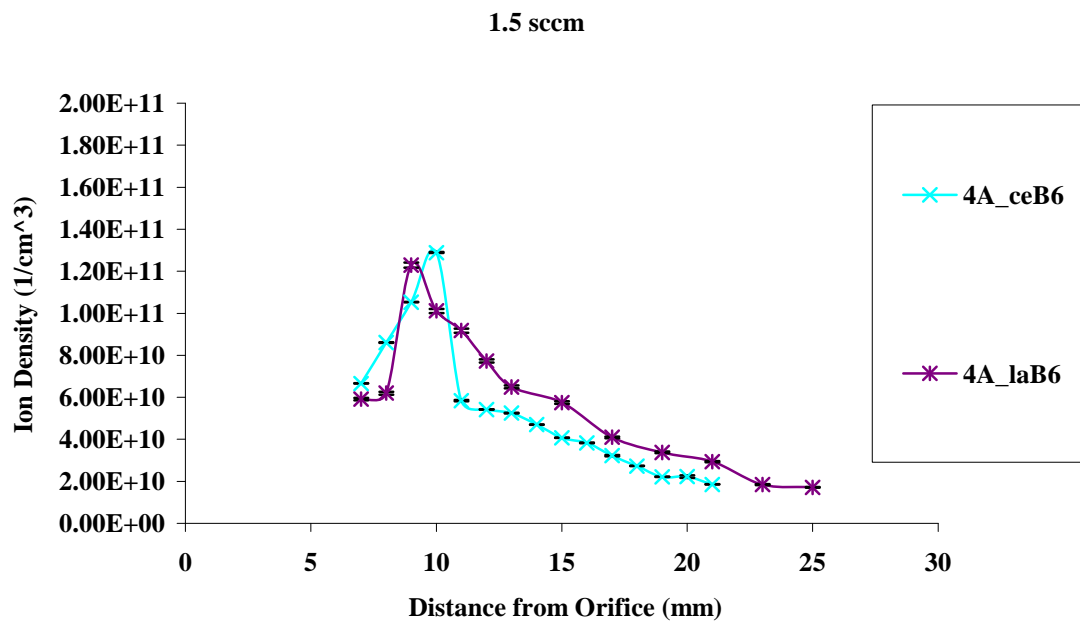
Figure 77. CeB$_6$ & LaB$_6$ Ion Density Comparison at 1.5 sccm (2)
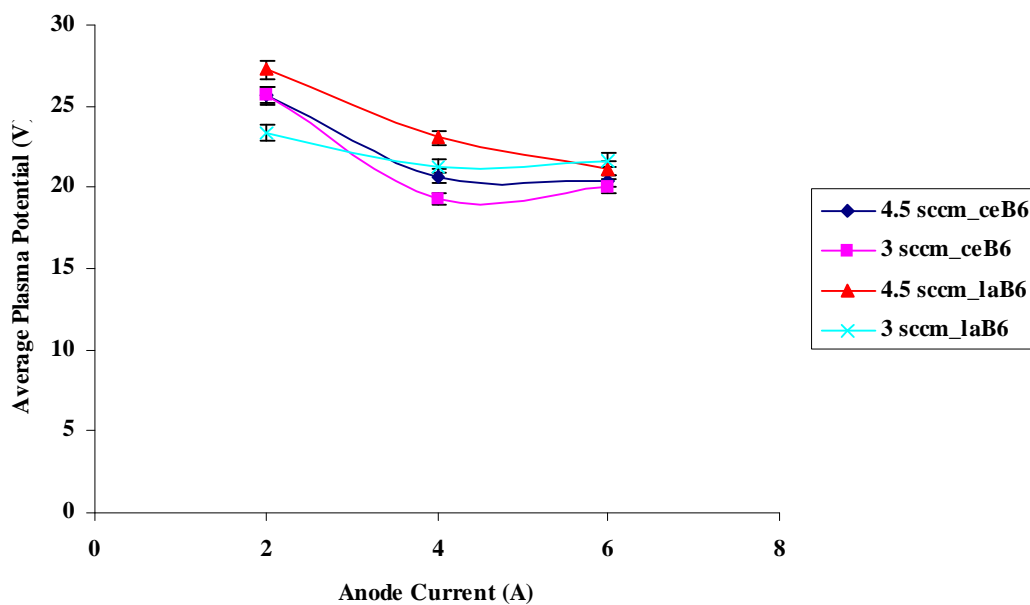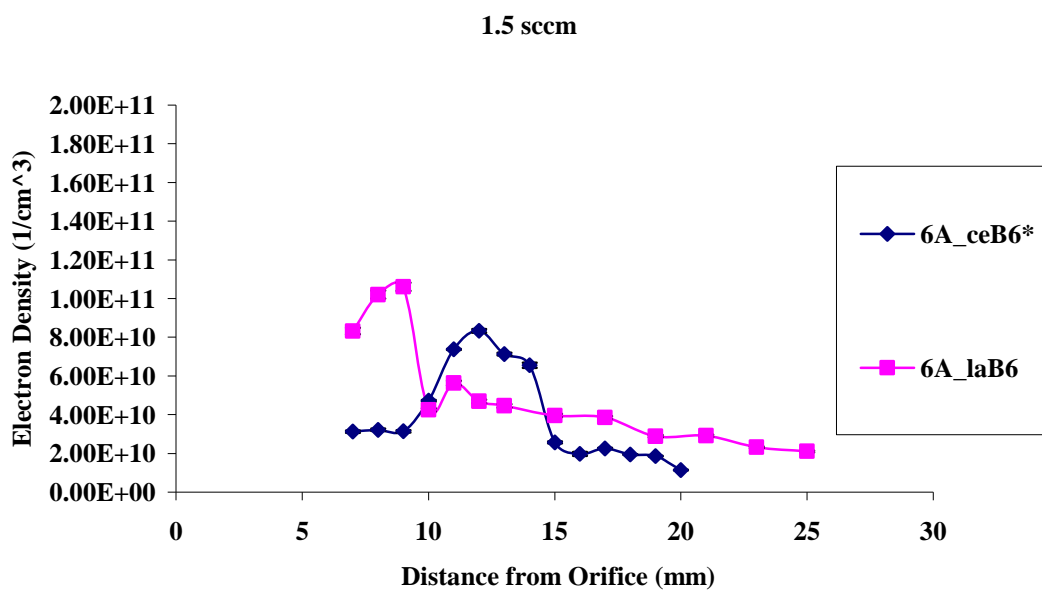
Figure 78. CeB$_6$ & LaB$_6$ Electron Density Comparison at 1.5 sccm
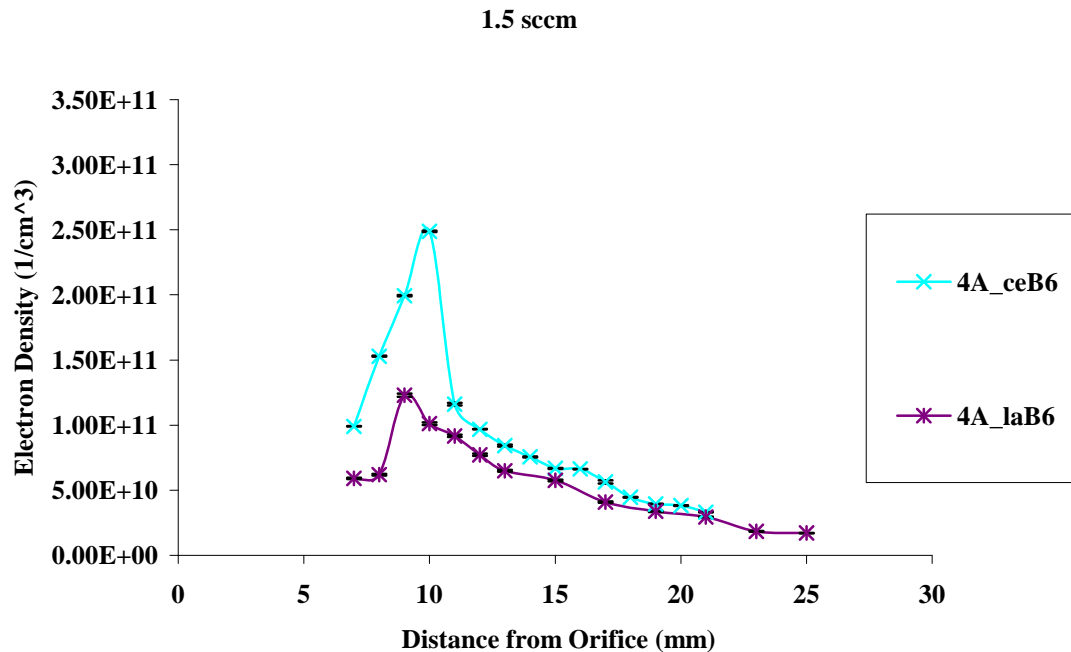
Figure 79. CeB$_6$ & LaB$_6$ Electron Density Comparison at 1.5 sccm (2)

Finally, the plasma floating potential in Figure 80 behaved the same way as previously described when plasma balls/plasmoids formed. Where the potential suddenly dropped, there was a sharp increase in density, and where the potential spiked, there was a decrease in density. This behavior occurred every time a plasmoid formed.
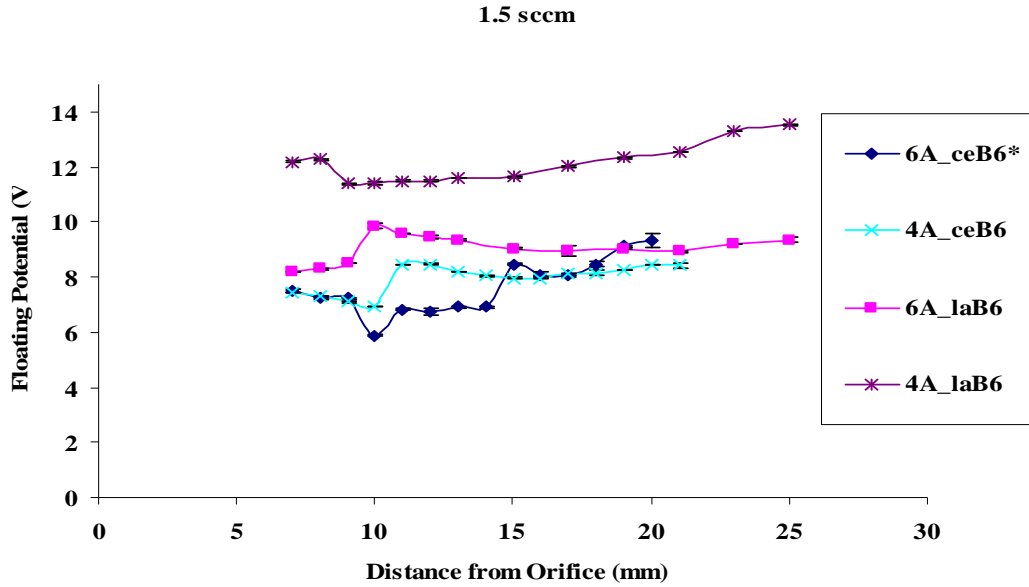
1.5 sccm

Figure 80. CeB$_6$ & LaB$_6$ Floating Potential Comparison at 1.5 sccm

The CeB$_6$ cathode's voltage waveforms were very similar to that of the LaB$_6$ cathode at 1.5 sccm. Spot mode occurred for anode currents below 6 A. There were some oscillations, but the amplitude was less than 5 volts, characteristic of normal ionization events.[15] When the anode current was set to 6 A with the keeper on, the cathode transitioned into plume mode. Having the keeper on or off did not induce or eliminate plume mode in this case. Keeper operation did reduce the amplitude and frequency of the anode current oscillations as it did for the LaB$_6$ cathode, but did not appear to eliminate plume mode. It is not entirely clear why this was the case, as the

LaB$_6$ cathode transitioned back into spot mode when the keeper was on in other instances.

As one can see in Figure 81 and Figure 83, the anode voltage oscillation is typically a sharp increase in potential, while the keeper electrode experiences a sudden drop. If density increases with decreasing potential, then the large positive spikes in anode voltage are an event where the anode power supply is struggling to regain the current it needs to continue the discharge. The anode effectively demands more plasma and the keeper behaves as if it compensates its potential to deliver. As the keeper potential drops the plasma density increases shortly to answer the current demand. Fourier analysis of the waveform in Figure 81 shows the two primary frequencies in the anode voltage oscillations were 59 and 644 kHz. The anode's voltage signal was dominated by frequencies below 1 MHz, having the highest strength for oscillations below 700 kHz. The keeper voltage oscillations were obviously lower in strength. Its two primary harmonics were 59 and 117 kHz. 59 kHz was the primary frequency for both the anode and keeper during plume mode. These data show a coupling effect between the anode and keeper when the cathode is in plume mode. Fourier analysis in Figure 84 confirmed the anode-keeper coupling as well. The keeper's signals were also weaker and more frequency harmonics coincided between the anode and keeper voltage signal in Figure 84 than Figure 82. 39 kHz was the primary harmonic for the keeper and the anode voltage signal in the latter case. Another harmonic that occurred in the keeper and anode voltage signal was 48 kHz. This further supports the coupling behavior between the anode and keeper oscillations during plume mode. All of the primary

109

frequency harmonics in the above figures were within the range needed for high-energy

ion production as postulated by Goebel et al.[34]
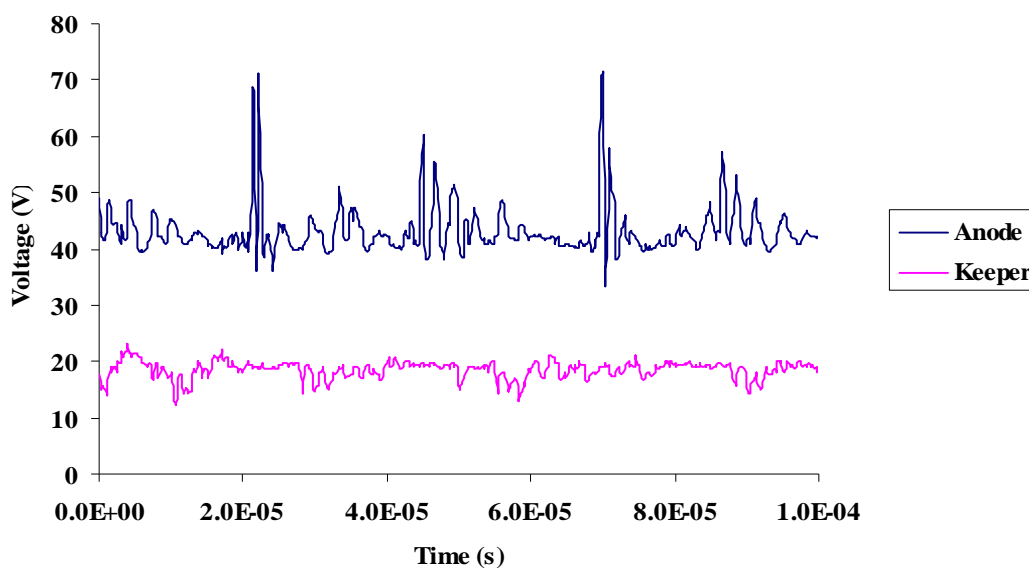
Figure 81. CeB$_6$ Cathode Plume Mode for 6A Anode, 1 A Keeper at 1.5 sccm
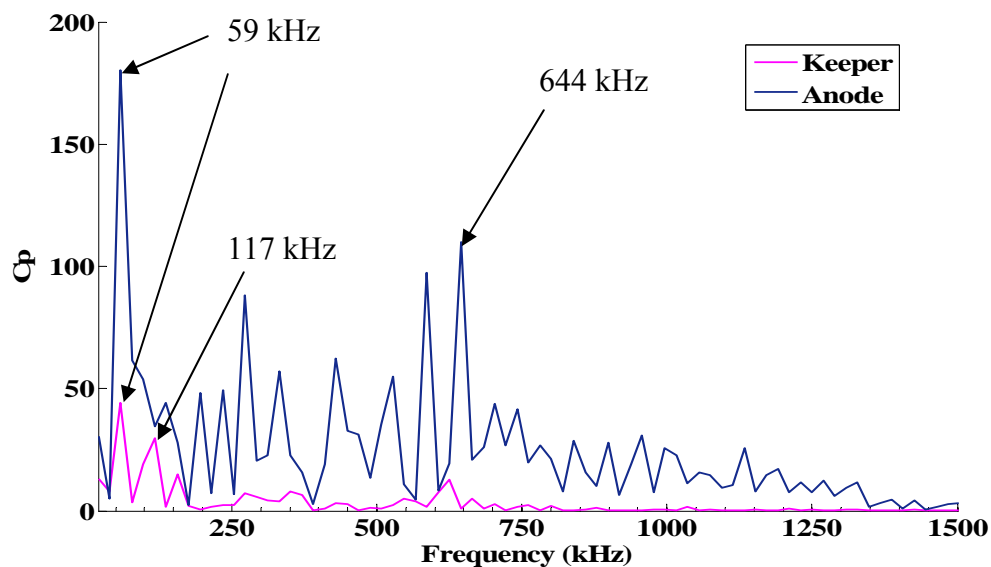
Figure 82. FFT Analysis of CeB$_6$ Cathode Plume Mode for 6A Anode, 1 A Keeper at 1.5
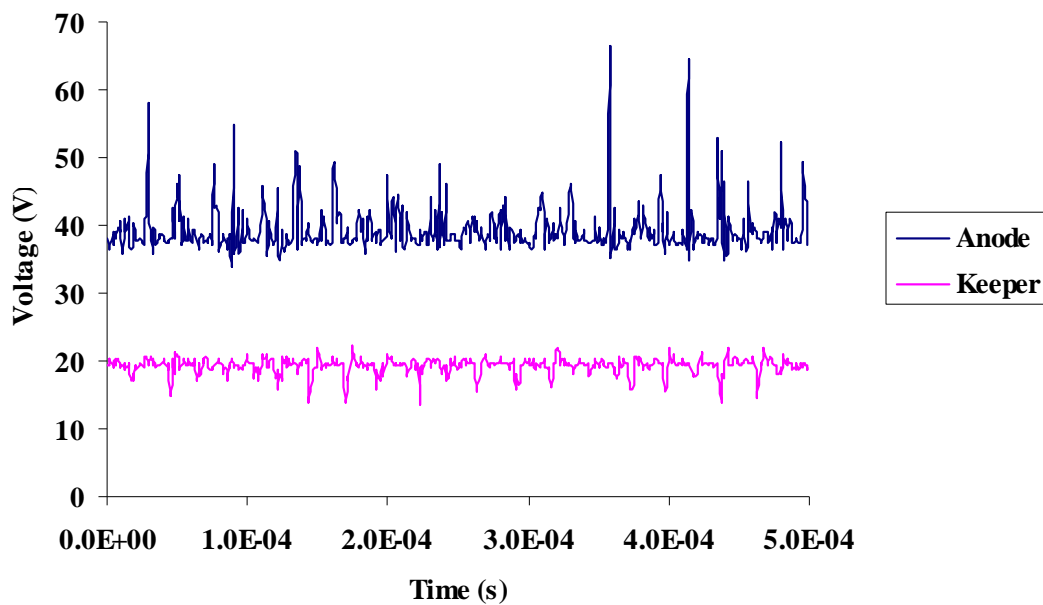
sccm

Figure 83. 2nd CeB$_6$ Cathode Plume Mode for 6A Anode, 1 A Keeper at 1.5 sccm
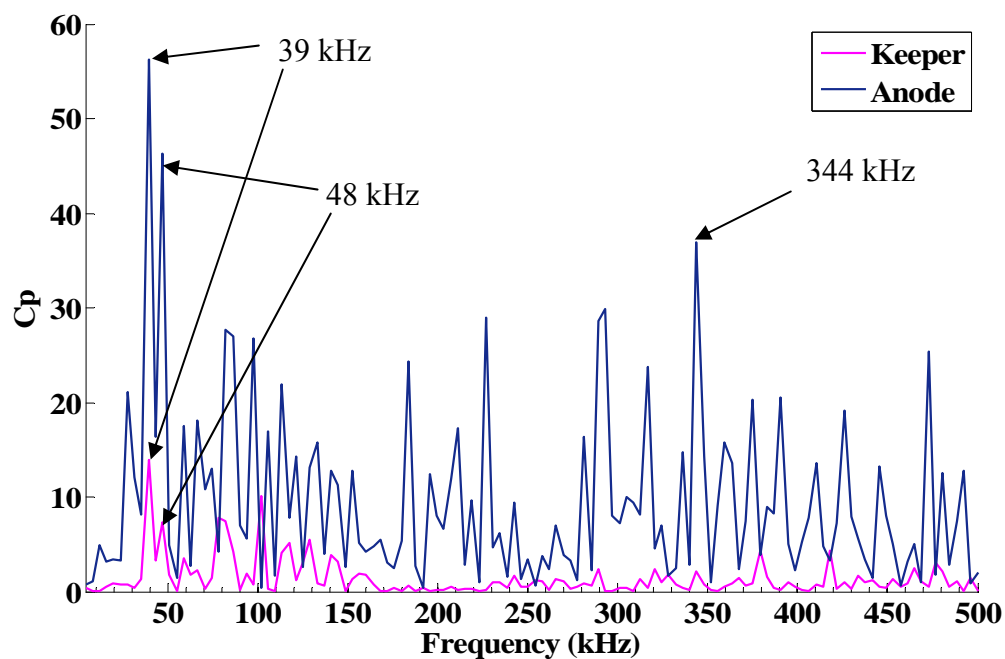
Figure 84. FFT Analysis for 2nd CeB$_6$ Cathode Plume Mode for 6A Anode, 1 A Keeper

at 1.5 sccm

111

For each test point determined to be in plume mode as the waveform in Figure 81 and Figure 83 shows, the color of the plasma was very different from other modes like Figure 39. During full plume mode, the plasma was blue and while during spot mode, it was light purple, Figure 85 and Figure 87. The intermediate is a mix of these and its color is a bluish purple, Figure 86. The camera settings were identical for each picture. When the plume is blue, there is higher presence of fully ionized xenon and low neutral density.[12,16] When the discharge is starved of propellant, the higher anode potentials of plume mode exhausts the neutral density supply and forces the plasma population to have more ionized xenon, resulting in a blue plume. During purple discharge, the ionization efficiency is poor, there is a higher concentration of excited neutrals, and less ionized xenon. The intermediate has a mix of neutrals and ions. These colors are dependant on the species and not their energies. Although the plume has lower ion densities during spot mode, it does not mean this is an inefficient mode. The only reason the discharge is purple during spot mode is there is no magnetic field to increase the path length of the electrons and improve ionization efficiency. If a magnetic field were present, both plumes would be blue. However, this is not critical for testing integration into a Hall thruster.
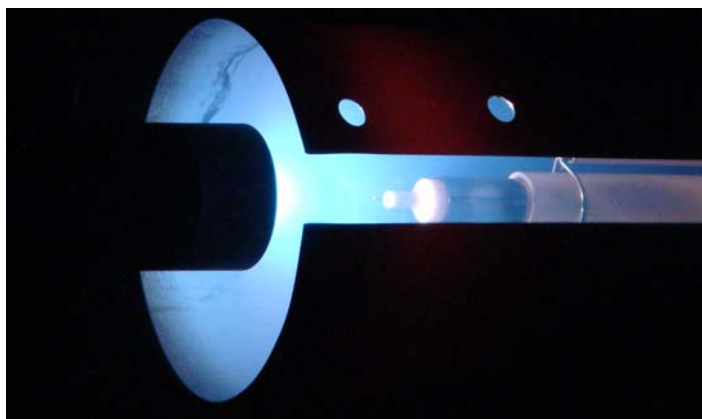
Figure 85. LaB$_6$ Cathode in Plume Mode
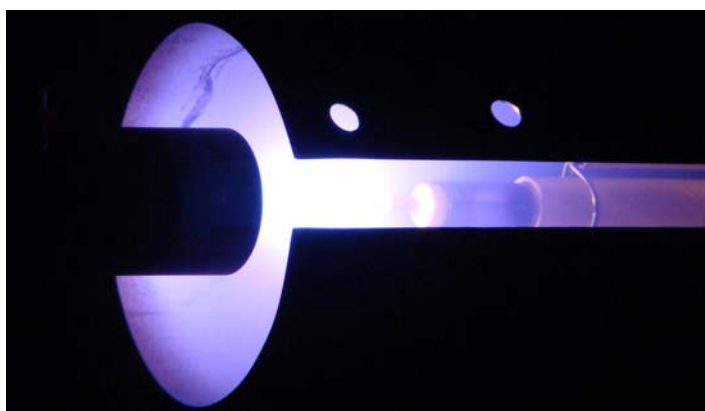
Figure 86. LaB$_6$ Cathode in Intermediate Mode
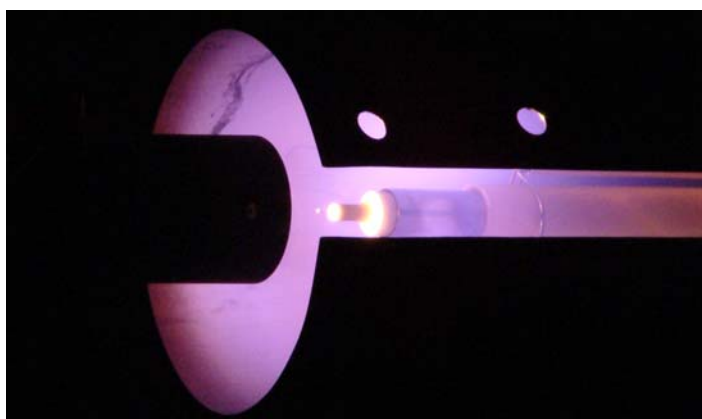
Figure 87. LaB$_6$ Cathode in Spot Mode

An interesting side note that highlights the importance of time resolved data for plasma discharges is Figure 88. Over the course of 10 minutes, at 1.5 A anode current and 1.5 sccm with both the heater and keeper off, the anode voltage increased with time. The poisoning section discusses the mechanism for this cause. Cooling may also increase the anode current as the temperature drops. The coupling plasma compensates for this decrease in emission from the insert and results in higher anode voltages.
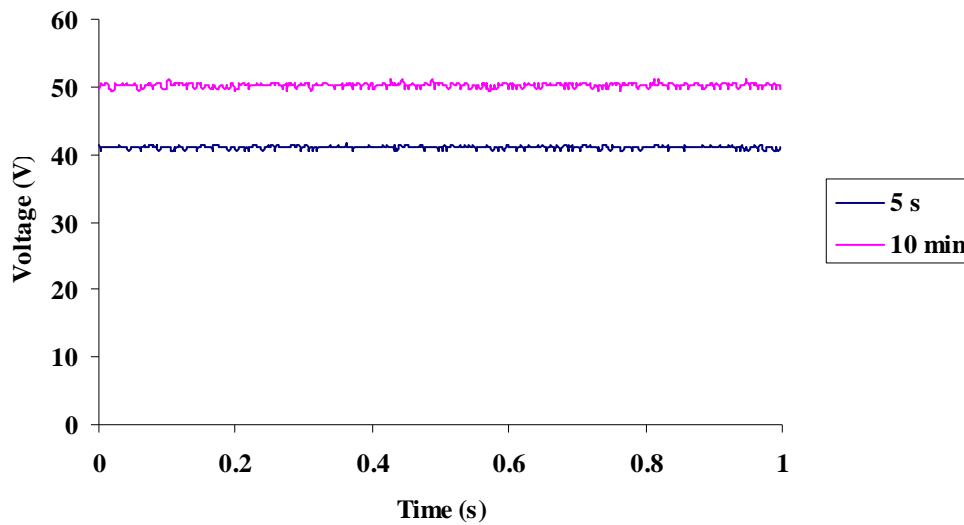
Figure 88. CeB$_6$ Anode Voltage for 1.5A Anode Current at 1.5 sccm

Collectively, the CeB$_6$ cathode performed very closely to the LaB$_6$ cathode. The electron temperatures were about the same and the plasma potentials were slightly lower than the LaB$_6$ cathode in some cases. It operated in spot mode for all conditions but one. The ion and electron densities were on the same order as the LaB$_6$ cathode. However, for the larger aspect ratio the minimum operating point for the LaB$_6$ cathode was 2.5 A with no heater or keeper power at 1.5 sccm. For the same orifice geometry, the CeB$_6$ cathode ran as low as 1.5 A at 1.5 sccm with the heater and keeper turned off. This showed CeB$_6$

114

had a lower operating limit because it may have had a lower work function and required less heat to maintain the same current density as its LaB_6 counterpart. On the other hand, it may have had a lower emissivity and actually run hotter, resulting in higher emission current densities. IR imaging helped to answer this question. Table 3 is a summary of the CeB_6 cathode with its respective voltages, currents, and mode of operation.

Mass Flow (sccm)	J_a (A)	J_k (A)	V_a (V)	V_k (V)	Mode
4.5	6	0	23.6	N/A	Spot
	4	1	23.43	17.12	Spot
		0	23.59	N/A	Spot
	2	1	23.54	22.62	Spot
		0	32.85	N/A	Spot
3	6	1	25.95	16.45	Spot
		0	25.09	N/A	Spot
	4	1	27.9	18.18	Spot
		0	29.28	N/A	Spot
	2	1	25.9	25.6	Spot
		0	32.47	N/A	Spot
1.5	6	1	42.9	18.53	Plume
		0	43.09	N/A	Plume
	4	1	27.89	N/A	Intermediate
		0	31.19	N/A	Intermediate
	2	1	30.68	27.89	Spot
		0	36.36	N/A	Spot

Table 3. CeB_6 Performance Summary

After review of this table, the CeB_6 hollow cathode did not provide a significant advantage over LaB_6. The heater power requirements were the same and the ignition power requirements were slightly lower for CeB_6. During operation the discharge and keeper power (when it was on) were essentially the same, varying by only a few watts, discussed in the IR imaging section. It also had a similar plume mode transition as the other cathodes.

Infrared Imaging Analysis

The primary purpose for IR imaging was to determine which cathode was hotter and how this played into evaporation (lifetime) and poisoning. Low current cathodes run at lower temperatures, as described by the Richardson-Duschman relationship. When the insert temperature is sufficiently high, poisoning from other gases are not a problem and does not affect the life of the boride cathodes. However, when the temperatures are too low, the tolerance to poisoning decreases and may reach a point where it provides no advantage over impregnated cathodes. Even if the boride cathodes were susceptible to poisoning at lower currents, they do provide the advantage of demonstrating the ability to regain performance after high temperature bake-out. IR imaging also provides the information necessary for correlating evaporation rate and temperature. Goebel makes a direct comparison between LaB_6 and impregnated cathode's evaporation rates and lifetimes.[2] He also provides correlations between evaporation rate and emission current density. His results show LaB_6 having a lower evaporation rate than type B impregnated cathodes at emission current densities below 14 A/cm^2. The temperature information collected here will reveal the operating temperatures of these cathodes and their potential evaporation rates can be deduced.

To collect this important temperature data, each cathode was positioned at the center of the vacuum chamber facing the ZnSe window. Both cathodes' geometry and distance to the anode was identical to guarantee the only variable between them was the insert material. The orifice plates were assumed parallel with the ZnSe window. The author made every effort to ensure this was the case. The FLIR® camera can select regions of the image for analysis, Figure 89 shows the LaB_6 cathode and the location

selected. Thermocam® software calculated the maximum and minimum temperatures of the circle indicator.   An average was not used because the emissivity changes with temperature over the orifice plate.
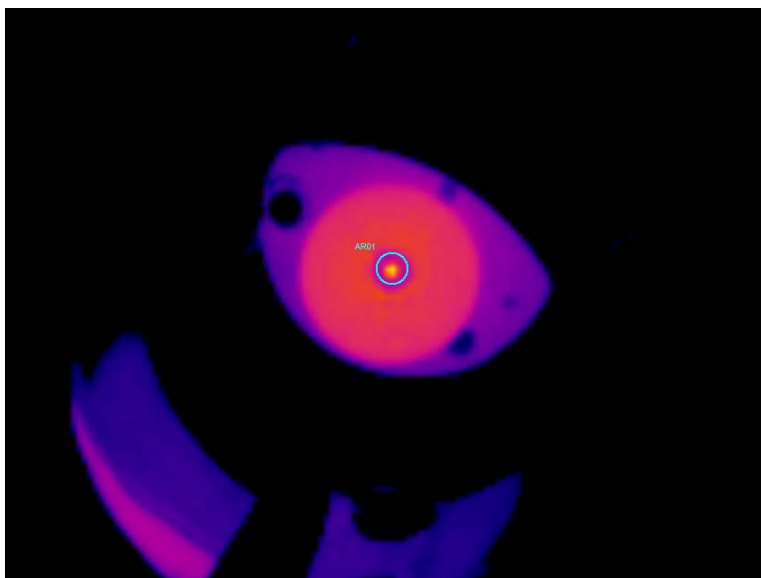
Figure 89. IR Image of LaB$_6$ Cathode with Circle Indicator

The first step with IR imaging was calibrating the camera with the total normal emissivity of the tantalum orifice plate. Emissivity values were available in literature, but considered unsuitable for these tests. The values reported from one source for a 2 mm tantalum wire operating in the range expected for these cathodes never exceeded 0.25.[44] After correcting for the ZnSe window, using this emissivity in the camera caused the orifice plate temperature to exceed the expected operating temperature by a few hundred degrees Celsius. This was not realistic since these cathodes were operating at very low current compared to past research.[2] Many factors play into emissivity values such as surface finish, material composition, etc. To ensure accurate results were possible, the best way to calibrate the camera was to put the cathode into the chamber,

turn the heater on to its power limit, and take thermocouple readings and IR images from the tantalum orifice plate directly. By using the Stefan-Boltzmann relationship for radiation, the emissivity of the tantalum orifice plate was calculated from equation 8.

$$\varepsilon = \frac{T_{IR}^4}{T_{TC}^4} \tag{8}$$

The thermocouple and IR camera temperatures were both known, a simple ratio allowed the emissivity of tantalum (assuming the camera detector is 1) to be calculated for a range of temperatures. In addition to emissivity, the camera accounted for a window transmissivity correction of 0.68. Each temperature measurement from the camera was an average of four samples. The resulting plot for emissivities as a function of temperature is in Figure 90, which includes standard deviation and camera accuracy errors. This calibration occurred for a set of images similar to Figure 91.
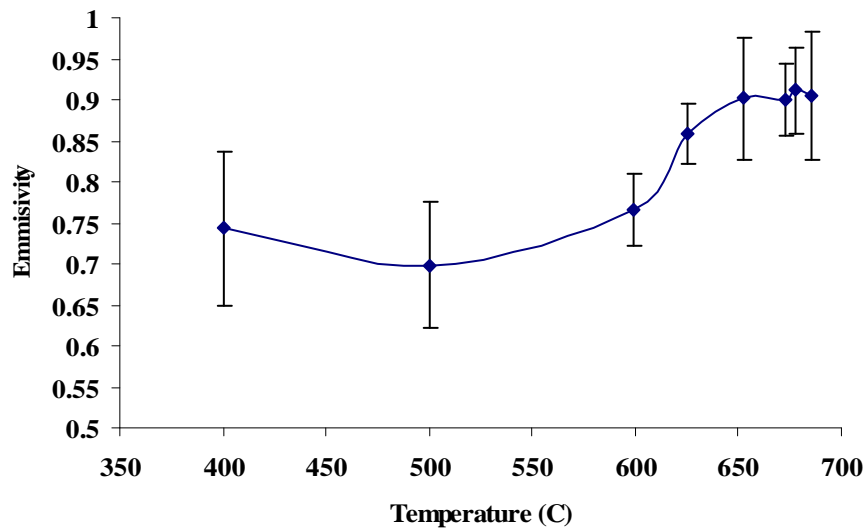
Figure 90. Emissivity Calibration Results

118
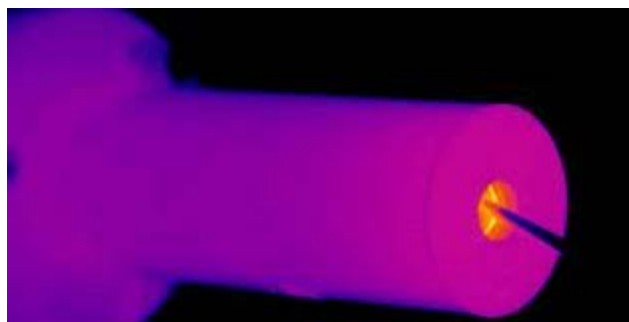
Figure 91. IR Image of LaB$_6$ Cathode with 11.9 A to Heater

The emissivities did not change much as the temperature approached 700°C. With this, the emissivity stayed at approximately 0.9 for temperatures at or above 700°C; and 0.72 for any temperatures below 600°C. In comparison, emissivity values reported for etched tantalum sheets operating below 600°C were 30% lower than observed here.[45] At 1000°C, the emissivity of tantalum in literature was 0.78, 13% lower than the value used here for this temperature. Cade also states the emissivity's rate of increase is lower for temperatures above 1000°C. Extrapolating his data results in an emissivity for tantalum of 0.89 at 1650°C. This is effectively the same emissivity used for these experiments. All temperatures on the orifice plate recorded by the camera were well above or below the 600°C and 700°C temperature thresholds. In the above image, the maximum temperature recorded with a correction of 0.9 is only 1000°C. This was not of great concern because the thermocouple was acting as a heat sink to the cathode, and the camera could not see the insert surface temperature, which may be a few hundred degrees higher. This is due to the thermal barrier created by the two orifice plates stacked in front of the inserts. The temperature drop is significant in a vacuum when contact resistance between the insert, protective sleeve, protective sleeve and orifice plate, and the two orifice plates is considered.

Correcting for the atmosphere, reflected chamber temperature, window, and emissivity of the orifice plate, Thermacam® software analyzed the images collected. Comparing LaB_6 to CeB_6 for one orifice geometry (0.5), the graphs provided show the cathode's temperature dependence on flow and current beginning with Figure 92.
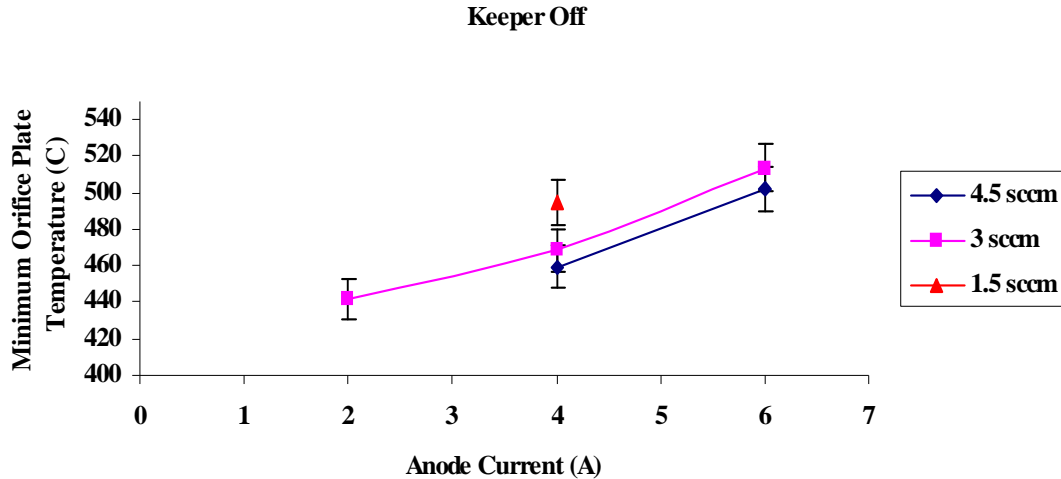
Keeper Off

Figure 92. LaB_6 Cathode IR Results with Keeper Off

The temperature varied as much as 500°C across the orifice plate. The temperature increased with anode current as expected and dropped with rising flow rate. The higher flow rate may increase convection and slightly lower the measured temperature. This same trend occurred with the keeper turned on, which acted to increase the overall temperature as expected, Figure 93.
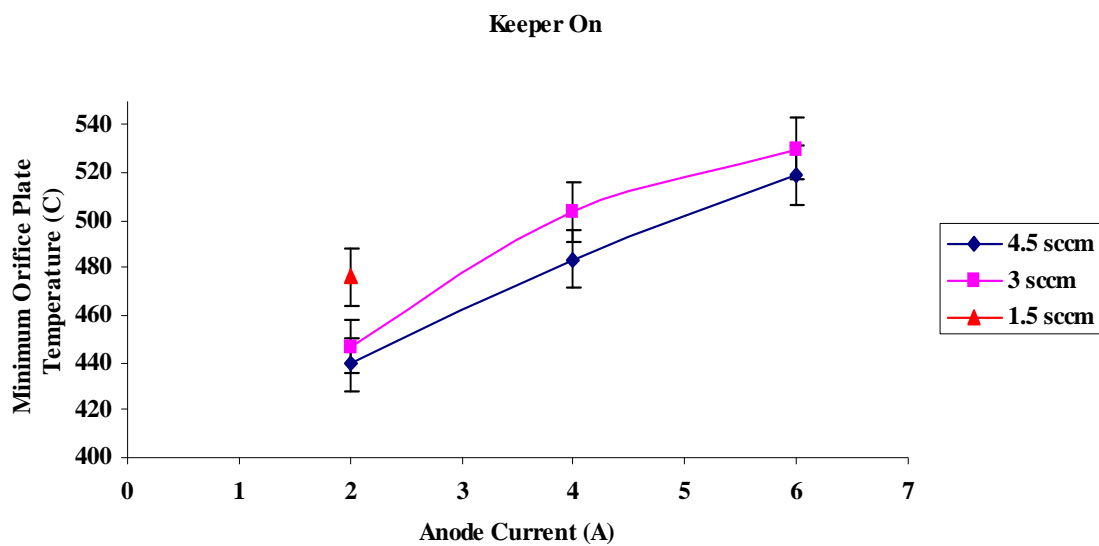
Figure 93. LaB$_6$ Cathode IR Results with Keeper On

As one may have already noticed, the temperatures reported appear considerably low. However, the maximum temperature of the orifice plate was a little closer to what was expected. See Figure 94.
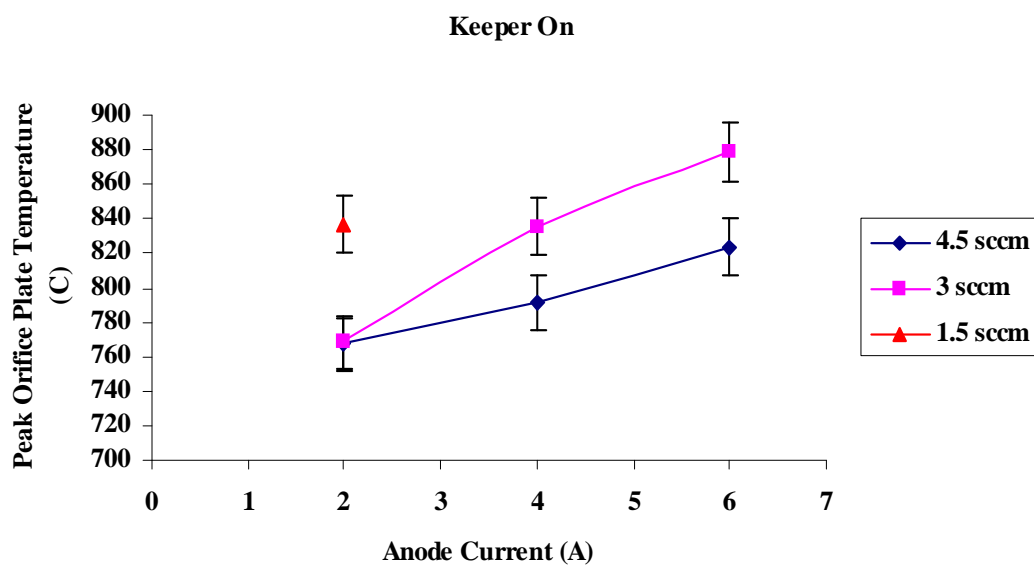
Figure 94. Peak Temperature LaB$_6$ IR Results with Keeper On

With the keeper off, the peak temperatures were slightly lower in both cathodes and followed the same behavior as Figure 94. In general, the CeB_6 cathode temperatures were higher, with the same trends observed in Figure 93 and Figure 94. These temperatures were still low and peak around 900°C at best. Several factors may attribute to this. First, there was a 0.635 mm gap between the insert and the orifice plate, provided by the insert protective sleeve. There was a temperature drop across the sleeve, contact resistance between the sleeve and insert, as well as the sleeve and orifice plate. This combination provided the thermal barrier discussed above. Second, there was no radiation shielding/heater filament around the end of the cathode tube housing the orifice plate (Figure 22). The thermocouple also acted as a heat sink to the cathode orifice and lowered its temperature during calibration. A lower thermocouple temperature would result in a higher emissivity than is truly exhibited. All of these factors contribute to the absolute temperature error, not the relative.

Figures 95 and 96 directly compare CeB_6 and LaB_6. Table 4 summarizes the nomenclature used to describe the test points of both cathodes. The figure compares each cathode's performance as a function of these test points. The cathodes showed temperature increasing with current (anode and keeper) and decreasing with flow rate. Surprisingly, the CeB_6 cathode temperatures were slightly higher than the LaB_6 cathode temperatures. They should be lower due to CeB_6's lower work function. Figure 96 represents the cathodes' peak temperature measurements. This trend occurred for all but one operating condition. As a result, calibration errors could not contribute to CeB_6 having higher temperatures since both cathodes had the same parameters applied during

122

imaging. A factor that could contribute to CeB_6 having higher operating temperatures is its power consumption.

Figure 97 and Figure 98 show the total power used, a sum of the keeper and anode power. This correlated well with the temperature trends observed, having the highest power levels for the highest current and lowest flows. However, no cathode provided a significant advantage over the other. Consequently, the CeB_6 cathode's power levels were not significantly higher than LaB_6's and could not be a factor in its higher operating temperatures. The error included for this data accounted for the resolution of the oscilloscope and data acquisition card

	Anode Current (A)	Keeper Current (A)	Flow Rate (sccm)
TP1	6	1	4.5
TP2	6	0	4.5
TP3	4	1	4.5
TP4	4	0	4.5
TP5	2	1	4.5
TP6	2	0	4.5
TP7	6	1	3
TP8	6	0	3
TP9	4	1	3
TP10	4	0	3
TP11	2	1	3
TP12	2	0	3
TP13	6	1	1.5
TP14	6	0	1.5
TP15	4	1	1.5
TP16	4	0	1.5
TP17	2	1	1.5
TP18	2	0	1.5

Table 4. Cathode Operating Test Points
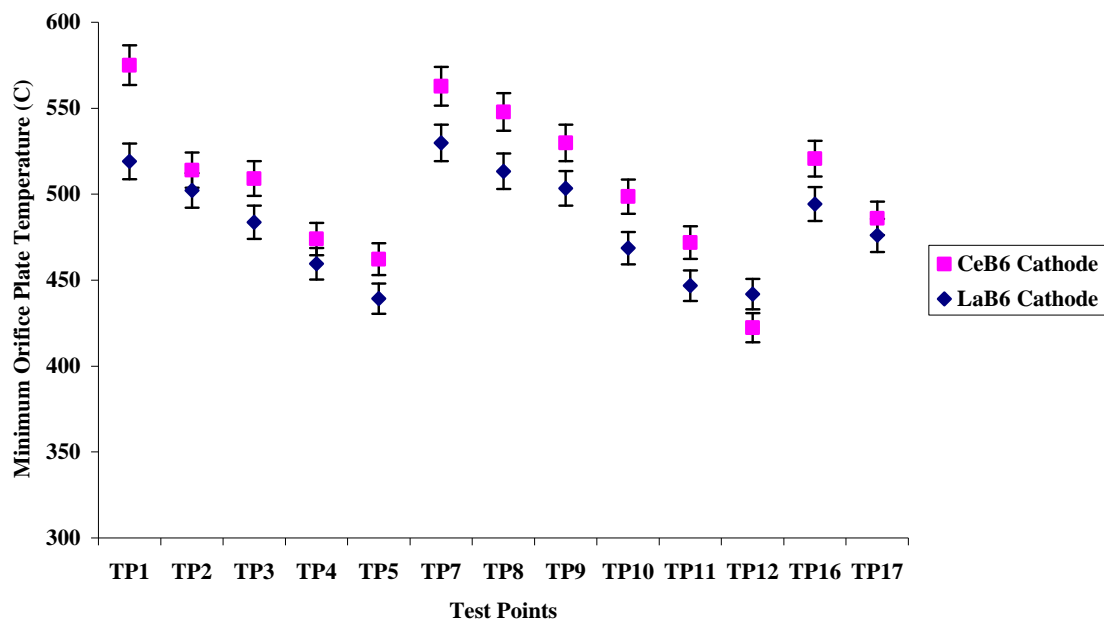
Figure 95. CeB$_6$ and LaB$_6$ Minimum Temperature Comparison
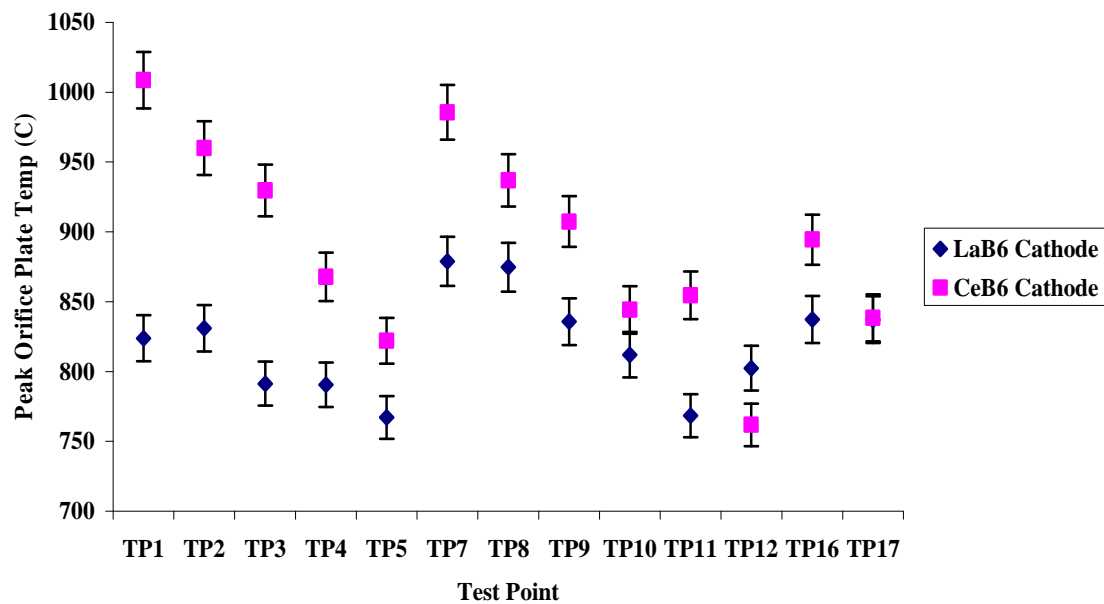
Figure 96. CeB$_6$ and LaB$_6$ Maximum Temperature Comparison

124
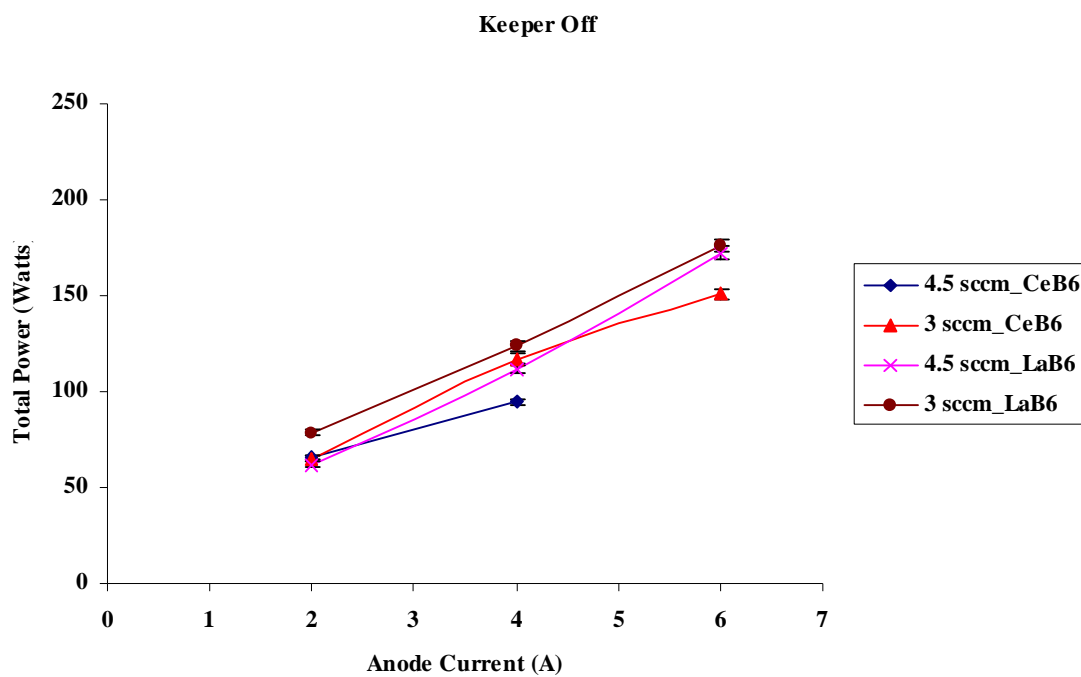
Keeper Off

Figure 97. CeB$_6$ and LaB$_6$ Power Comparison with Keeper off
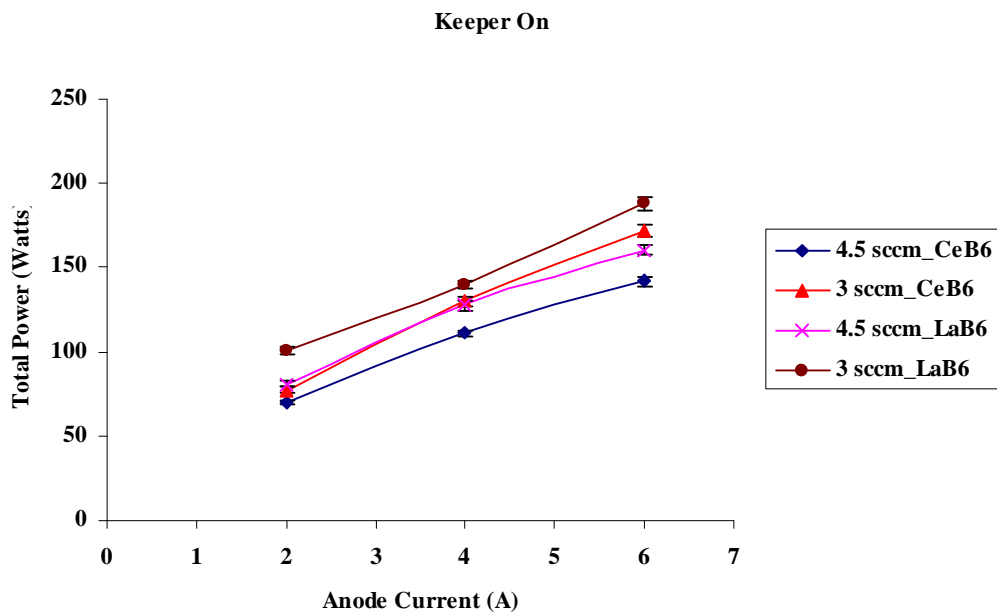
Keeper On

Figure 98. CeB$_6$ and LaB$_6$ Power Comparison with Keeper on

125

As previously mentioned, the insert temperature may be higher than the orifice plate temperature. The absolute orifice plate temperatures were lower than expected but not a concern since the relative temperature trends between CeB_6 and LaB_6 were consistent. Despite lower absolute temperatures, the LaB_6 cathode performance did not degrade from poisoning. However, the CeB_6 cathode did require more power after low flow and low current test points, and given these temperature data, the formation of oxides and contaminants was entirely possible. As for the higher CeB_6 insert temperature, there are several possible explanations. First, the CeB_6 cathode may have better thermal efficiency. This may attribute to the slightly higher temperatures, but is unlikely to have a significant contribution due to the similarity between the cathodes. Second, with a lower theoretical density than the LaB_6 insert (and possibly due to the formation of contaminates), the CeB_6 insert may actually have a closer work function to LaB_6 than expected. It may even be higher. If this were true, it would explain why the temperatures were higher. Third, the inside diameter may have increased, causing the temperature of any insert to increase. This may have occurred if the evaporation rate were higher for CeB_6 than LaB_6. However, after examination, both cathode's inside diameter did not change. Lastly, the CeB_6 insert work function may indeed be 2.5 eV, but its emissivity may be lower, causing it to sustain higher temperatures and emit more current. If this were true, higher temperatures would explain the higher plasma densities and lower potentials for some conditions of the CeB_6 cathode. Appendix B contains the remaining plots for the CeB_6 cathode temperature data.

Poisoning Mechanisms

Spectral analysis and microscope imaging gave even more information regarding the behavior of the inserts after testing. The images presented here are after 52 hours of testing the LaB_6 insert and 37 hours for the CeB_6 one.

<div align="center">

LaB_6 Results

</div>

The only motivation behind investigating the possible poisoning mechanism for the LaB_6 insert was to compare it to the CeB_6 insert. Over the course of testing, the LaB_6 cathode did not require higher flow or power to start. This cathode consistently started at the conditions outline in the Cathode Ignition section. Figure 99 shows the end of the cylindrical LaB_6 insert closest to the orifice plate. After performing spectral analysis for different locations on the insert surface in Figure 99, the primary contaminate on the surface was carbon. There were some trace amounts of tantalum and oxygen. When the author took the insert sample out originally, the carbon deposited on the LaB_6 insert appeared upstream from the orifice. To test LaB_6's resistance to contamination, the insert ends were swapped and reinserted so the carbon rich end was next to the orifice. Despite having an accumulation of carbon on the insert surface, the emission capability of the LaB_6 insert did not degrade. The spectral graph, Figure 100, used to make these conclusions only gives elemental information and is for a small region of the insert. As a result, the actual constituents in their compound form were not determined.
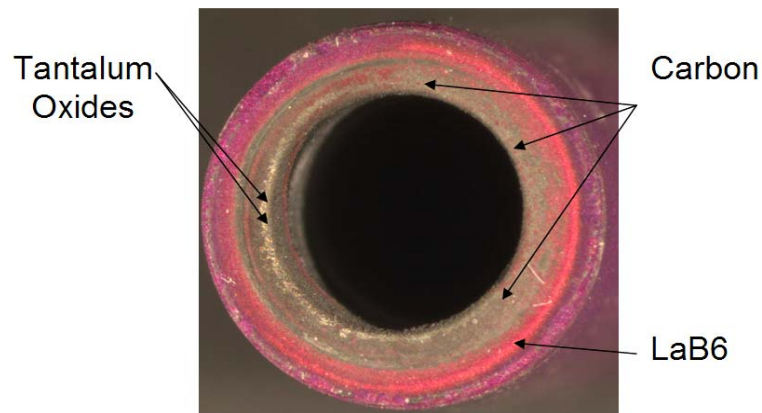
Figure 99. LaB$_6$ Insert (Near Orifice Plate)

LaB6 Insert W/ Tantalum and Oxides
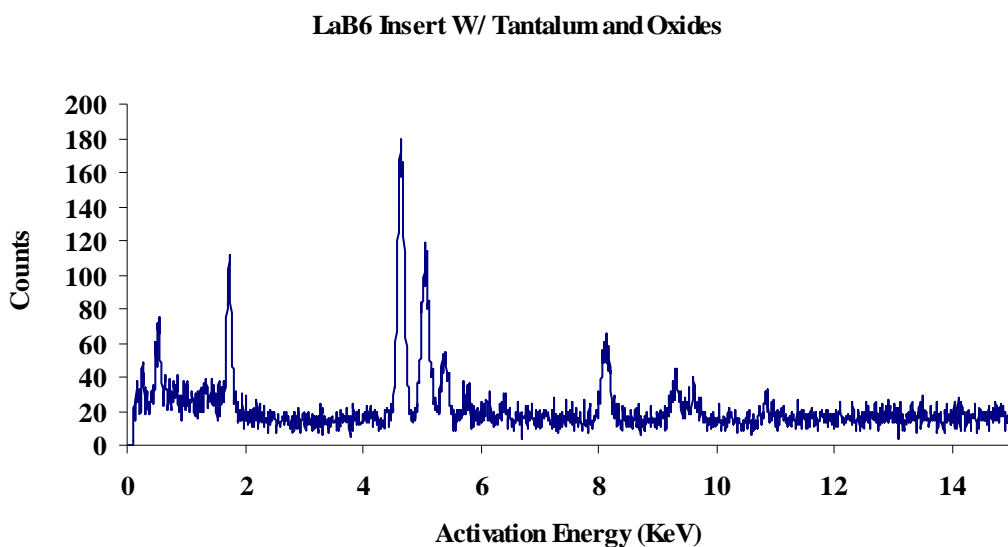
Figure 100. Spectral Analysis for LaB$_6$ Insert (near orifice plate)

The spectrum in Figure 100 is for the region in Figure 99 calling out "tantalum oxides". When performing the analysis, the scanning electron microscope analyzed a circular spot of a given size then moved to the next one. The beam focused onto the small lighter region of the black ring on the insert, and the software identified tantalum,

carbon, and oxygen, along with other normal elements such as lanthanum and boron. The color microscope images provided a visual reference for the spectral data. Based upon the known colors of carbon, tantalum, and LaB$_6$, it was thought the lighter grey area was some kind of tantalum oxide when Edax called out tantalum and oxygen. Carbon dioxide and lanthanum oxides were ruled out because of their state of matter and colors at room temperature, respectively. Figure 101 shows a normal LaB$_6$ insert spectrum acting as the baseline for other scans.

LaB6(Normal)
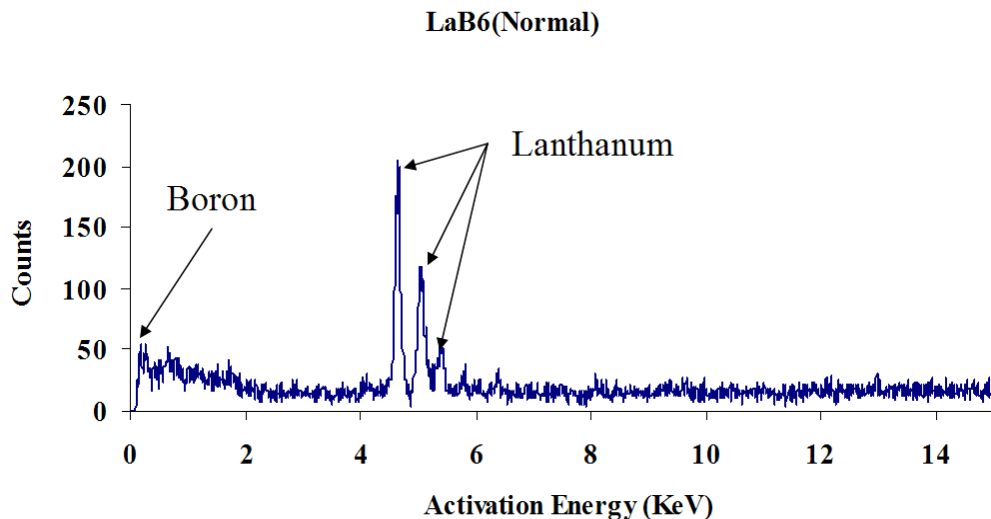
Figure 101. Normal LaB$_6$ Insert Spectrum

The next image is for the opposite end of the insert. When initially removed, this end had some oxides and tantalum present, and after rotating it around as mentioned above, the tantalum and oxide levels reduced and some carbon began to form, all occurring after an additional 15 hours of testing. Again, this demonstrates the robust nature of the LaB$_6$ insert. Using the same reasoning described above, the main contaminate here is carbon with some small amounts of tantalum.
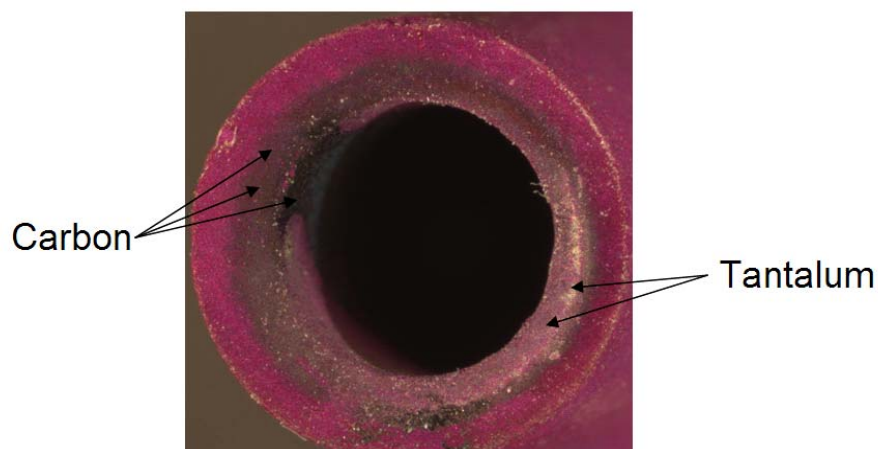
Figure 102. LaB$_6$ Insert (End Opposite of Orifice Plate)

The images of the locations presented were the only areas with any contaminates. The sides of the insert were free from contamination, confirmed by spectral analysis. Figure 103 is an image of the LaB$_6$ insert after 52 hours of testing. It shows no signs of evaporative losses, having only a 0.59% +/- 0.007% decrease in mass over the course of its use and no dimensional change. For comparison, Figure 104 shows the insert before testing with slightly different lighting.

Figure 103. LaB$_6$ Insert after 52 Hours of Testing

Figure 104. LaB$_6$ Insert before Testing

130

Although some contaminates were detected on the LaB$_6$ inserts, they did not have a measurable effect on its performance. Whether the contamination mechanism was by diffusion or something else was unclear with this analysis. The source of the carbon and tantalum contamination was from the obvious candidates of the orifice plate and carbon components in the cathode. The oxides however could be from two possible sources: one being the propellant lines, the other the small air gap present inside of the cathode, shown in Figure 105. The protection sleeves formed a snug fit inside the cathode tube, with the ends pressed against the sleeves by the presence of a spring inside the cathode tube. This configuration effectively formed a small air pocket inside the cathode, while it may not be a perfect seal; it is a virtual leak and may provide enough air to form oxides on the insert.

Cathode Tube   Protection Sleeves

Air Gap   LaB6
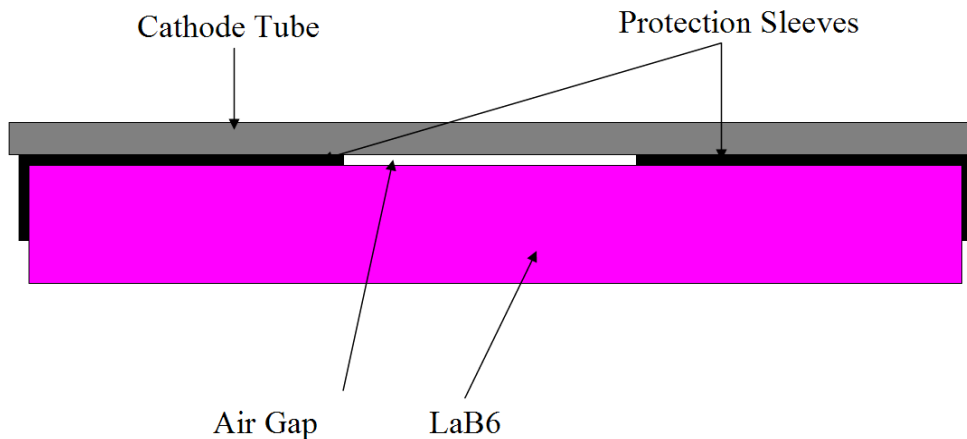
Figure 105. Possible Air Pocket

CeB$_6$ Results

The CeB$_6$ cathode behaved much differently than the LaB$_6$ cathode after close review by microscopy and spectral analysis. The most noticeable change was the decrease in outer diameter, Figure 106.
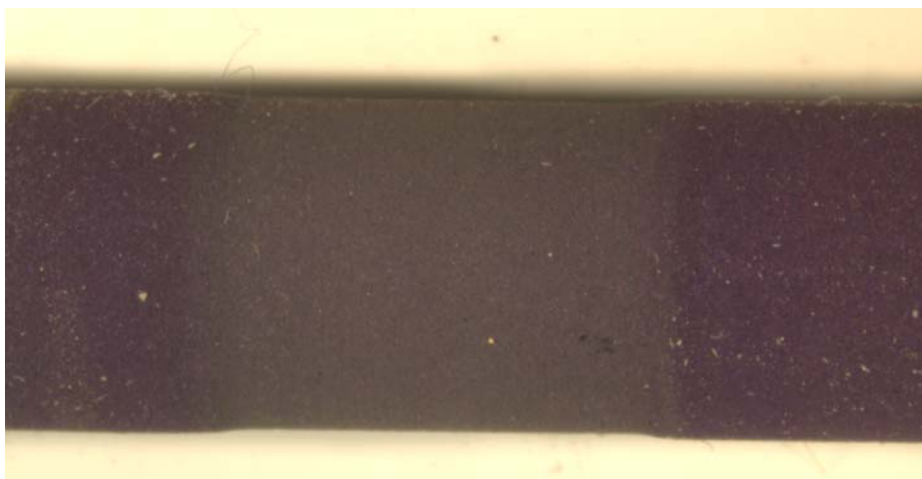
Figure 106. CeB$_6$ Insert w/ Diameter Change

After weighing the insert, the mass had dropped by 7.83% +/- 0.008% after only 37 hours of run time. Since the CeB$_6$ cathode operated for a shorter period than LaB$_6$ and lost more mass, its evaporation rate appears to be higher than expected. The thinner region of the CeB$_6$ insert in Figure 106 coincided with the air pocket described in Figure 105. Poisoning of this exposed portion of the insert may have increased its evaporation rate and contributed to the large mass loss. The covered regions showed some signs of CeB$_6$ evaporation by the coating left on the inside of the protection sleeves, Figure 107. This evaporative deposition occurred for both the LaB$_6$ cathode and CeB$_6$ cathode.
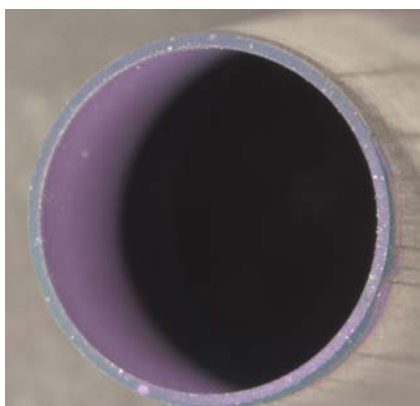
Figure 107. CeB$_6$ Insert Protection Sleeve after Testing

Spectral analysis indicated the region of decreased diameter contained tantalum. The presence of tantalum may have accelerated the evaporation rate of the insert. The microscope did not detect any oxides and very little carbon in this portion of the insert. The concentrations of boron were not low when compared to the uncontaminated baseline spectrum. This eliminates the possibility of boron loss through evaporation or diffusion. Further investigation would provide more information and help clarify the process of this contamination and evaporation phenomenon.

Another portion of the insert contained some tantalum as well, Figure 108. It was not clear if the region of tantalum formed by diffusion or some other process. Destructive analysis may shed light on this contamination mechanism as well.

Tantalum
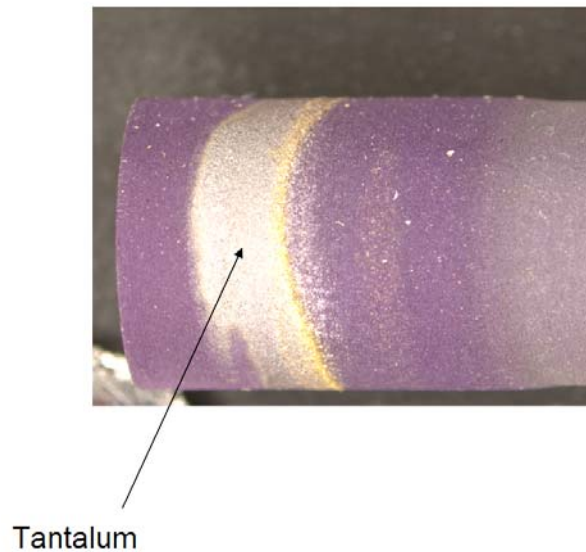
Figure 108. CeB$_6$ Insert w/Stripe

The end of the insert closest to the orifice had oxygen and some carbon present with little other than cerium and boron. The activation energy of some elements was too high for the Edax to detect and may be more than the 15 keV limit, such as molybdenum. Nevertheless there were some contaminates on this surface, Figure 109. The opposite end only showed some signs of carbon, Figure 110.

Oxide
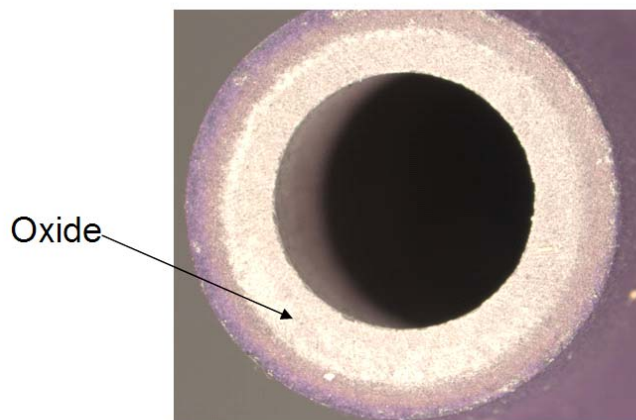
Figure 109. CeB$_6$ Insert (End near Orifice)
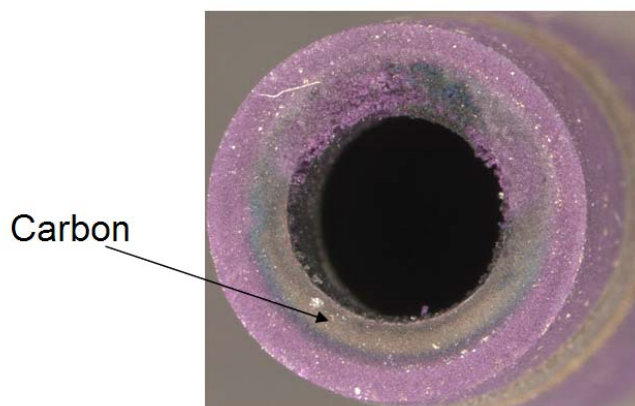
Figure 110. CeB_6 Insert (End Opposite of Orifice)

The air pocket described earlier or oxygen adsorbed by the molybdenum cathode tube may have contributed to the contamination of this insert. Unlike the LaB_6 insert, CeB_6 did show some signs of ignition degradation with time. Specifically after running the CeB_6 cathode at or below 1.5 A and 1.5 sccm, it required higher flow rates and longer heating time to start. Contamination may have also increased the anode and keeper voltages during operation.

Based on the poisoning data, this LaB_6 insert was more resistant to contamination than the CeB_6 insert. CeB_6 was also supposed to have a lower evaporation rate, but with these observations, that did not appear to be the case. However, its evaporation rate may have been accelerated by the presence of contaminates and requires more investigation. Without attempting high temperature bake-out for either cathode after contamination, determining if they could regain full emission capability was unclear as well. Oxygen and water vapor pressures in the vacuum chamber were well below the required values for contamination, confirmed by the residual gas analyzer (RGA) plot in Figure 111. The remaining spectral graphs are included in appendix A.
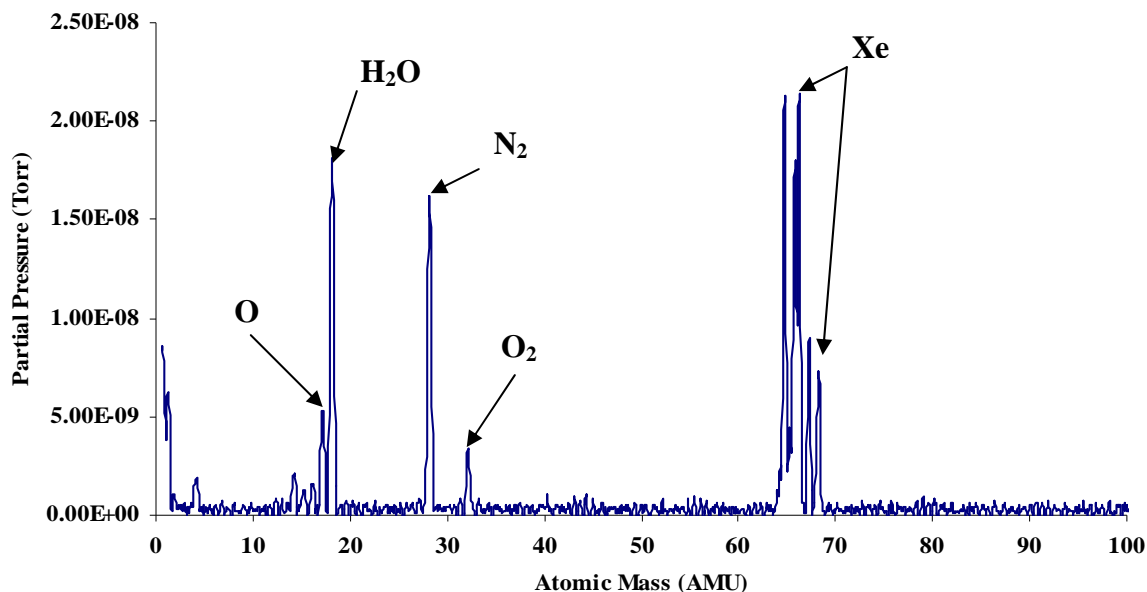
Figure 111. RGA Scan for SPASS Facility during Cathode Testing

High-Speed Imaging Results

High-speed imaging assisted in depicting the behavior of the cathode coupling plasma during spot and plume mode. The camera can observe more than an oscilloscope. It can see an oscillation that the oscilloscope might indicate as small. Intensity variations between frames were used to visually distinguish between large and small oscillations. For example, if one frame was very bright and one following it is pitch black, this is a large oscillation. If one frame is only slightly brighter than one following it, then the oscillation is smaller in magnitude. Brightness correlated with oscillation amplitude.

During spot mode, the camera observed very small flickers, typical of normal plasma oscillations. However, the plasma did not oscillate uniformly. The images taken show a non-uniform distribution of light intensity. Uniform plasmas occurred when the light intensity was symmetric about the cathode centerline. The regions of higher

136

intensity light indicated concentrations of high energy electrons. For spot mode, the changes in intensity only appeared to shift the plasma up and down relative to cathode centerline rather than move it along the centerline. The following frames are an illustration of the cathode during spot mode. The top left frame is the earliest and each successive frame is 50 microseconds apart.
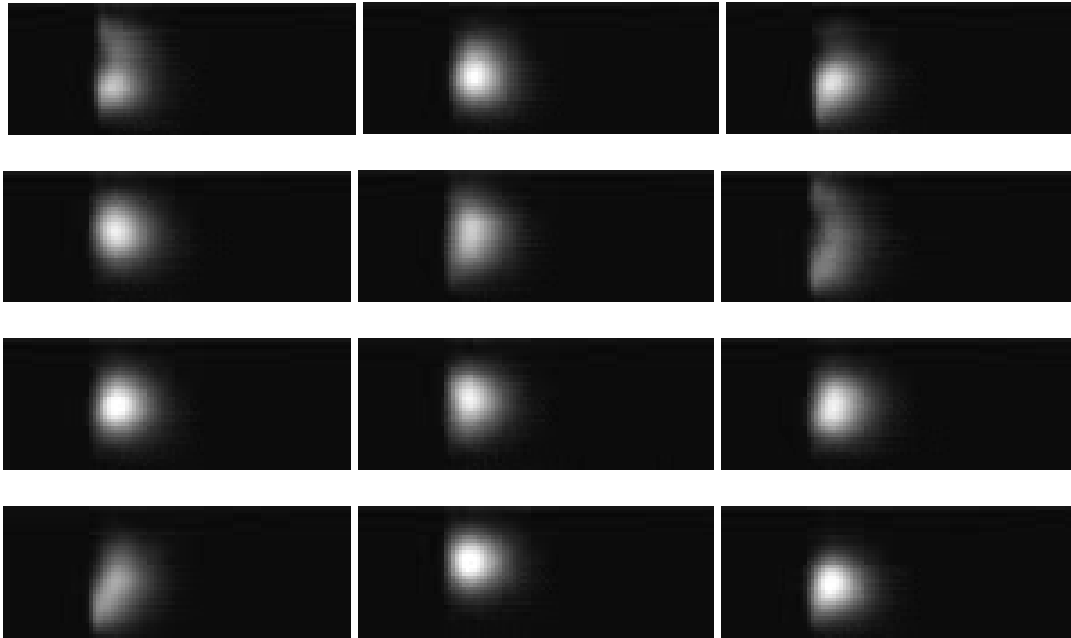
Figure 112. High-Speed Images of LaB$_6$ Cathode at 4 A Anode, 0 A Keeper, 4.5 sccm

The frame numbering starts at 1 in the top left and 12 on the bottom right. Frames 1, 6, and 10 all show lower intensity plasma than the other frames. Frames 3, 6, and 10 show examples of non-uniform plasma. The last two frames seemed misaligned but they are actually images of the plasma as it formed in two different locations relative to cathode centerline. The light collected in these images is of the highest intensity within the plasma and may exclude lower energy electrons.

During plume mode, the oscillations were more prominent. Captured 17 microseconds apart, the frames in Figure 113 appear dimmer than Figure 112 because of the shorter exposure time.
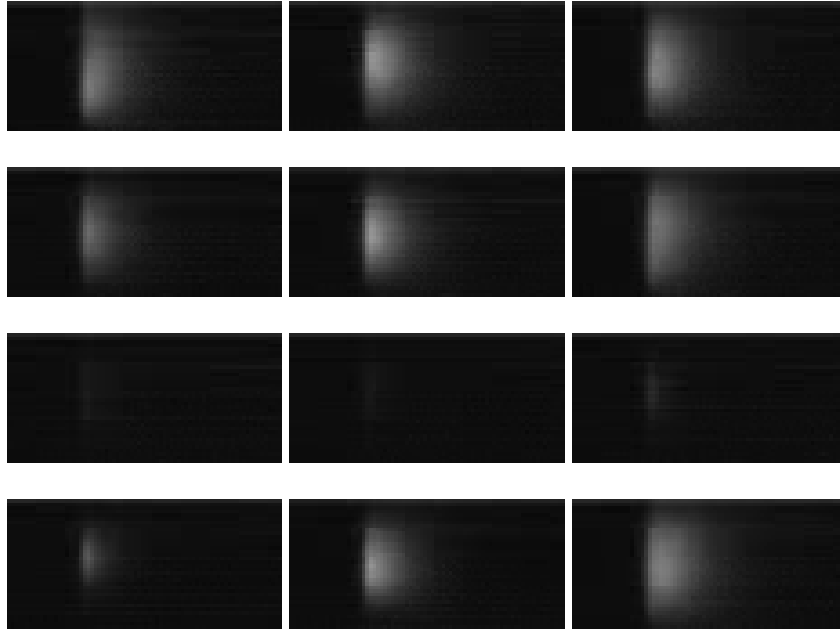
Figure 113. High-Speed Images of LaB$_6$ Cathode at 6 A Anode, 1 A Keeper, 1.5 sccm

The images show how much the electron energy changed during plume mode. Ion density is clearly very low at frames 7-9. Unlike spot mode, these images show the plasma disappearing and reappearing. From the total sample of frames taken, events like the one shown in frames 7-9 occur 60 times in 0.016 seconds. With a frequency of 3.5 kHz, this is close to one harmonic observed by Martin and Williams but not typical of the high frequency oscillations plume mode is characteristic of. Instead, this frequency is similar to those observed to result from power supply regulation. Thus, a higher frame rate and larger aperture may be required for better analysis.

V. Conclusions and Recommendations

Conclusions of Research

Based upon the findings of this research, the LaB_6 cathode proved the superior electron emitter, not from an electron emission standpoint, but rather on lifetime and poisoning resistance. Neither cathode provided a significant power savings advantage over the other. The CeB_6 cathode had slightly lower electron temperatures and plasma potentials, and higher electron and ion densities for some operating conditions. It also demonstrated lower flow and current capability than the AR.5 LaB_6 cathode.

CeB_6's superior plasma characteristics did not appear to result from a lower work function, but rather a lower emissivity. Without additional emissivity studies for the CeB_6 insert, this research could not quantify its true emissivity, only deduce it based upon the findings here. A low emissivity and lower work function may provide and advantage over LaB_6, allowing the CeB_6 cathode to ignite at lower potentials while operating with high temperatures. Elevated temperatures should provide additional resistance to poisoning for any cathode, but did not help CeB_6 in this research. Despite higher operating temperatures, the CeB_6 cathode succumbed to the effects of contamination and showed degradation in performance by requiring more heater power and flow to start after running at low flow and current.

The CeB_6 insert's large mass decrease resulted from a higher evaporation rate than published or was accelerated by poisoning.[7] The CeB_6 insert lost more mass than the LaB_6 insert, leading one to conclude this sample's life could be shorter than the LaB_6 cathode, especially since it operated 15-18 hours less. In contrast, the LaB_6 cathode did not show any signs of degradation and lost very little mass.

139

Reducing the aspect ratio improved the performance of the LaB_6 cathode (and would do the same for CeB_6) by lowering the electron temperatures and plasma potentials, and increasing the ion and electron densities. There was no significant change in power consumption but this orifice geometry allowed the LaB_6 cathode to run at power levels as low as the CeB_6 cathode. After operating at these conditions, the LaB_6 cathode did not require more flow and power to light as its CeB_6 counterpart began to show.

Both cathodes also had similar spot and plume mode transitions. Each was either in or close to plume mode at 1.5 sccm with equal or greater than 6 A anode current and the keeper turned off. All cathodes stabilized or transitioned out of plume mode with the keeper on for a wide range of anode currents and did not require excessive flow to maintain spot mode emission.

With these conclusions, the LaB_6 cathode is a viable electron emitter for low power electric propulsion technology. Poisoning does not affect the insert, despite having lower operating temperatures at low current. Even with a higher work function, the operating range was as wide as impregnated cathodes. The CeB_6 cathode had slightly better emission traits than LaB_6. The evaporation and poisoning effects observed may limit its life and make a CeB_6 insert with this density difficult to integrate into hollow cathodes. Nevertheless, the lanthanum hexaboride cathode would provide lifetime benefits over impregnated cathodes for a wide range of currents (1.4A-100A). The tables summarizing the cathode's performance are included here again.

Mass Flow (sccm)	J_a (A)	J_k (A)	V_a (V)	V_k (V)	Mode
6	6	1	26.26	15.89	Spot
		0	25.57	N/A	Spot
	4	1	27.91	18.22	Spot
		0	27.72	N/A	Spot
	2	1	30.44	20.34	Spot
		0	31.18	N/A	Spot
4.5	6	1	26	16.22	Spot
		0	26.72	N/A	Spot
	4	1	27.43	17.83	Spot
		0	27.84	N/A	Spot
	2	1	30.23	20.63	Spot
		0	30.95	N/A	Spot
3	6	1	28.46	17.06	Spot
		0	29.36	N/A	Spot
	4	1	30.16	19.24	Spot
		0	30.89	N/A	Spot
	2	1	37.51	25.51	Spot
		0	39.18	N/A	Spot
1.5	6	1	32.17	19.48	Intermediate
		0	48.17	N/A	Plume w/probe
	4	1	31.62	21.31	Spot
		0	34.36	N/A	Spot
	2	1	38.89	25.46	Spot
		0	42.34	N/A	Spot

Table 1. AR.25 LaB6 Performance Summary

Mass Flow (sccm)	J_a (A)	J_k (A)	V_a (V)	V_k (V)	Mode
4.5	4	1	26.1	17.6	Spot
	2	1	32.4	23.6	Spot
3	6	1	27.78	25.15	Spot
		0	31.45	N/A	Spot
	4	1	28	18.4	Spot
	2	1	33.3	23.75	Spot
1.5	6	1	30.43	19.88	Intermediate
		0	34	N/A	Intermediate
	4	1	31.9	24.05	Spot
		0	35.24	N/A	Intermediate

Table 2. AR.5 LaB6 Performance Summary

Mass Flow (sccm)	J_a (A)	J_k (A)	V_a (V)	V_k (V)	Mode
4.5	6	0	23.6	N/A	Spot
	4	1	23.43	17.12	Spot
		0	23.59	N/A	Spot
	2	1	23.54	22.62	Spot
		0	32.85	N/A	Spot
3	6	1	25.95	16.45	Spot
		0	25.09	N/A	Spot
	4	1	27.9	18.18	Spot
		0	29.28	N/A	Spot
	2	1	25.9	25.6	Spot
		0	32.47	N/A	Spot
1.5	6	1	42.9	18.53	Plume
		0	43.09	N/A	Plume
	4	1	27.89	N/A	Intermediate
		0	31.19	N/A	Intermediate
	2	1	30.68	27.89	Spot
		0	36.36	N/A	Spot

Table 3. CeB6 Performance Summary

Recommendations for Future Research

The first suggestion addresses the CeB_6 insert. It is unclear why the insert's outside diameter decreased the most in the region exposed to the air pocket. It appeared the evaporation rate of the insert was lower in the regions covered by the protective sleeves. Future studies should look into using one sleeve to cover the entire length of the insert and determine if it would reduce the insert's evaporation rate and prolong its lifetime. A possible added benefit to this modification would be to remove the air pocket that exists in the current design and eliminate it as a possible poisoning source. Future work should also extend the contamination investigation with destructive analysis to determine if the contaminates are forming on the surface or have diffused into the bulk of the insert. Until recently the highest theoretical density possible for the CeB_6 insert was 70%, new samples may go as high as the LaB_6 insert (80-90%).[46] The higher density samples may perform better and would be a worthy subject to apply the preceding recommendations. It would be ideal if single crystals could be arranged in a geometry to substitute the hollow polycrystalline insert. Single crystals have 100% theoretical density and because the work function depends on their plane orientation, they can be positioned so the lowest work function plane faces the insert plasma. Some of these alternative insert geometries prototyped from A-P-Tech® are included in appendix C. A final experiment should measure the emissivity of the polycrystalline insert, since the availability of this data is scarce. A combination of these tests would fully determine if CeB_6 is a viable hollow cathode emitter.

The next phase of research for LaB$_6$ should investigate a 3.2 mm cathode. This

reduces the power and flow requirements. The 6.4 mm cathode used in this study had a

large thermal mass and was not tailored for low current designs. A challenge to designers

of the 3.2 mm cathodes, especially ones using LaB$_6$, is minimizing conduction of heat to

the base of the cathode. This heat loss reduces the temperature of the insert and

sometimes requires heater operation, more heater power, or special care in the cathode

tube design. LaB$_6$ requires more power to ignite, adding another challenge to the design.

Without excessive flow and power, it may be difficult to make an orifice small enough

for a low current cathode, yet large enough so it can light. Large orifice diameters allow

the cathode to light with less power, but require more flow to maintain spot mode. A

good trade-off is a small orifice, with a very shallow depth. With the work presented

here, an aspect ratio of 0.25 allowed the cathode to run at low flow and current, its depth

was not restricted by electron beam welding temperatures because the orifice plate was

pressed between the insert and the lip of the cathode tube. However, a solution is a

chamfer on the cathode orifice, ultimately reducing the depth and allowing the orifice

plate to be electron beam welded.

An additional challenge with the LaB$_6$ cathode is its higher work function,

requiring a very good thermal design and careful material selection for key components.

A suggested material by Domonkos is titanium, due to its low thermal conductivity, high

strength, and low sputter yield. Another possible candidate for the cathode tube would be

pyrolytic graphite. Graphite has a low sputter yield, good compatibility with the LaB$_6$

insert, and is very anisotropic. During the initial investigation into the use of this

material for a cathode tube, the author found several companies capable of making the

144

tube out of this material. However, the plane orientation was such that the high thermal

conductivity plane (comparable to copper) was along the length of the tube, and the low

was radially across it.[47] This would allow the heat to very quickly transfer from the insert

to the base, but effectively act as an insulator between the insert and the heater, making a

thermally inefficient design. The challenge was finding a company that made the

pyrolytic graphite such that the plane orientation would maximize heat transfer radially

and minimize it axially. Mintech Pyrogenic Group in Easton, Pennsylvania can make a

very small pyrolytic graphite cathode tube, 3.2-6.4 mm diameter at 2.5 cm in length. The

design could be similar to the one presented in this research, in Figure 114, with the

exception of the dimensions.
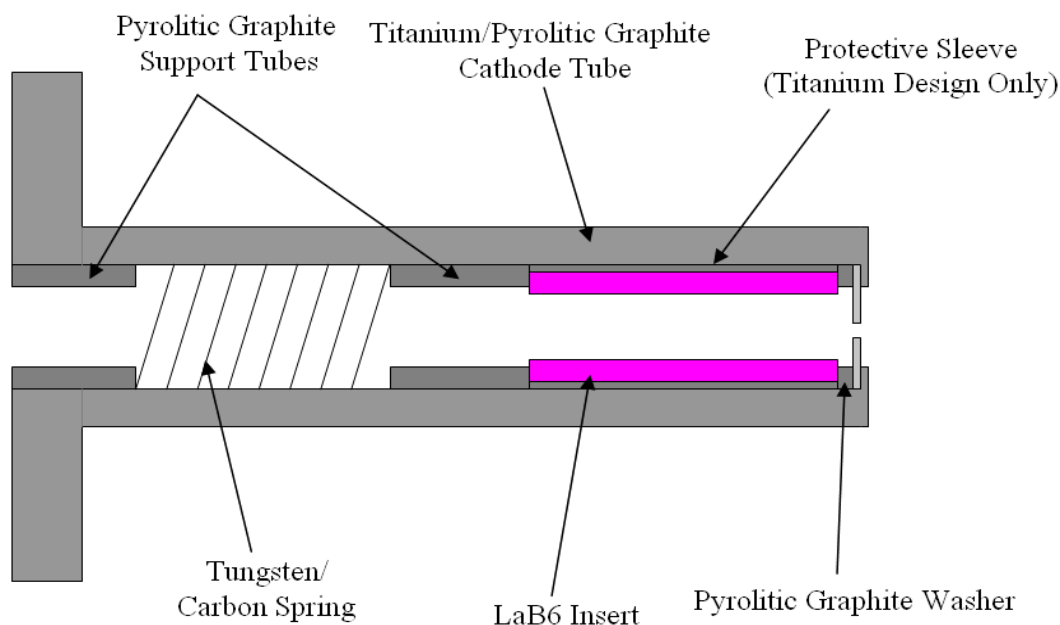
Figure 114. 3.2 mm LaB$_6$ Cathode Design

Some important considerations not immediately apparent in the above figure are

the diameter (3.2 mm) and the length (2.5 cm). The insert length would be 10 mm and

the remaining parts scale accordingly. The figure above is a rough drawing of the basic cathode concept, not paying any special attention to the relative dimensions but rather the raw assembly. The cathode tube wall would actually be much thinner as well as some of the other parts. The primary benefit of the smaller dimensions of the cathode would reduce the thermal mass and improve its thermal efficiency. If not a pyrolytic graphite tube, a titanium one would provide a good alternative. Pyrolytic graphite support tubes would act as insulators between the insert and cathode base. A single graphite protective sleeve with a small pyrolytic washer would at as one between the insert and the orifice plate. The very high cross plane resistance and excellent compatibility with LaB_6 makes pyrolytic graphite a material worthy of investigation for use in 6.4 and 3.2 mm cathodes whether it is as a cathode tube or internal components. Special care with the radiation shielding would minimize losses through the heater wire.

Another challenge with an anisotropic material is the coefficient of thermal expansion (CTE). For the design presented above, the lowest CTE would be radially and highest axially. Consequently, dimensional tolerances would be an important consideration when constructing this cathode. The final step would be to test the 3.2 mm cathode with this anode geometry and apply a magnetic field. The magnetic field is not as important for Hall thrusters as it is for ion thrusters. After experimentation in a triode, the cathode could then integrate into an ion or hall thruster.

Appendix A. Spectral Analysis Data

CeB6 Insert (Orifice End)
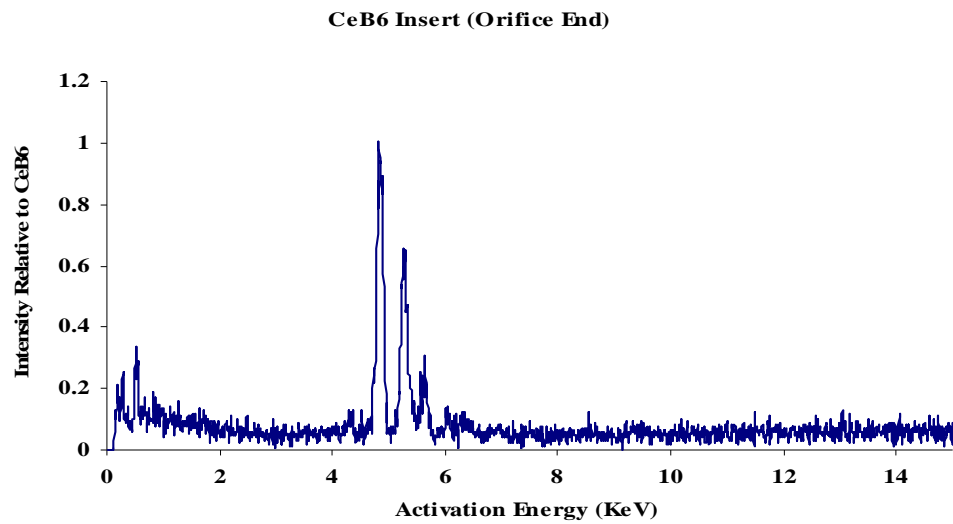
Figure 115. CeB$_6$ Insert End near Orifice Spectrum

CeB6 Insert (Thin side)
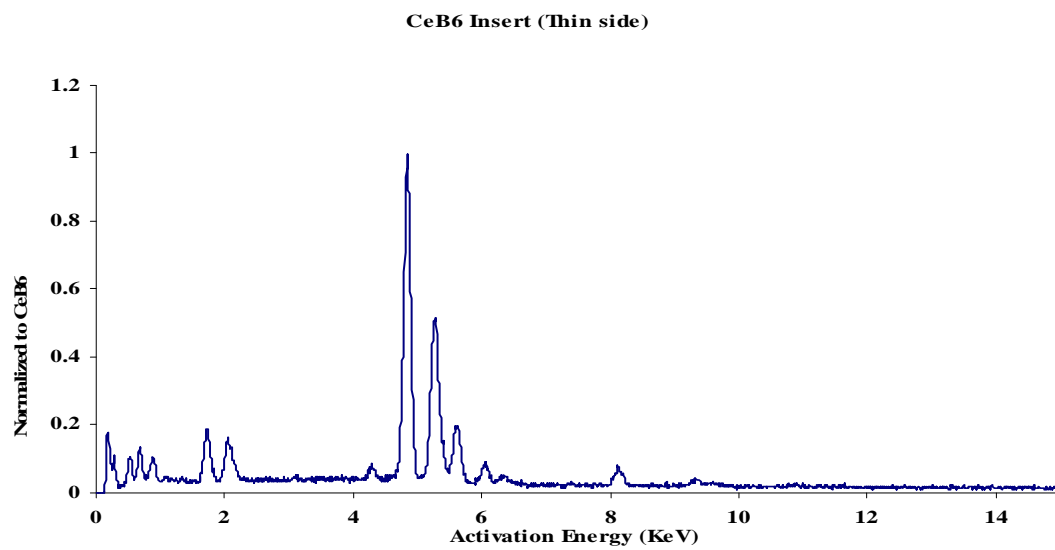
Figure 116. Side of CeB$_6$ Insert Spectrum

CeB6 Insert (Upstream Side)
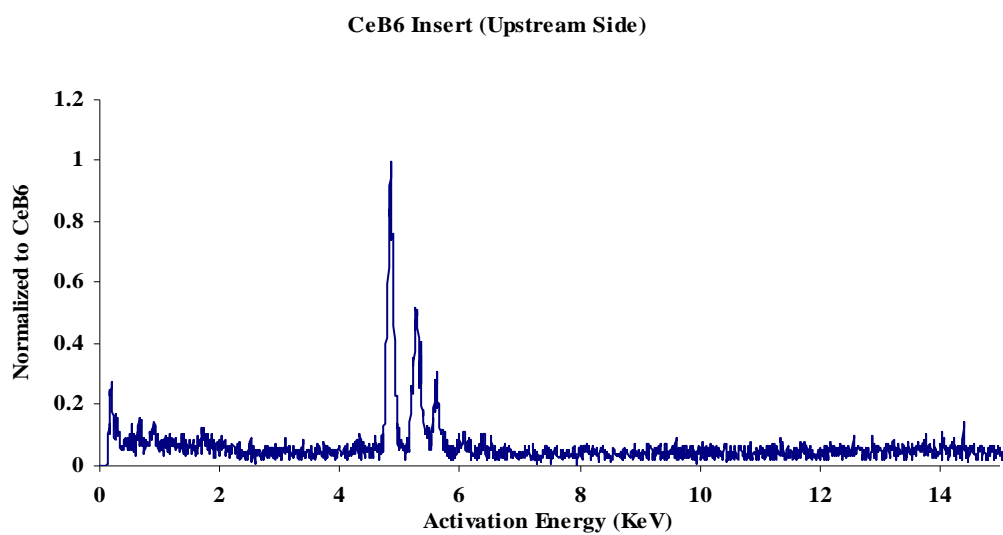
Figure 117. CeB$_6$ Insert End Opposite of Orifice Spectrum

Normal CeB6 Insert Spectrum
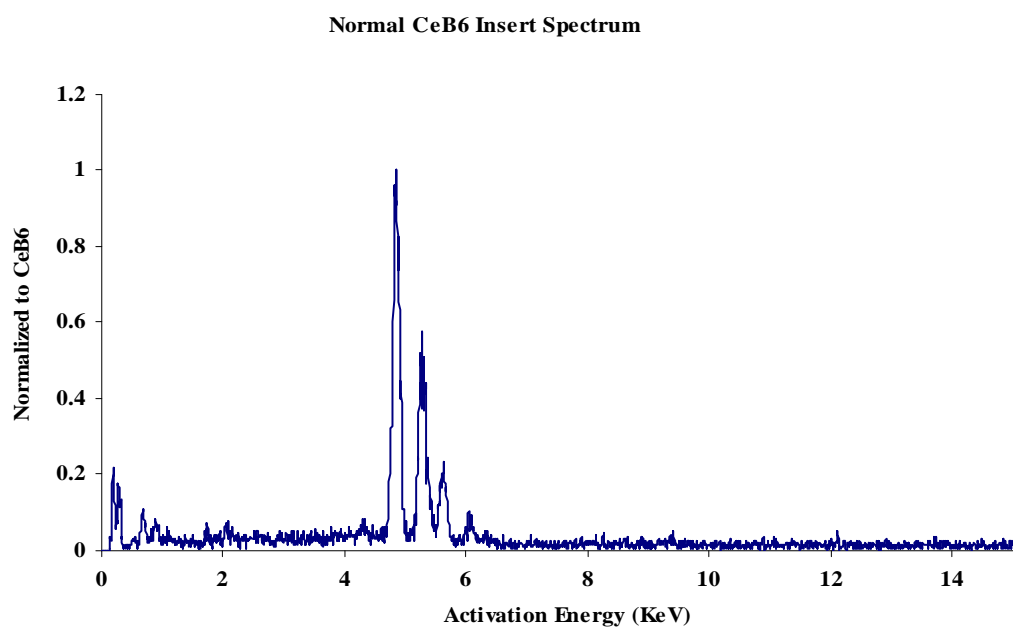
Figure 118. Normal CeB$_6$ Insert Spectrum
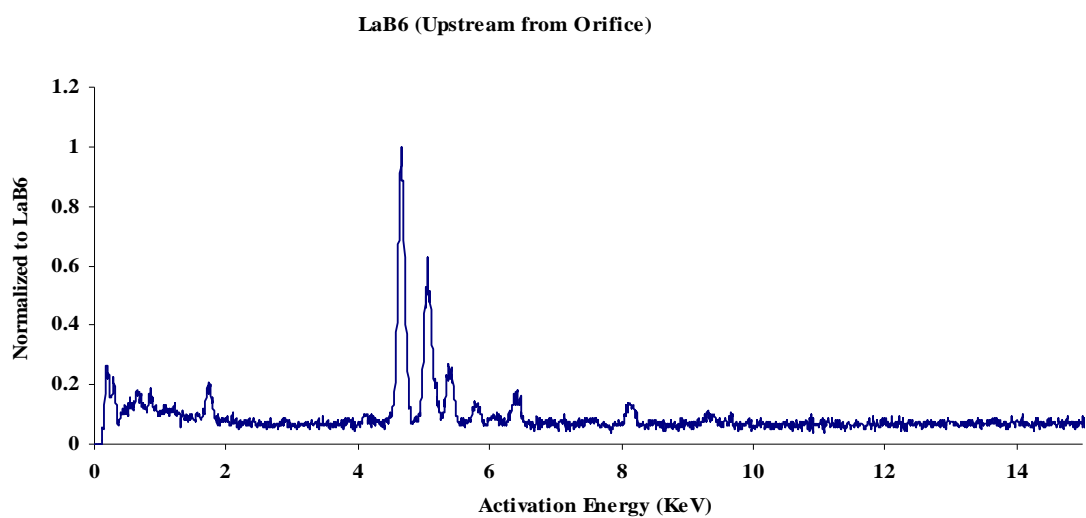
Figure 119. Insert end opposite from Orifice Plate Spectrum
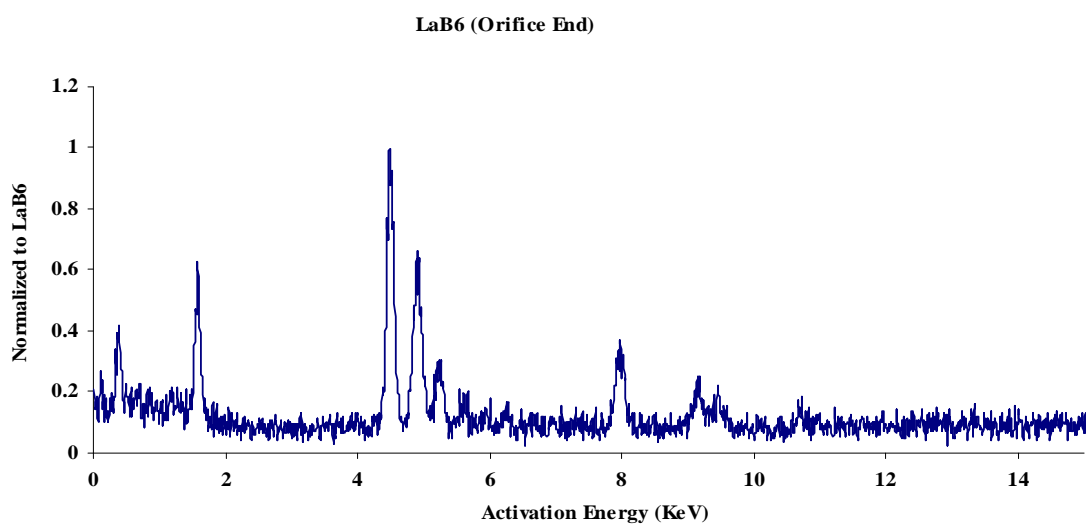
Figure 120. Insert end near Orifice Plate Spectrum

149

Normal LaB6 Spectrum
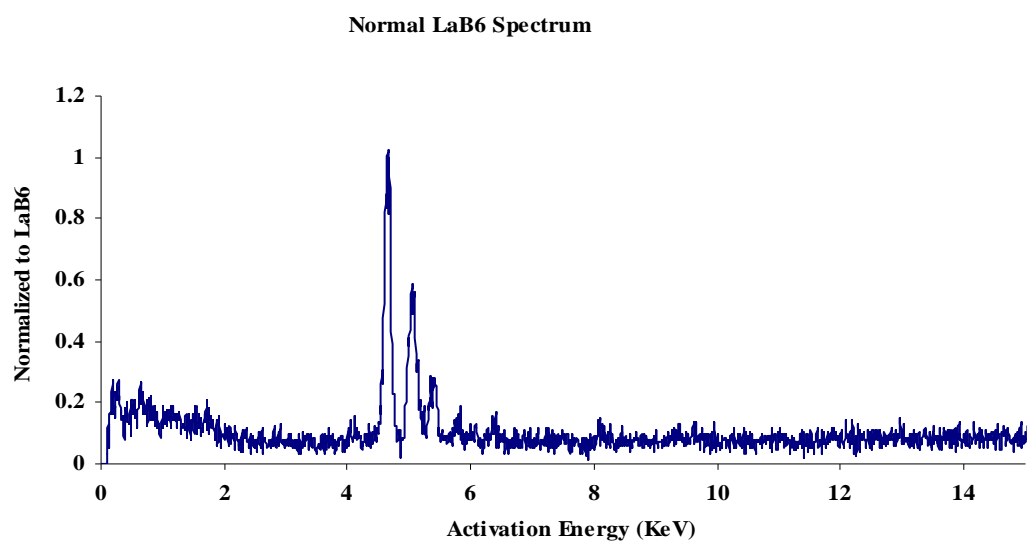
Figure 121. Normal LaB$_6$ Insert Spectrum

Appendix B. CeB$_6$ Temperature Data
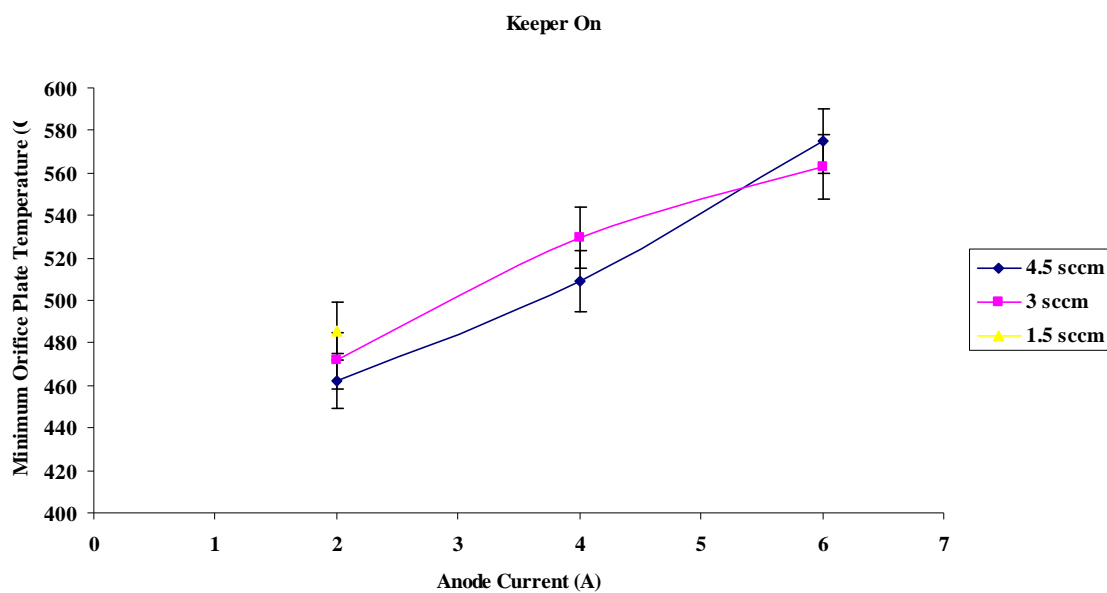
Keeper On

Figure 122. Minimum Orifice Plate Temperature (Keeper On)
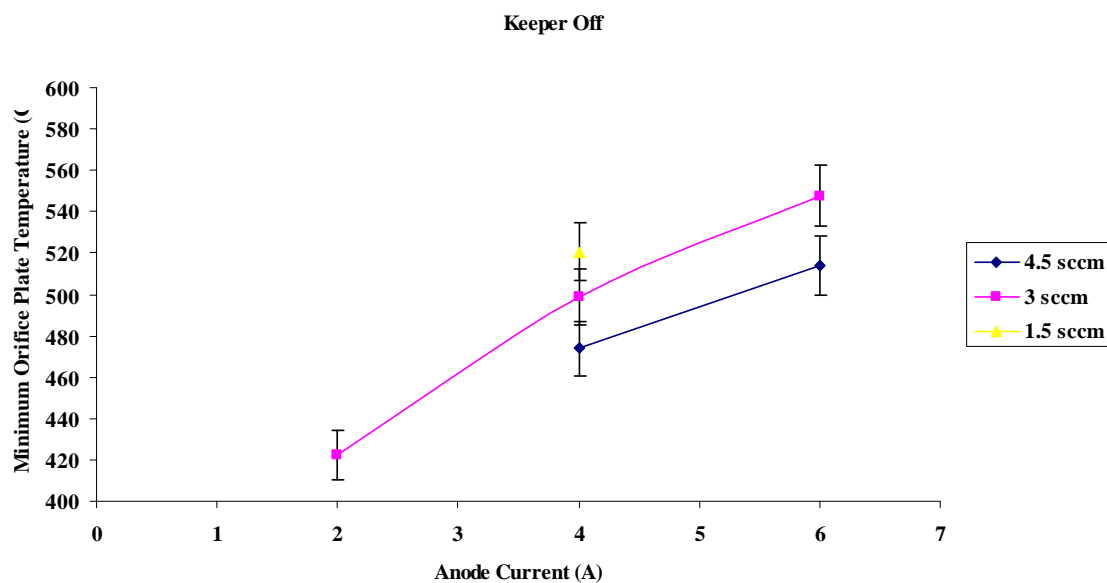
Keeper Off

Figure 123. CeB$_6$ Minimum Orifice Plate Temperature (Keeper Off)
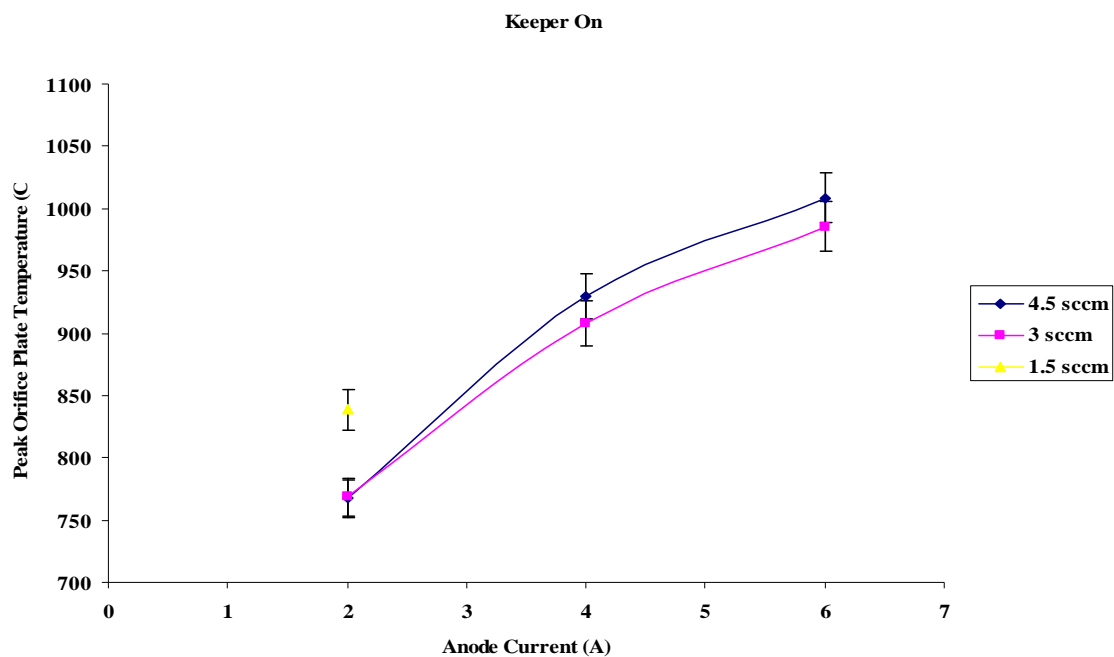
Figure 124. CeB$_6$ Peak Orifice Plate Temperature (Keeper On)
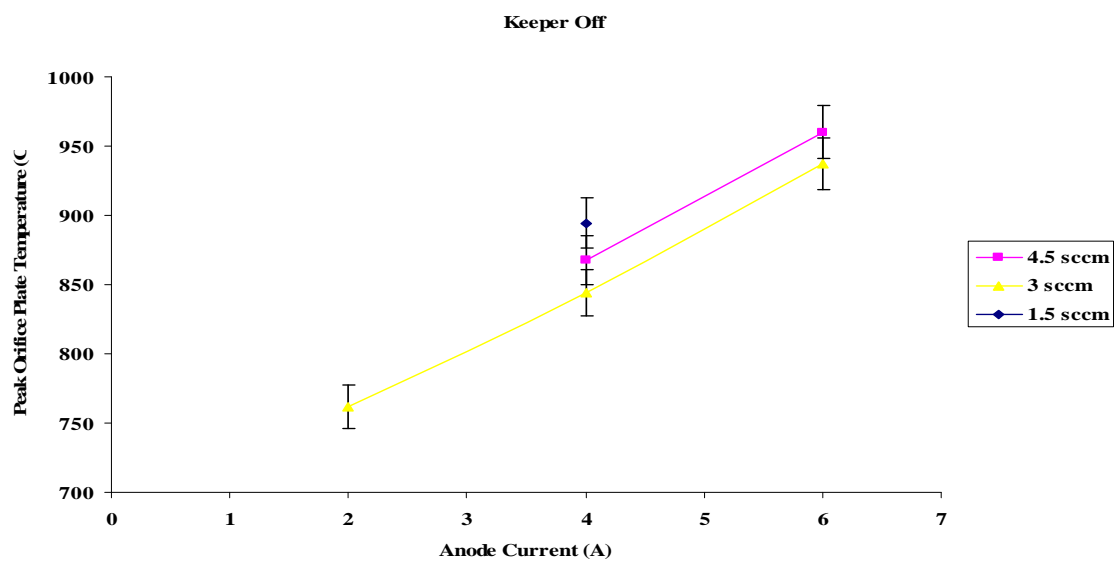
Figure 125. CeB$_6$ Peak Orifice Plate Temperature (Keeper Off)

152

Appendix C. Alternative Cathode Insert Geometries
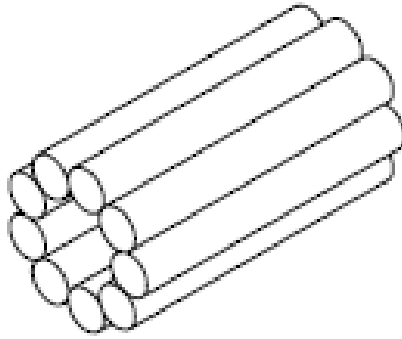
Figure 126. Single Crystal (100% density) Hollow Cathode Insert Arrangement[48]
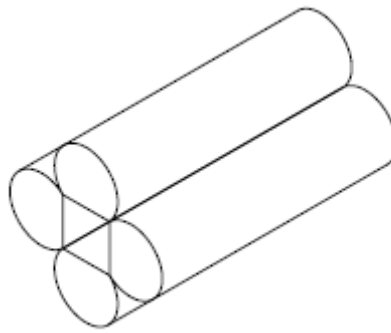
Figure 127. Single Crystal (100% density) Hollow Cathode Insert Arrangement (2)[48]

Appendix D. Preliminary CeB$_6$ and LaB$_6$ Cathode Results

Low Current Cerium Hexaboride and Lanthanum Hexaboride Hollow Cathodes

Dustin J. Warner[*] and Richard D. Branam[†]
Air Force Institute of Technology, Wright-Patterson AFB, OH, 45433

William A. Hargus, Jr.[‡]
Air Force Research Laboratory, Space Propulsion Branch, Edwards AFB, CA 93523

Dan M. Goebel[§]
Jet Propulsion Laboratory, California Institute of Technology, Pasadena, CA 91109

A Cerium Hexaboride (CeB6) and Lanthanum Hexaboride (LaB6) hollow cathode have been built for testing and evaluation as a low current electron source (<10A). This study monitored the DC and AC voltage characteristics during the evaluation of cathode performance for three different flow rates, and several anode and keeper current levels. The CeB6 cathode has a broader operating regime than the LaB6 cathode, running at lower current and flow levels than its LaB6 counterpart. The minimum current for the LaB6 cathode is approximately 3A at 1.5 sccm of xenon with no power to the heater. The minimum for the CeB6 cathode is approximately 1.5A at 1.5 sccm of xenon with no heater power.

Nomenclature

A	=	Richardson Constant
k	=	Boltzman's Constant
T	=	Temperature (K)
e	=	Charge of an Electron (C)
j	=	Current Density (A/cm^2)
ε	=	Permittivity of Free Space
φ	=	Work Function (eV)
E	=	Electric Field (V/m)
V	=	Volts
C	=	Coulomb
cm	=	centimeters
eV	=	Electron Volt
l	=	Liter

I. Introduction

RECENT research introduced a lanthanum hexaboride (LaB6) hollow cathode with a similar geometry of traditional hollow cathodes.[1] Historically, LaB6 cathodes require the use of the cathode heater to sustain stable operation. Therefore, the power required to create the same current levels as lower work-function impregnated cathodes was much higher for the LaB6 cathode. Recently, Goebel et. al. modified the LaB6 cathode geometry to allow it to sustain a discharge without the continual use of the heater. Nevertheless, impregnated cathodes have demonstrated reliable operation for thousands of hours.[2] They have also demonstrated operation over a wide range of current levels from a few hundred milliamps to hundreds of amps. However, as the temperature of the insert increases with the current demanded, the evaporation rate rises as well.[1] This has lead to some investigation into LaB6 as an alternative to impregnated cathodes as high current electron sources. LaB6 is reported to have a lower evaporation rate than impregnated cathodes at emission current densities of roughly 10A/cm^2.[1] LaB6 has also demonstrated a much higher resistance to poisoning from oxygen and water vapor than impregnated cathodes.[3] This

---

[*] Graduate Student, Department of Aeronautics and Astronautics, 2950 Hobson Way, Student Member, AIAA
[†] Assistant Professor, Department of Aeronautics and Astronautics, 2950 Hobson Way, Senior Member, AIAA
[‡] Senior Researcher, Space Propulsion Branch, Edwards AFB, CA 93523, Member
[§] Principal Scientist, Advanced Propulsion Group, Jet Propulsion Laboratory, Pasadena, CA, Senior Member AIAA

1
American Institute of Aeronautics and Astronautics
092407

demonstrates LaB6 cathodes as a viable alternative to conventional impregnated cathodes due to its resistance to poisoning and prospect for longer life.

While LaB6 demonstrates reliable, robust operation at current levels from 10A-100A, no published work in the US has investigated its feasibility as low current electron sources (<10A).[1] However, Russia has already used low current LaB6 cathodes for several low power hall thrusters.[4] This is mainly because LaB6 has a higher work function than the barium, calcium, and alumina impregnated cathodes. As a result, the LaB6 cathodes operate at higher temperatures (1650°C for ~10A/ cm^2) and require better thermal designs with higher power levels to maintain stable operation. One of the primary concerns of the lower current cathodes is heat loss by conduction to the base of the cathode, sometimes requiring continual heater operation for the cathode to maintain stable discharge. This is usually not of great concern for higher power applications, as the fraction of cathode power is small when compared to the total power of the system. On the other hand, cathode power is a large part of the total system for low power applications, and has been the subject of extensive investigation.[5]

Another material very similar to LaB6 is Cerium Hexaboride (CeB6). It has a slightly lower work function than LaB6, demonstrates the same resistance to poisoning as LaB6, and has a lower evaporation rate at similar emission current densities.[6,7] While used in many applications, using CeB6 in a hollow cathode emitter is relatively new. Christman, et. al. directly compares CeB6 and LaB6 single crystal emitters and investigates the very subjects mentioned here. He observed CeB6 has virtually the same capability as LaB6 as far as total emission current, and capable of providing 2-4 times the life of LaB6 if operated at sufficient temperatures to resist poisoning (>1300°C) and reaches stable operation much faster than LaB6.[7] Mitamura also found the life of CeB6 could be about four times that of LaB6 and that it has a higher emission current than LaB6 at similar temperatures.[8] Christman also observed CeB6 and LaB6 both demonstrate superior resistance to contamination from most gases. The original electron emission capability was regained after high temperature bake-out, with the exception of carbon. He found that after one hour of high temperature bake-out the CeB6 crystal regained 30% of its original emission where the LaB6 regained roughly 24%. After further heating, the CeB6 crystal regained 100% of its emission capability and the LaB6 crystal showed little change with further heating. Swanson and McNeely found that CeB6 and LaB6 had similar characteristics and both offer promise for electron emitters.[9] Another study completed by Davis, et. al., suggests CeB6 as a viable cathode technology as well.[10] This resistance to poisoning by the CeB6 crystal demonstrates its promise as an electron emitter for hollow cathodes.

To investigate the feasibility of LaB6 and CeB6 cathodes for low current applications, two cathodes developed and tested for electric propulsion applications are presented here. One cathode constructed for each insert material from a design acquired from Goebel at JPL is studied. This study also presents the modifications made to the original orifice design to reduce the flow requirements for spot-mode emission. Described in below are the details of the aforementioned cathodes and their performance during this investigation.

II. CeB6 and LaB6 Properties

Figure 1. Polycrystalline LaB6 Hollow Cathode Insert

LaB6 was first demonstrated as a hollow cathode by Goebel et. al. in 1978 and as an emitter for plasma sources in 1985.[11,12] Later it was used in a hollow cathode configuration for ion and hall thrusters in 2005. The work function of this insert material ranges from 2.66 eV to 2.91 eV.[1] The work function of CeB6 is between 2.5-2.62 eV.[9,10] These values both depend on the surface stoichiometry of each crystal and the crystal plane orientation.

Figure 1 shows an example of a hollow cathode insert, constructed in a hollow cylinder geometry. Due to the geometry of this insert, the CeB6 and LaB6 inserts are made from polycrystalline material. Because of the brittle nature of the single crystal of LaB6 and CeB6 used in direct emission cathodes, figure 2, it is difficult to machine into a hollow cathode insert tube.[13] As a result, polycrystalline material is press-sintered into a single rod, then machined to the final tube geometry. The density is approximately 70-90% of theoretical density. Due to the polycrystalline nature of the insert, the resulting work function is an averaging of each crystal.
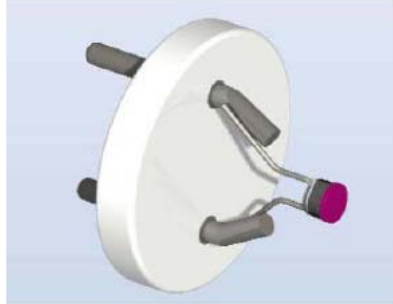
Figure 2. Single Crystal LaB6 Electron Emitter

Nevertheless, the Richardson-Duschman Equation describes the electron emission of a given material.

$$j = A \cdot T^2 \cdot e^{\frac{-q \cdot \phi}{k \cdot T}} \tag{1}$$

With an electric field present from the plasma sheath forming within the cathode insert, an effective work function is inserted into equation 1. This is the Schottkey-effect, described by:

$$\phi_{eff} = \phi - \sqrt{\frac{q \cdot |E|}{4\pi \cdot \varepsilon_0}} \tag{2}$$

The result is an overall lowering of the cathode work function. After initial breakdown, the hollow cathode typically does not require a heater to operate and can self-sustain discharge. The electric field also increases the peak current capability of the hollow cathode.

Another consideration for both LaB6 and CeB6 are their evaporation rates. According to vendor data and some available literature, CeB6 and LaB6 have very similar evaporation rates.[10,13] However, CeB6 has a slightly lower evaporation rate at 1800K, attaining a value of approximately 12nm/hr.[9] In comparison, LaB6 has an evaporation rate of 16.8 nm/hr at the same temperature. Unlike the impregnated cathodes, the only life-limiting characteristic of CeB6 and LaB6 is the evaporation and sputter erosion rate of the insert material.

Finally, the third consideration for the use of these cathodes as insert materials is their resistance to poisoning. A study completed by Gallagher extensively investigated the effects of poisoning for LaB6.[3] Christman found CeB6 demonstrates a similar resistance as well.[7] According to other studies, LaB6 can withstand pressures of 10^{-4} torr of oxygen exposure and experience no degradation of electron emission after high temperature bake-out.[13] Christman found similar results in his comparison of CeB6 and LaB6. Additionally, operation of LaB6 at temperatures above 1600°C allows the material to act as an electron source for oxygen plasma formation.[1] These results demonstrate the robust and reliable nature of boride cathodes.

III. Methodology

A. Vacuum Facility

The Space Propulsion Analysis and Simulation System (SPASS) vacuum facility is two meters in diameter and three meters long. A Leybold-Trivac rotary vane vacuum pump is used to bring the chamber pressure down to 80 mtorr. Atmospheric to rough vacuum pressure was monitored using a Kurt J. Lesker mini-convectron gauge. This pressure data was recorded and logged via Labview. Four CVI Torrmaster cryogenic pumps were used to maintain the chamber to pressures as low as $3*10^{-8}$ torr. The combined pumping speed of the system is ~16,000 l/s for xenon. An ExTorr residual gas analyzer (RGA) monitors the high-vacuum pressure. This partial and total pressure data was collected and recorded through manufacturer provided hardware and software. The RGA could report atomic masses ranging from 1-100 AMU and partial pressures ranging from $1*10^{-3}$ to $1*10^{-10}$ torr.

Figure 3. SPASS Facility

3
American Institute of Aeronautics and Astronautics
092407

158

B. Propellant and Power Systems

All tests were performed using grade five xenon. Flow was controlled through MKS flow meters and an MKS type 247 4-channel readout. Each flow meter was calibrated for 0-10 sccm of xenon. Figure 4 depicts the propellant system schematic.

A Matsusada REk 650V, 2.5A DC power supply controlled the cathode keeper voltage and current. A 150Ω 1000 watt resistor was placed in series with the keeper, in addition to a 5A calibrated shunt resistor, used to measure the current through the circuit. An HP Agilent 6033A 20V, 30A DC power supply drove the cathode heater. The anode used an HP 6038A 60V, 10A DC power supply. The maximum power output for each power supply was 250 watts, limiting the operating range of the cathodes. Calibrated shunt resistors were placed in series with the heater and anode. Figure 9 depicts the schematic of the set-up.
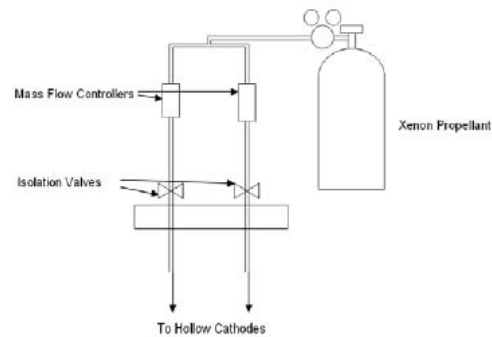
Figure 4. Propellant System Schematic

C. Cathode Assembly and Data Acquisition System

The cathodes presented here are of identical geometry based on a design obtained from Dan Goebel and the Jet Propulsion Laboratory. The authors constructed the cathode tube from molybdenum. The orifice plate was originally thoriated tungsten with a 45-degree chamfer and 3mm orifice. As this was better suited for higher current applications, the author modified the orifice plate and replaced it with a tantalum orifice plate, shown in figure 6. Initial tests used a .25mm thick orifice plate with a 1mm hole drilled through its center using electronic-discharge machining (EDM). Stacking the plates on top of each other offered a simple method to vary the aspect ratio, the ratio of the diameter of the orifice to its depth. The tests performed here used an aspect ratio of 0.5.

1. Cathode Tube
2. Keeper
3. Mounting Flange
4. Heater Filament
5. Insert
6. Support Tubes
7. Orifice Plate
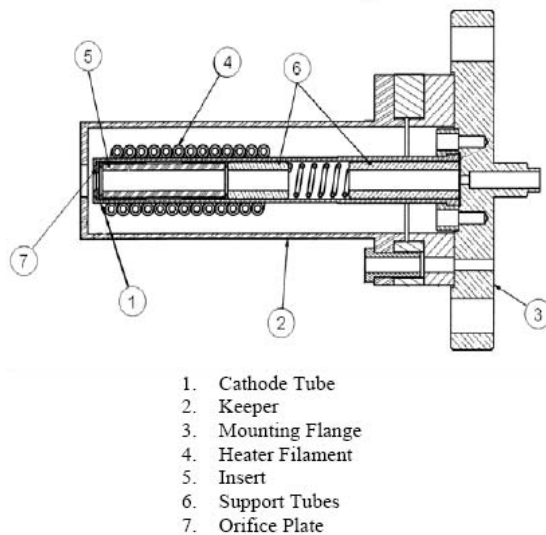
Figure 5. Hollow Cathode Assembly

Each insert is 6.4 mm in diameter with an inside diameter of 3.8 mm and a length of 2.5 cm. This geometry provides a total emitting surface area of 3.0 cm^2. Two small Poco graphite sleeves, grade DFP-1, protect both inserts from the refractory metal cathode tube. This prevents the flow of boron into the refractory metal, which would dramatically increase the work function.[14] A graphite tube backed by a carbon spring supports the insert. The spring provides the pressure needed to seat the orifice to the cathode tube. A Grafoil® gasket provides a seal between the cathode tube and mounting flange. Figure 5 shows a drawing of the cathode assembly.

Most cathodes employ the use of tantalum sheathed, magnesium oxide insulated, tantalum heater filaments to bring the insert up to its required operating temperature. The maximum operating temperature for these heaters is too low for the boride cathodes. As a result, an alumina insulated, tantalum-sheathed, tantalum heater filament is used. It has maximum operating temperature of roughly 1800°C.[1] Wrapped around the cathode approximately 12

times, the heater filament used in this study could provide nearly 140 watts of power over the insert region. Figure 7 shows the cathode tube with heater and shielding.

Due to the nature of the boride cathodes, heat loss by conduction and radiation are considerable. Care was taken to ensure the power required to run the cathode is low enough for the boride-based insert to operate effectively for low-current applications. For this design, tantalum radiation shielding (0.125mm thick) was wrapped around the heater filament 13 times. A thicker piece of tantalum foil wrapped around the outside of the shielding ensures a secure fit. Figure 7 shows the cathode with the keeper electrode removed and radiation shielding in place.

Figure 6. Tantalum Orifice Plates

Figure 7. Open Cathode with Radiation Shielding
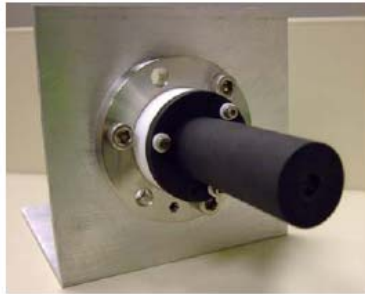
Figure 8. Cathode with Graphite Keeper

The final component of the hollow cathode is the keeper electrode. The keeper, constructed entirely out of Poco graphite, has an orifice of approximately 6 mm. The orifice is located approximately 1 mm from the cathode tube. Figure 8 shows the cathode in its entirety.

All tests performed use the triode configuration shown in figure 9. The anode is 5 cm in diameter and 13 cm long. It is positioned 2 cm downstream of the cathode keeper. The cathode is tested at anode current levels of 2, 4, and 6 A. The cathode keeper current was set to 0, 0.5, and 1 A for each anode current level. These test points were all run at 3 different flow rates, 1.5, 3, and 4.5 sccm. This resulted in 27 different operating points for each cathode.

A National Instruments SCXI 1321 4-channel readout measures the current through each shunt resistor. The voltage and waveform data for the keeper and anode were measured through a Tektronics TDS 420A 200 MHz digitizing oscilloscope.

IV. Results & Discussion

Observed by Goebel et. al., high frequency oscillations (50-500 kHz) at the edge of regions of dense plasma downstream of the cathode may create high-energy ions that accelerate the erosion of the cathode and its subsequent components.[15] Several additional studies have investigated the conditions required to minimize cathode erosion.[16,17,18] Originally completed by Rawlin and Pawlik, these studies have collectively lead to the identification of two modes of cathode operation.[19] One of which is spot-mode; characterized by low amplitude and frequency voltage and current oscillations,

Figure 9. Power Supply Schematic

and higher flow rates. Plume-mode is characterized by high frequency and amplitude voltage and current oscillations. Higher discharge voltages, electron temperatures, and lower flow rates also characterize plume-mode.

160

Two common methods are available for observing this phenomena, waveform monitoring and Langmuir probe measurements. Although Langmuir probe data may be a more sensiti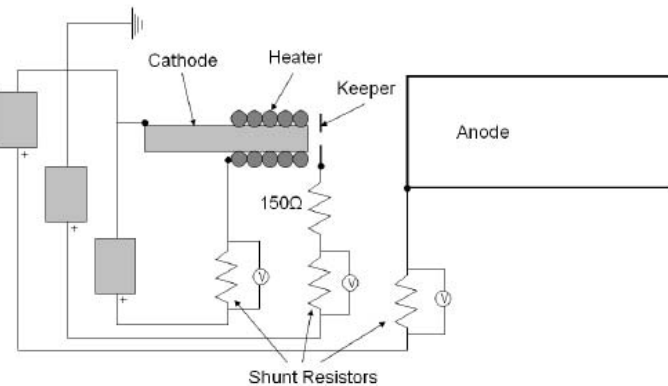ve indicator of the onset of plume-mode, we employed waveform monitoring for the initial tests due to availability of equipment. Each condition ran for approximately 10 minutes before data collection to determine spot or plume-mode operation.

A. Cathode Ignition

The Lab6 cathode has operated for roughly 20 hours to date. The robust nature of the cathode insert requires no special conditioning. The typical ignition process for this cathode is listed below. The cathode consistently started at these conditions without any complications or observable degradation.

1) Set heater current to 11.25 A and warm-up until the voltage reaches approximately 11V (~10 minutes).
2) Pump propellant lines out to the bottle.
3) Set flow to 4.5 sccm and allow to flow for 5 minutes.
4) Set keeper to 600 V,1 A, then cathode is started.

The CeB6 cathode ignition sequence is identical, with the exception of the keeper voltage, which is set to 500 V. Both were able to start with approximately 120-130 watts to the heater. The CeB6 cathode has approximately 15 hours of operation to date. Figure 10 is a picture of the LaB6 cathode during the moment of ignition, captured with a high-speed camera. The keeper orifice is to the left of the picture and the cylindrical anode is on the right.
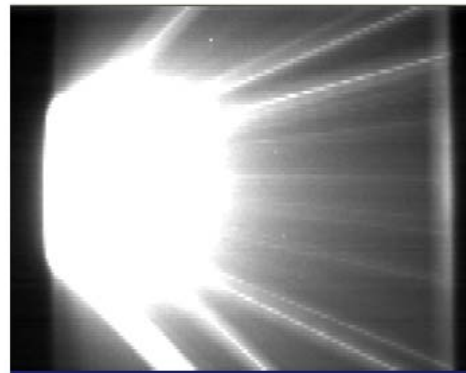
Figure 10. Moment of Cathode Ignition

B. Low-Current and Flow Operating Ranges

In addition to waveform monitoring to determine spot and plume-mode operation, both cathode flow rates and current levels were decreased until the discharge became unstable. Stable operation for the LaB6 cathode was as low as 2 A to the anode, 1 A to the keeper with the heater turned off at 2 sccm of flow. Large AC voltage oscillations that occurred during the low flow rates and currents characterized unstable operation. The amplitude of these oscillations was on the order of tens of volts or more and the frequency was on the order of several hertz.

The CeB6 cathode maintained a stable discharge at as low as 1.5 A to the anode with the keeper and heater turned off at 1.5 sccm of xenon.

C. Spot and Plume Mode Transitions

This work determined the transition from spot to plume-mode by waveform monitoring. The cathode entered plume-mode when the voltage levels oscillated more than one volt at a frequency of 50 kHz or greater. When the oscillations were lower than one volt the cathode was considered to be in spot-mode. Other typical factors played in as well: flow rate and voltage levels.

Tables 1, 2, and 3 display the mode of operation at different test points for the LaB6 cathode. For the 6 A and 4 A case at 1.5 sccm, the voltage limit was exceeded for the power supply and this data was not included for both the CeB6 and LaB6 cathode. The exception is the 4A case at 1.5 sccm for the CeB6 cathode. Figure 11 displays the anode voltage during this test point. Tables 4-7 summarize the operation modes for the CeB6 cathode.

161
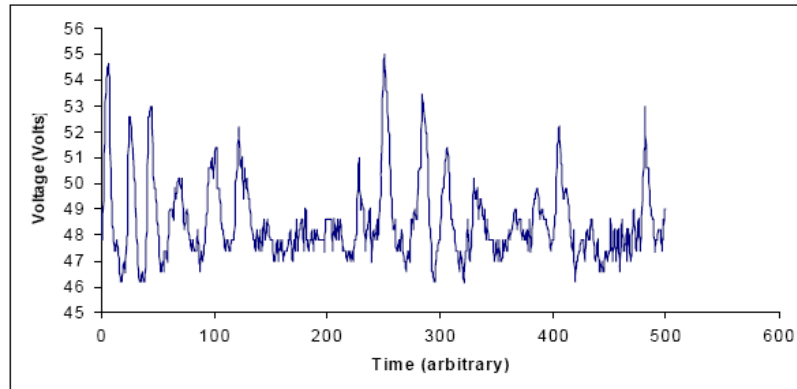
Figure 11. Anode Voltage Waveform for CeB6 cathode at 4A anode current, 1A Keeper current and 1.5 sccm.

Table 1. LaB6 Cathode at 4.5 sccm

Anode Current	Keeper Current	Anode Voltage	Keeper Voltage	Mode
6	1	31.15	16.04	Spot
6	0.5	30.82	15.72	Spot
6	0	32.26	N/A	Spot
4	1	34.85	19.04	Spot
4	0.5	34.09	19.47	Spot
4	0	35.04	N/A	Spot
2	1	41.3	26.2	Spot
2	0.5	41.9	28	Spot
2	0	46.7	N/A	Spot

Table 2. LaB6 Cathode at 3 sccm

Anode Current	Keeper Current	Anode Voltage	Keeper Voltage	Mode
6	1	35.12	17.74	Plume
6	0.5	35.73	17.13	Spot
6	0	36.6	N/A	Spot
4	1	36.36	19.72	Spot
4	0.5	37.47	19.76	Spot
4	0	39.4	N/A	Spot
2	1	47.4	27.635	Spot
2	0.5	42.66	26.53	Spot*
2	0	45.6	N/A	Spot*

* 30-40 W Heater Power Required

162

Table 3. LaB6 at 1.5 sccm

Anode Current	Keeper Current	Anode Voltage	Keeper Voltage	Mode
2	1	45.86		Spot*
2	0.5	44.47		Spot*
2	0	46.98	N/A	Spot*

*30-40W Heater Power Required

Table 4. CeB6 Cathode at 4.5 sccm

Anode Current	Keeper Current	Anode Voltage	Keeper Voltage	Mode
6	1	29.5	15.56	Spot
6	0.5	29.48	15.55	Spot
6	0	29.56	N/A	Spot
4	1	29.7	21.9	Spot
4	0.5	32.1	19.54	Spot
4	0	32.66	N/A	Spot
2	1	32.4	28.2	Spot
2	0.5	35.5	26	Spot
2	0	38.2	N/A	Spot

Table 5. CeB6 Cathode at 3 sccm

Anode Current	Keeper Current	Anode Voltage	Keeper Voltage	Mode
6	1	31.6	18.5	Spot
6	0.5	32	15.4	Spot
6	0	32.9	N/A	Spot
4	1	33.3	22.9	Spot
4	0.5	35.9	19.6	Spot
4	0	36.4	N/A	Spot
2	1	35.3	29.1	Spot
2	0.5	38.7	26.5	Spot
2	0	41.8	N/A	Spot

Table 6. CeB6 Cathode at 1.5 sccm

Anode Current	Keeper Current	Anode Voltage	Keeper Voltage	Mode
4	1	48.5	24.7	Plume
2	1	40.8	31.7	Spot
2	0.5	43.2	27.1	Spot
2	0	47.2	N/A	Spot

163

Figure 12 gives an idea of the typical plume-mode operation. The difference in frequency is attributed to the fact the data was taken at different test points. Figure 13 displays typical spot-mode for the keeper. The finest resolution of the oscilloscope was 400 mV, hence the rough discritization in data.
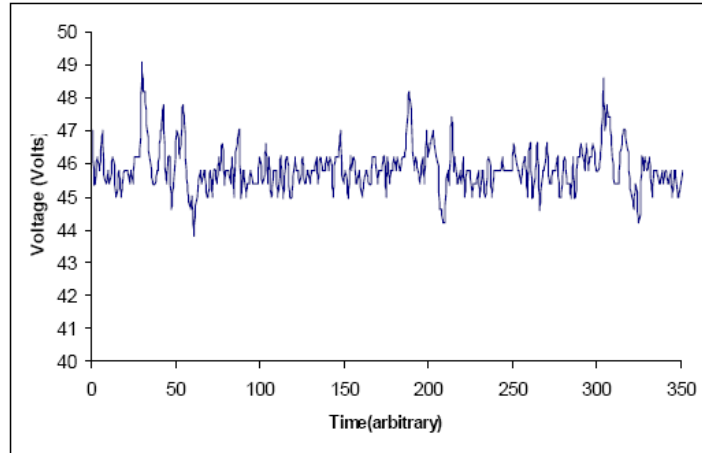

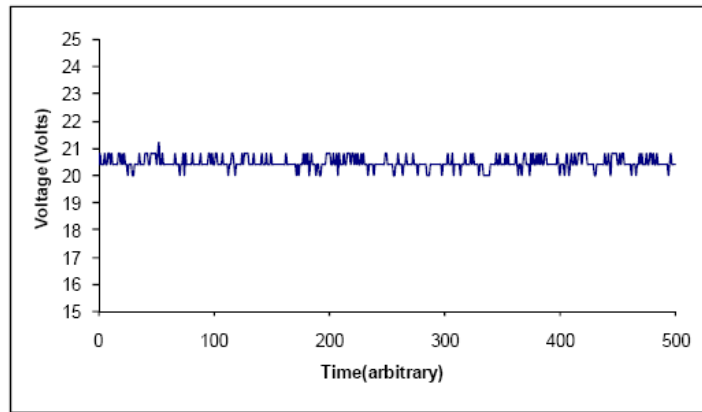**Figure 12. Plume-Mode Anode Voltage Waveform**

Figure 13. Spot-Mode Keeper Voltage Waveform

As a whole, the CeB6 cathode and LaB6 cathode performed in a very similar fashion over the course of these preliminary tests. For the given orifice geometry and anode configuration, most test points operate in spot-mode.

164

V. Conclusions

The results presented here indicate CeB6 and LaB6 cathodes are capable of operating as low current, low flow cathodes. Due to the temperature requirements, the LaB6 cathodes may not be able to sustain stable discharge at current levels below 2.5 A without the use of a heater. However, future improvements to the thermal efficiency of the 6.4 mm cathode could widen the operating range of the LaB6 cathode. The results also indicate challenges in scaling the LaB6 cathode down to smaller sizes due to the difficulty in minimizing heat conduction to the base of the cathode. The CeB6 cathode may provide an alternative to LaB6 if it meets or exceeds the resistance to poisoning and life characteristics of LaB6. Improvements to the thermal design may broaden the operating limits of the CeB6 cathode as well. Future work for these cathodes will investigate a smaller orifice and determine the operating limits of that configuration, as well as the effects of poisoning. Future studies will also begin plasma measurements for both cathodes. Nevertheless, the results presented here demonstrate with some thermal improvements the LaB6 cathode and the current CeB6 cathode as viable, low current electron emitters.

Acknowledgments

References

[1] Goebel, D.M. and Watkins, D.M., "LaB6 Hollow Cathodes for Ion and Hall Thrusters,"AIAA-2005-4239, 41st Joint Propulsion Conference, Tucson, AZ, Jul 2005.

[2] Sarver-Verhey, T. R., "Destructive Evaluation of a Xenon Hollow Cathode After a 28,000 Hour Life Test," NASA/CR—1998-208678.

[3] Gallagher, H. E., "Poisoning of LaB6 Cathodes." Journal of Applied Physics, 40(1), January 1969.

[4] Kim, Vladimir.," Electric Propulsion Activity in Russia." IEPC-01-05, 27th International Electric Propulsion Conference, Pasadena, CA, 15-19 October, 2001.

[5] Domonkos, Matthew T., "Evaluation of Low-Current Orificed Hollow Cathodes" PhD Dissertation, University of Michigan, 1999.

[6] Togawa, K., et al., "Emittance Measurement on the CeB6 Electron Gun for the Spring 8 Compact Sase Source." 351-354, FEL Conference, 2004.

[7] Christman, L. A., Schwind, G. A., Swanson, L. W., "A Comparison of CeB6 and LaB6 Thermionic Cathodes." 49th Annual Meeting of the Electron Microscopy Society of America, August 1991.

[8] Mitamura, S. et. Al., "CeB6 Electron Emitter and the Application." IMC16, Sapporoo, 2006.

[9] Swanson, L.W., Mcneely, D.R., "Work Functions of the 001 Face of the Hexaborides of Ba, La, Ce, and Sm." Journal of Surface Science Vol. 83 1979 pp. 11-28.

[10] Davis, P. R., et. al., "Comparison of Thermionic Cathode Parameters of Low Index Single Crystal Faces of LaB6, CeB6, and PrB6" Oregon Graduate Center, 8 April 1989.

[11] Goebel, Dan M.; Crow, J T.; Forrester, A T., "LaB6 Hollow Cathode for Dense Plasma Production." Rev. Sci. Instrum., 49 (4), April 1978.

[12] D.M. Goebel, Y. Hirooka and T. Sketchley, "Large area lanthanum hexaboride electron emitter", Rev. Sci. Instrum., 56, p.1717-1722 (1985).

[13] Personal conversations with Larry Southall, A-P-Tech, OR.

[14] Lafferty, J M., "Boride Cathodes." Journal of Applied Physics, 22(3), March 1951.

[15] Goebel, D. M., Jameson, K., Katz, I., and Mikellides, I. G., "Energetic Ion Production and Keeper Erosion in Hollow Cathode Discharges," IEPC-2005-266, 29th International Electric Propulsion Conference, Princeton University, Oct. 31-Nov. 4, 2005.

[16] Mirtich, M. J. and Kerslake, W. R., "Long Lifetime Hollow Cathodes for 30-cm Mercury Ion Thrusters," AIAA Paper 76-985, AIAA International Electric Propulsion Conference, Key Biscayne, FL, Nov. 1976.

[17] Shroff, A. M., Palluel, P., and Tonnerre, J. C., "Performance and Life Tests of Various Types of Impregnated Cathodes," Applications of Surface Science, Vol. 8, 1981, pp. 36-49.

[18] Sarver-Verhey, T. R., "Continuing Life Test of a Xenon Hollow Cathode for a Space Plasma Contactor," NASA Contractor Report 195401, Nov. 1994.

10
American Institute of Aeronautics and Astronautics
092407

Bibliography

1 Sarver-Verhey, T. R., "Destructive Evaluation of a Xenon Hollow Cathode After a 28,000 Hour Life Test," NASA/CR—1998-208678.

2 Goebel, D.M. and Watkins, D.M., "LaB6Hollow Cathodes for Ion and Hall Thrusters,"AIAA-2005-4239, 41stJoint Propulsion Conference, Tucson, AZ, Jul 2005.

3 Hofer, Richard R; Johnson, Lee K.; Goebel, Dan M.; Fitzgerald, Dennis J., "Effects of an Internally- Mounted Cathode on Hall Thruster Plume Properties," AIAA 2006-4482, 42nd Joint Propulsion Conference, Sacramento, CA, Jul 2006.

4 Goebel, Dan M.; Crow, J T.; Forrester, A T., "LaB6 Hollow Cathode for Dense Plasma Production." Rev. Sci. Instrum., 49(4), April 1978.

5 Tang, R., et al., "Breakdown and Ignition Limits in LaB6 Hollow Cathode Discharges" International Conference on Plasma Science, Traverse City, MI, June 2006.

6 Gallagher, H. E., "Poisoning of LaB6 Cathodes." Journal of Applied Physics, 40(1), January 1969.

7 Christman, L. A., Schwind, G. A., Swanson, L. W., "A Comparison of CeB6 and LaB6 Thermionic Cathodes." 49th Annual Meeting of the Electron Microscopy Society of America, August 1991.

8 Lafferty, J M., "Boride Cathodes." Journal of Applied Physics, 22(3), March 1951.

9 D.M. Goebel, Y. Hirooka and T. Sketchley, "Large area Lanthanum Hexaboride Electron Emitter", Rev. Sci. Instrum., 56, p.1717-1722 (1985).

10 Sommerville, Jason D.; King, Lyon B., "Effect of Cathode Position on Hall-Effect Thruster Performance and Cathode Coupling Voltage," AIAA 2007-5174, 43rd Joint Propulsion Conference, Cincinnati, OH, Jul 2007.

11 Pacros, Anne, "Instruments and Testing for a Hall Thruster Pume Experiment on the Space Shuttle." MS Thesis, Massachusetts Institute of Technology, 2002.

12 Azziz, Yassir, "Experimental and Theoretical Characterization of a Hall Thruster Plume." PhD Dissertation, Massachusetts Institute of Technology, 2007.

13 Kamhawi, Hani, "Development of a Hollow Cathode Assembly for the High Voltage Hall Accelerator." AIAA 2007-5172, 43rd Joint Propulsion Conference, Cincinnati, OH, July 2007.

14 Kim, Vladimir.," Electric Propulsion Activity in Russia." IEPC-01-05, 27th International Electric Propulsion Conference, Pasadena, CA, 15-19 October, 2001.

15 Goebel, Dan M., Katz, Ira C., "Fundamentals of Electric Propulsion: Ion and Hall Thrusters" Wiley, NY 2008.

16 Thomas, Cliff, Sommier, Emmanuelle, Gascon, Nicholas, Capelli, Mark., "The Magnetic Interference Hall Accelerator." AIAA 2006-4993, 42nd Joint Propulsion Conference, Sacramento, CA, July 2006.

17 Domonkos, Matthew T., "Evaluation of Low-Current Orificed Hollow Cathodes" PhD Dissertation, University of Michigan, June 1999.

18 Mirtich, M. J., "Investigation of Hollow Cathode Performance for 30-cm Thrusters," NASA TM X-68298, 1973.

19 Wirz, Richard; Goebel, Dan; Marrese, Colleen; Mueller, Juergen, "Development of Cathode Technologies for a Miniature Ion Thruster." AIAA-2003-4722, 39th Joint Propulsion Conference, Huntsville, AL, Jul 2003.

20 Wirz, Richard, "Dsicharge Plasma Processes of Ring Cusp Ion Thrusters" PhD Dissertation, California Institute of Technology, April 2005.

21 Rawlin, V. K. "13,000 Hour Test of a Mercury Hollow Cathode." NASA Technical Memorandum X-2785 June 1973.

22 Williams, J.D., "An Experimental Investigation of Hollow Cathode-Based Plasma Contactors" PhD Dissertation, Colorado State University, 1991.

23 Veeco "3 cm DC (ITI) Ion Source." http://www.veeco.com/products/Process_Equipment/Ion_Sources/3cm_DC__ITI_Ion _Source/, August 2007.

24 Davis, Paul R., et al., "Comparison of Thermionic Cathode Parameters of Low Index Single Crystal Faces of LaB6, CeB6, and PrB6."

25 Kimball Physics "ES-440 LaB6 Single Crystal"
   http://www.kimphys.com/cathode/catalog_PDF/LaB6_cathode_ES440.pdf

26 Personal conversations with Larry Southall, A-P-Tech, OR.

27 Polk, J. E., et. al., "Characterization of Hollow Cathode Performance and Thermal
   Behavior" AIAA-2006-5150, 46th Joint Propulsion Conference, Sacramento, CA,
   Jul 2006.

28 Mitamura, S. et. al., "CeB6 Electron Emitter and the Application." IMC16, Sapporo,
   2006.

29 Davis, P. R., et. al., "Comparison of Thermionic Cathode Parameters of Low Index
   Single Crystal Faces of LaB6, CeB6, and PrB6"

30 Storms, E K., Mueller B A., "A Study of Surface Stoichiometry and Thermionic
   Emission using LaB6." Journal of Applied Physics, 50(5), May 1975.

31 Wolski, W., "Pressed Boride Cathodes." NASA TM-77821, NASA, Washington
   D.C., June 1985.

32 Foster J.E., Williams G.J., Patterson M.J., "Characterization of an Ion Thruster
   Neutralizer" NASA Technical Memorandum 2005-213883 September 2005.

33 Mandell, M. J. and Katz I., "Theory of Hollow Cathode Operation in Spot and Plume
   modes,"AIAA-94-3134, 30th Joint Propulsion Conference, Indianapolis, IN, June
   1994.

34 Goebel, D. M., Jameson, K., Katz, I., and Mikellides, I. G., "Energetic Ion Production
   and Keeper Erosion in Hollow Cathode Discharges," IEPC-2005-266, 29th
   International Electric Propulsion Conference, Princeton University, Oct. 31-Nov. 4,
   2005.

35 Martin, R. M. and Williams, J. D., "Direct Measurements Nearby a Hollow Cathode
   Using a High Speed Electrostatic Probe."   AIAA 2006-4820, 42nd Joint Propulsion
   Conference, Sacramento, CA, July 2006.

36 Martin, Russell M. and Williams, John D., "Direct and Remote Measurements of
   Plasma Properties Nearby a Hollow Cathode" IEPC-2005-294, The 29th International
   Electric Propulsion Conference, Princeton University, October 2005.

168

37 Swanson, L. W. and Mcneely D. R, "Work Functions of the (100) Face of Ba, La, Ce, and SM" Surface Sciences 83 (1979) 11-28

38 Siegfried, D. E., "A Phenomenological Model for Orificed Hollow Cathodes." PhD Dissertation, Colorado State University, 1983.

39 Goebel, Dan M., Jameson, Kristina K., Watkins, Ron M., and Katz, Ira, "Hollow Cathode and Keeper-Region Plasma Measurements Using Ultra-Fast Miniature Scanning Probes," AIAA-2004-3430, 40th Joint Propulsion Conference, For Lauderdale, Florida, July 11-14, 2004.

40 Hutchinson, Ian H. "Principles of Plasma Diagnostics" Cambridge University Press, Cambridge, 2002.

41 SmartProbe User Manual

42 Chen, Francis F. "Langmuir Probe Diagnostics" Mini-Course on Plasma Diagnostics, IEEE-ICOPS Meeting, Jeju, Korea, June 2003.

43 Mikellides, Ioannis G., Katz Ira, Goebel Dan M., Jameson, Kristina K., Polk James E., "The Partially Ionized Gas and Associated Wear in Electron Sources for Ion Propulsion, II: Discharge Hollow Cathode." AIAA 2007-5192 43rd Joint Propulsion Conference, Cincinnati, OH, July 2007.

44 Milosevic, N.D., Vukovic, G.S., Pavicic, D.Z., and Maglic, K.D.,"Thermal Properties of Tantalum between 300 K and 2300 K" International Journal of Thermophysics, Vol 20, No. 4, 1999.

45 Cade, C.M., "The Thermal Emissivity of Some Materials Used in Thermionic Valve Manufacture" IRE Transactions on Electronic Devices,

46 Cerac, Inc. Wisconsin

47 Bunker, Robert C., Ewing Mark E., Shipley, John L., "Pyrolytic Graphite Gauges for Measuring Large Heat Fluxes." NASA Technical Brief, MFS-31572

48 A-P-Tech, McMinnville, Oregon.

Vita

2nd Lieutenant Dustin J. Warner graduated from Glenwood High School in Chatham, IL in 2002. He completed is Bachelor of Science degree in mechanical engineering at Colorado State University, Fort Collins, CO in 2006. Upon graduation, he received his commission from AFROTC Detachment 90.

His first assignment was as a direct accession student to the department of Aeronautics and Astronautics at AFIT in 2006. Upon completion of his degree, he will follow-on to NASIC. There he will perform duties as an analyst for space launch vehicle propulsion.

REPORT DOCUMENTATION PAGE

1. REPORT DATE (DD-MM-YYYY)	2. REPORT TYPE	3. DATES COVERED (From – To)
	Master's Thesis	March 2007 – March 2008

4. TITLE AND SUBTITLE	5a. CONTRACT NUMBER
ADVANCED CATHODES FOR NEXT GENERATION ELECTRIC PROPULSION TECHNOLOGY	5b. GRANT NUMBER
	5c. PROGRAM ELEMENT NUMBER
6. AUTHOR(S)	5d. PROJECT NUMBER
Warner, Dustin J., 2nd Lt., USAF	5e. TASK NUMBER
	5f. WORK UNIT NUMBER

7. PERFORMING ORGANIZATION NAMES(S) AND ADDRESS(S)	8. PERFORMING ORGANIZATION REPORT NUMBER
Air Force Institute of Technology Graduate School of Engineering and Management (AFIT/ENY) 2950 Hobson Way, Building 640 WPAFB OH 45433-8865	AFIT/GA/ENY/08-M07

9. SPONSORING/MONITORING AGENCY NAME(S) AND ADDRESS(ES)	10. SPONSOR/MONITOR'S ACRONYM(S)
AFRL/RZS Att: Mr. Michael Huggins 1 Ara Rd. Edwards, AFB CA 93524	11. SPONSOR/MONITOR'S REPORT NUMBER(S)

12. DISTRIBUTION/AVAILABILITY STATEMENT

APPROVED FOR PUBLIC RELEASE; DISTRIBUTION UNLIMITED.

13. SUPPLEMENTARY NOTES

14. ABSTRACT

The research presented here investigated the feasibility of a 6.4 mm Lanthanum Hexaboride (LaB_6) and Cerium Hexaboride (CeB_6) hollow cathode for low power electric propulsion applications (100-300W). Two orifice geometries, one anode configuration, several anode and keeper currents, and a range of flow rates were tested for the LaB_6 cathode. The CeB_6 cathode underwent the same tests, with the exception of the second orifice geometry due to time constraints.

The required instruments include an oscilloscope to monitor the keeper and anode voltages, a Langmuir probe measured electron temperature, plasma densities, and plasma potential for the coupling plasma, infrared imaging studied the thermal characteristics of each cathode, electron microscopy for surface contaminant analysis, and high-speed imaging for coupling plasma observations. The oscilloscope, Langmuir probe, and high-speed camera determined the cathodes' mode of operation and gave information that indicated stable spot mode or unstable, destructive plume mode.

The CeB_6 cathode operated in spot mode as low as 1.5 A and 1.5 sccm with no heater or keeper power, and as high as 6 A, 1.5 sccm with 1 A keeper current. Increasing the flow rate and keeper current mitigated plume mode. The CeB_6 cathode was more susceptible to poisoning than the LaB_6 cathode, requiring more heater power and flow to start after running at low flow and current for long periods. The CeB_6 cathode also operated at slightly higher temperatures than the LaB_6 cathode, indicating a higher emissivity.

The LaB_6 cathode ran in spot mode as low as 2.5 A, at 1.5 sccm with no heater or keeper power. However, when the aspect ratio was reduced to 0.25, the cathode operated as low as 1.4 A, with 1.5 sccm until the cathode exceeded the voltage limit of the power supply. The same spot/plume mode characteristics were observed for LaB_6 as CeB_6. LaB_6 was more resistant to poisoning than the CeB_6 insert tested here, and operated at slightly lower temperatures. Neither cathode provided a significant power savings advantage compared to each other, nor significant plasma performance. The LaB_6 cathode demonstrated the capability for use as a low current electron emitter while the CeB_6 cathode requires further investigation. A comprehensive study of both cathodes is presented here including suggestions for a 3 mm LaB_6 cathode intended for future research.

15. SUBJECT TERMS

Lanthanum Hexaboride, Cerium Hexaboride, electric propulsion, hollow cathodes, hall thrusters, ion thrusters, plasma contactors, insert

16. SECURITY CLASSIFICATION OF:			17. LIMITATION OF ABSTRACT	18. NUMBER OF PAGES	19a. NAME OF RESPONSIBLE PERSON
a. REPORT	b. ABSTRACT	c. THIS PAGE			Richard D. Branam, Maj., USAF
U	U	U	UU	172	19b. TELEPHONE NUMBER (Include area code) (937) 255-6565x7485 (richard.branam@afit.edu)